REPORT DOCUMENTATION PAGE

Form Approved OMB NO. 0704-0188

1. REPORT DATE (DD-MM-YYYY)	2. REPORT TYPE	3. DATES COVERED (From - To)
13-12-2022	Final Report	29-Sep-2018 - 28-Sep-2022

4. TITLE AND SUBTITLE
Final Report: Control of Organic Matter with Strong Coupling

5a. CONTRACT NUMBER
W911NF-18-1-0472

5b. GRANT NUMBER

5c. PROGRAM ELEMENT NUMBER
106012

6. AUTHORS

5d. PROJECT NUMBER

5e. TASK NUMBER

5f. WORK UNIT NUMBER

7. PERFORMING ORGANIZATION NAMES AND ADDRESSES

Norfolk State University
700 Park Avenue
McDemmond Center for Applied Research, Suite 601
Norfolk, VA 23504 -8060

8. PERFORMING ORGANIZATION REPORT NUMBER

9. SPONSORING/MONITORING AGENCY NAME(S) AND ADDRESS (ES)

U.S. Army Research Office
P.O. Box 12211
Research Triangle Park, NC 27709-2211

10. SPONSOR/MONITOR'S ACRONYM(S)
ARO

11. SPONSOR/MONITOR'S REPORT NUMBER(S)
72497-RT-REP.43

12. DISTRIBUTION AVAILIBILITY STATEMENT

Approved for public release; distribution is unlimited.

13. SUPPLEMENTARY NOTES

The views, opinions and/or findings contained in this report are those of the author(s) and should not contrued as an official Department of the Army position, policy or decision, unless so designated by other documentation.

14. ABSTRACT

15. SUBJECT TERMS

16. SECURITY CLASSIFICATION OF:			17. LIMITATION OF ABSTRACT	15. NUMBER OF PAGES	19a. NAME OF RESPONSIBLE PERSON
a. REPORT	b. ABSTRACT	c. THIS PAGE			Mikhail Noginov
UU	UU	UU	UU		19b. TELEPHONE NUMBER 757-823-2204

RPPR Final Report
as of 14-Mar-2023

Agency Code: 21XD

Proposal Number: 72497RTREP **Agreement Number: W911NF-18-1-0472**
INVESTIGATOR(S):

Name: Chi Yang
Email: cyang@nsu.edu
Phone Number: 7578239531
Principal: N

Name: Mikhail A Noginov
Email: mnoginov@nsu.edu
Phone Number: 7578232204
Principal: Y

Name: Natalia Noginova Ph.D.
Email: nnoginova@nsu.edu
Phone Number: 7578232298
Principal: N

Organization: **Norfolk State University**
Address: 700 Park Avenue, Norfolk, VA 235048060
Country: USA

DUNS Number: 074754805 EIN: 546002808
Report Date: 28-Dec-2022 Date Received: 13-Dec-2022
Final Report for Period Beginning 29-Sep-2018 and Ending 28-Sep-2022
Title: Control of Organic Matter with Strong Coupling
Begin Performance Period: 29-Sep-2018 **End Performance Period:** 28-Sep-2022
Report Term: 0-Other

Submitted By: Mikhail Noginov Email: mnoginov@nsu.edu
Phone: (757) 823-2204

STEM Degrees: **STEM Participants:**

Major Goals: Scores of physical phenomena, including light emission, donor-acceptor energy transfer, wetting and chemical reactions, can be strongly modified in the vicinity of metamaterials (rationally designed metal-dielectric composites) and other non-local dielectric environments. They, arguably, occur in the weak coupling regime of light-matter interaction, when the rates of the processes are affected, while the energy states of the interacting systems remain intact. Despite the richness of physical phenomena enabled by the weak coupling, an even greater control of light-matter interactions can be achieved in the strong coupling regime (of e.g. excitons in molecular ensembles and resonant cavities), when the eigen-energies of interacting states differ significantly (by ~1 eV!) from those of individual not interacting constituents. We argue that such a strong change of the energy eigenvalues may constitute creation of a new hybridized matter, with greatly modified quantum mechanical wave-functions, spectroscopic properties, dispersion, surface potentials, electron transport and pathways of chemical reactions. Our studies of weak and strong coupling phenomena revealed that we just scratched the surface of the complex multi-faceted problem and, while providing for some answers, uncovered an even larger number of intriguing questions (below) to be answered in the this research program. (1) Where is the crossover of the classical and quantum regimes of a strong coupling? (2) Can two types of molecules form a new coherent state (coherent matter) enabled by their strong coupling with a cavity? (3) Why chemical reactions and the energy transfer are always inhibited on top of metal/dielectric substrates? Can rationally designed dielectric environments accelerate these processes? (4) Does the strong coupling exist in the absence of photons and can this effect be observed experimentally? (5) Can the strong coupling control magnetoresistivity in organic semiconductors? (6) Can a strong coupling occur in random inhomogeneous composite media? The understanding of these phenomena will lead to development of advanced organic and polymeric materials for future U.S. Air Force applications. Student development was among the major goals of this project. While two graduate students were planned to be recruited and trained in the proposed research program, a much larger number of students, including underrepresented minorities, benefited from the project through participation in research and professional

development activities.

Accomplishments: See attached

Training Opportunities: 15 graduate and 4 undergraduate students were requited and trained in the project; 7 of them were females and 6 were AA minority. Some of them were paid directly (stipend and tuition) and others indirectly (via purchase of materials and supplies).

Results Dissemination: The research findings were disseminated via patents, journal publications and conference presentations.

Honors and Awards: Mikhail A. Noginov has received Norfolk State University Distinguished Scholarship Award (in 2022).

Protocol Activity Status:

Technology Transfer: Discussions with AFRL scientists have been held. However, they did not result in collaborations yet.

PARTICIPANTS:

Participant Type: PD/PI
Participant: Mikhail A Noginov
Person Months Worked: 6.00 **Funding Support:**
Project Contribution:
National Academy Member: N

Participant Type: Co-Investigator
Participant: Natalia Noginova
Person Months Worked: 4.00 **Funding Support:**
Project Contribution:
National Academy Member: N

Participant Type: Staff Scientist (doctoral level)
Participant: Chi Yang
Person Months Worked: 6.00 **Funding Support:**
Project Contribution:
National Academy Member: N

Participant Type: Graduate Student (research assistant)
Participant: Md G. R. Chowdhurry
Person Months Worked: 12.00 **Funding Support:**
Project Contribution:
National Academy Member: N

Participant Type: Graduate Student (research assistant)
Participant: Kanij M Khabir
Person Months Worked: 12.00 **Funding Support:**
Project Contribution:
National Academy Member: N

RPPR Final Report
as of 14-Mar-2023

Participant Type: Graduate Student (research assistant)
Participant: Leila Hesami
Person Months Worked: 12.00 **Funding Support:**
Project Contribution:
National Academy Member: N

ARTICLES:

Publication Type: Journal Article Peer Reviewed: Y **Publication Status:** 1-Published
Journal: Journal of the Optical Society of America B
Publication Identifier Type: DOI Publication Identifier: 10.1364/JOSAB.36.00E132
Volume: 36 Issue: 7 First Page #:
Date Submitted: 9/11/19 12:00AM Date Published: 7/1/19 4:00AM
Publication Location:
Article Title: Effect of metal–dielectric substrates on chemiluminescence kinetics
Authors: V. N. Peters, C. Yang, S. Prayakarao, M. A. Noginov
Keywords: Chemiluminescence; control of chemical reactions; hyperbolic metamaterials
Abstract: We studied chemiluminescence of rhodamine 6G (R6G) dye in a series of R6G:DNPO:PMMA films deposited onto a variety of metallic, metal–dielectric, and dielectric substrates. We found that chemiluminescence kinetics on top of Ag and Au films covered by an insulating MgF2 layer had longer decay times than those on top of purely dielectric substrates, MgF2 films on glass. We infer that Ag- and Au-based substrates with an insulating MgF2 layer on top affected the reaction rates by influencing polarization energies of reactants and surrounding molecu- lar dipoles. At the same time, the chemiluminescence kinetics on top of Ag and Au surfaces (without an insulating MgF2 spacer) were substantially shorter than those on top of dielectric substrates, probably because of conven- tional chemical catalysis. The peak emission intensities on top of metallic substrates (with and without the MgF2 layer on top) were lower than those on top of purely dielectric substrates, likely due to inhibition of the
Distribution Statement: 3-Distribution authorized to U.S. Government Agencies and their contractors
Acknowledged Federal Support: **Y**

Publication Type: Journal Article Peer Reviewed: Y **Publication Status:** 1-Published
Journal: Journal of Nanophotonics
Publication Identifier Type: DOI Publication Identifier: 10.1117/1.JNP.13.026007
Volume: 13 Issue: 02 First Page #: 1
Date Submitted: 9/11/19 12:00AM Date Published: 5/1/19 12:00AM
Publication Location:
Article Title: Study of electrical conductivity of the poly(3 hexylthiophene-2, 5-diyl) polymer in resonant Fabry–Perot cavities
Authors: Joshua Asane, Vanessa Peters, Rohan Alexander, Tylisia Wallace, D'Angelo Peters, Mikhail Noginov
Keywords: strong coupling; poly(3-hexylthiophene-2, 5-diyl) polymer; conductivity; resonant cavity.
Abstract: Enhancing electrical conductance in organic semiconductors has been a focus of intense research over the last few decades. The improvement can be made by optimizing either the material or the device architecture. As it has been shown by Orgiu et al., strong coupling of organic molecules with a nanostructured plasmonic substrate can significantly improve the mol- ecules' electrical conductivity. We searched for the effect of strong coupling with a Fabry–Perot cavity on the conductivity of the semiconducting poly(3 hexylthiophene-2, 5-diyl) (P3HT) polymer. Despite the observation of the strong coupling evidenced by a very large Rabi splitting of 1.0 eV, the increase of electrical conductivity with increase of the P3HT film thickness was primarily affected by an increase of the polymer's order in thick P3HT films.
Distribution Statement: 3-Distribution authorized to U.S. Government Agencies and their contractors
Acknowledged Federal Support: **Y**

RPPR Final Report
as of 14-Mar-2023

Publication Type: Journal Article Peer Reviewed: Y **Publication Status:** 1-Published
Journal: Journal of the Optical Society of America B
Publication Identifier Type: DOI Publication Identifier: 10.1364/JOSAB.36.002312
Volume: 36 Issue: 8 First Page #: 2312
Date Submitted: 9/11/19 12:00AM Date Published: 7/1/19 4:00AM
Publication Location:
Article Title: Non-resonant enhancement of spontaneous emission of HITC dye in metal-insulator-metal waveguides
Authors: Srujana Prayakarao, Deionjalei Miller, Devon Courtwright, Carl E. Bonner, Mikhail A. Noginov
Keywords: plasmonics, spontaneous emission
Abstract: We have experimentally studied the non-resonant enhancement of spontaneous emission of HITC laser dye in metal-insulator-metal (MIM) waveguides (also referred to as Fabry–Perot cavities). We have found that in the cavities, whose size was too small to support a fundamental or any higher order resonance, the emission decay rate increased, by nearly an order of magnitude, with reduction of the cavity size. At the same time, the emission intensity increased when the cavity size was reduced from ?200 to ?30 nm and dropped sharply when the cavity was smaller than ?30 nm. This emission enhancement, consistent with the perpendicular orientation of the emitting dipole with respect to the mirrors, is in a good agreement with the theoretical predictions known from the literature.
Distribution Statement: 3-Distribution authorized to U.S. Government Agencies and their contractors
Acknowledged Federal Support: **Y**

Publication Type: Journal Article Peer Reviewed: Y **Publication Status:** 1-Published
Journal: Nano Letters
Publication Identifier Type: DOI Publication Identifier: 10.1021/acs.nanolett.8b04268
Volume: 19 Issue: 2 First Page #: 1015
Date Submitted: 9/11/19 12:00AM Date Published: 1/1/19 5:00AM
Publication Location:
Article Title: Manipulation of Magnetic Dipole Emission from Eu
Authors: Aleksandr Vaskin, Soheila Mashhadi, Michael Steinert, Katie E. Chong, David Keene, Stefan Nanz, Aim
Keywords: Magnetic dipole emission, dielectric metasurfaces, Mie resonances, Purcell enhancement
Abstract: Mie-resonant high-index dielectric nanopar- ticles and metasurfaces have been suggested as a viable platform for enhancing both electric and magnetic dipole transitions of fluorescent emitters. While the enhancement of the electric dipole transitions by such dielectric nanoparticles has been demonstrated experimentally, the case of magnetic- dipole transitions remains largely unexplored. Here, we study the enhancement of spontaneous emission of Eu3+ ions, featuring both electric and magnetic-dominated dipole transitions, by dielectric metasurfaces composed of Mie- resonant silicon nanocylinders. By coating the metasurfaces with a layer of an Eu3+ doped polymer, we observe an enhancement of the Eu3+ emission associated with the electric (at 610 nm) and magnetic-dominated (at 590 nm) dipole transitions. The enhancement factor depends systematically on the spectral proximity of the atomic transitions to the Mie resonances as well as their multipolar order, both controlled by the nanocylin
Distribution Statement: 3-Distribution authorized to U.S. Government Agencies and their contractors
Acknowledged Federal Support: **Y**

RPPR Final Report
as of 14-Mar-2023

Publication Type: Journal Article Peer Reviewed: Y **Publication Status:** 1-Published
Journal: Optica
Publication Identifier Type: DOI Publication Identifier: 10.1364/OPTICA.6.000318
Volume: 6 Issue: 3 First Page #: 318
Date Submitted: 9/11/19 12:00AM Date Published: 3/1/19 5:00AM
Publication Location:
Article Title: Effect of strong coupling on photodegradation of the semiconducting polymer P3HT
Authors: Vanessa N. Peters, Md Omar Faruk, Joshua Asane, Rohan Alexander, D'angelo A. Peters, Srujana Pra
Keywords: Strong coupling; Photodegradation; P3HT
Abstract: Photonic structures are commonly designed to manipulate scattered or emitted light. However, in recent years, they were demonstrated to affect a variety of phenomena, including chemical reactions, which lie outside the traditional electrodynamics domain. In this work, we have studied the effect of a Fabry–Perot cavity on the chemical reaction of practical importance—photodegradation of the semiconducting polymer 2,5-poly(3-hexylthiophene) (P3HT), which is the material of choice in organic photovoltaics. Experimentally, Fabry–Perot cavities, composed of two silver mir- rors and filled with P3HT polymer, were photoexposed over tens of hours, and the concentration of the remaining thiophene rings (composing P3HT) was studied as a function of time. It has been found that in the regime of strong coupling with the cavity, characterized by one of the largest values of the Rabi splitting reported in the literature (1.0 eV), the normalized rate of photodegradation is reduced threefold.
Distribution Statement: 3-Distribution authorized to U.S. Government Agencies and their contractors
Acknowledged Federal Support: **Y**

Publication Type: Journal Article Peer Reviewed: Y **Publication Status:** 1-Published
Journal: physica status solidi (b)
Publication Identifier Type: DOI Publication Identifier: 10.1002/pssb.201800045
Volume: 256 Issue: 3 First Page #: 1800045
Date Submitted: 9/12/19 12:00AM Date Published: 3/1/19 3:00PM
Publication Location:
Article Title: Coupling of the First and Second Excited States of R6G Dye with the Fabry-Perot Cavity
Authors: Ekembu K. Tanyi, Erin Harrison, Cansu On, Mikhail A. Noginov
Keywords: Strong coupling; Excitons, Surface Plasmons
Abstract: Coupling of macroscopic ensembles of highly concentrated R6G molecules with aluminum and silver Fabry–Perot cavities of different sizes, in which one or two standing wave modes are in resonance with the absorption transition(s) of the dye molecules, have been studied. (i) It has been found that strong coupling of the cavity with one molecular eigenstate (S0?S1 transition) does not perturb the energies of the other molecular states. (ii) The S0?S2 absorption transition is too weak to strongly couple to the resonant cavity ("?" standing wave mode). However, the resonant cavity causes a blue shift of the S0?S2 excitation band. (iii) The splitting of the dispersion curve is theoretically predicted and experimentally observed at strong coupling of the cavity resonance ("?" standing wave mode) with the material resonances of Ag, including bound electron and "epsilon equal zero" transitions.
Distribution Statement: 3-Distribution authorized to U.S. Government Agencies and their contractors
Acknowledged Federal Support: **Y**

RPPR Final Report
as of 14-Mar-2023

Publication Type: Journal Article Peer Reviewed: Y **Publication Status:** 1-Published
Journal: ACS Applied Nano Materials
Publication Identifier Type: DOI Publication Identifier: 10.1021/acsanm.9b00147
Volume: 2 Issue: 3 First Page #: 1713
Date Submitted: 9/11/19 12:00AM Date Published: 2/1/19 5:00AM
Publication Location:
Article Title: Enhancement of Electrochromic Polymer Switching in Plasmonic Nanostructured Environment
Authors: Mohammad Shahabuddin, Thomas McDowell, Carl E. Bonner, Natalia Noginova
Keywords: plasmonics, charge transfer, nanostructures, cyclic voltammetry
Abstract: We explore color switching properties of thin polyaniline (PANI) films deposited on plasmonic nanomesh structures in comparison with the films deposited on flat gold. The nanostructured systems show a much steeper color switching with increasing voltage than the films prepared on flat substrates. A strong difference between nanostructured and flat systems is also observed at small voltages, where nanostructured samples often demonstrate an additional feature in cyclic voltammetry curves and nonmonotonous changes in optical properties. Possible origins of the observed effects are discussed in terms of acceleration of charge transport in nanostructured plasmonic environment and interface-related effects. The results can provide opportunities for enhancing and controlling the electrochromic polymer performance in smart windows or display applications.
Distribution Statement: 3-Distribution authorized to U.S. Government Agencies and their contractors
Acknowledged Federal Support: **Y**

Publication Type: Journal Article Peer Reviewed: Y **Publication Status:** 1-Published
Journal: Applied Physics Letters
Publication Identifier Type: DOI Publication Identifier: 10.1063/1.5117875
Volume: 115 Issue: 15 First Page #: 151103
Date Submitted: 7/26/20 12:00AM Date Published: 10/1/19 4:00AM
Publication Location:
Article Title: Plasmonic laser with distributed feedback
Authors: E. K. Tanyi, S. Mashhadi, C. On, Md. O. Faruk, E. Harrison, N. Noginova, M. A. Noginov
Keywords: plasmic laser
Abstract: We have demonstrated a low-threshold surface-emitting plasmonic laser radiating two symmetrical beams (at 30┐ from the normal to thesample) characterized by a narrow (└1 nm) spectral width, and explained its performance in terms of the distributed feedback mechanism. The results of our study provide an extra degree of freedom to the plasmonic laser design.
Distribution Statement: 2-Distribution Limited to U.S. Government agencies only; report contains proprietary info
Acknowledged Federal Support: **Y**

RPPR Final Report
as of 14-Mar-2023

Publication Type: Journal Article Peer Reviewed: Y **Publication Status:** 1-Published
Journal: Journal of the Optical Society of America B
Publication Identifier Type: DOI Publication Identifier: 10.1364/JOSAB.36.003579
Volume: 36 Issue: 12 First Page #: 3579
Date Submitted: 7/26/20 12:00AM Date Published: 11/1/19 4:00AM
Publication Location:
Article Title: Effect of nonlocal metal–dielectric environments on concentration quenching of HITC dye
Authors: Srujana Prayakarao, Samantha R. Koutsares, Carl E. Bonner, Mikhail A. Noginov
Keywords: Control of the energy transfer
Abstract: Understanding and harnessing energy transfer in organic and inorganic systems is of high fundamental and practical importance. In this work, we have experimentally studied the effect of lamellar hyperbolic metamaterials and metal/dielectric interfaces on the concentration-dependent luminescence quenching in thin polymeric poly (methyl methacrylate) films doped with 2-[7-(1,3-dihydro-1,3,3-trimethyl-2H-indol-2-ylidene)-1,3,5-heptatrienyl]-1,3,3-trimethyl-3H-indoliumiodide dye molecules. The rate of the concentration quenching (energy transfer to quenching centers) was found to be approximately proportional to the square of the dye concentration. The concentration quenching was strongly inhibited in the vicinity of metallic films and lamellar metal–dielectric metamaterials with hyperbolic dispersion. The characteristic length-scale of the inhibition (the distance between the dye molecules and the metallic surface, at which the inhibition becomes significant) was found to be ? 47 nm.
Distribution Statement: 2-Distribution Limited to U.S. Government agencies only; report contains proprietary info
Acknowledged Federal Support: **Y**

Publication Type: Journal Article Peer Reviewed: Y **Publication Status:** 1-Published
Journal: ACS Photonics
Publication Identifier Type: DOI Publication Identifier: 10.1021/acsphotonics.9b00734
Volume: 6 Issue: 12 First Page #: 3039
Date Submitted: 7/26/20 12:00AM Date Published: 12/1/19 5:00AM
Publication Location:
Article Title: Control of Physical and Chemical Processes with Nonlocal Metal–Dielectric Environments
Authors: Vanessa N. Peters, Srujana Prayakarao, Samantha R. Koutsares, Carl E. Bonner, Mikhail A. Noginov
Keywords: spontaneous emission, energy transfer, strong coupling
Abstract: In this Perspective, we make the case that (meta) material platforms that were originally designed to control the propagation of light can affect scores of physical and chemical phenomena, which are often thought to lie outside of the traditional electrodynamics domain. We show that nonlocal metal-dielectric environments, which can be as simple as metal?dielectric interfaces, can control spontaneous and stimulated emission, Förster energy transfer, wetting contact angle, and rates of chemical reactions. The affected phenomena can occur in both strong and weak coupling regimes and the large coupling strength seems to enhance the effects of nonlocal environments. This intriguing field of study has experienced a rapid growth over the past decade and many exciting discoveries and applications are expected in the years to come.
Distribution Statement: 2-Distribution Limited to U.S. Government agencies only; report contains proprietary info
Acknowledged Federal Support: **Y**

Publication Type: Journal Article Peer Reviewed: Y **Publication Status:** 1-Published
Journal: Journal of the Optical Society of America B
Publication Identifier Type: DOI Publication Identifier: 10.1364/JOSAB.376752
Volume: 37 Issue: 4 First Page #: 1065
Date Submitted: 7/26/20 12:00AM Date Published: 3/1/20 5:00AM
Publication Location:
Article Title: Low-loss volume modes in a lamellar hyperbolic metamaterial slab
Authors: S. R. Koutsares, E. K. Tanyi, S. J. Daniel, R. S. Savelev, M. Rahmani, D. Neshev, I. V. Shadrivov, M. A.
Keywords: low loss meta material
Abstract: We have studied, both theoretically and experimentally, the excitation of volume modes in a lamellar metal/dielectric metamaterial with hyperbolic dispersion. The highly efficient light penetration through tens of metamaterial layers is consistent with a relatively low propagation loss. The volume modes were found to be highly sensitive to the surface roughness of the layers, which can be a detrimental factor in device applications.
Distribution Statement: 2-Distribution Limited to U.S. Government agencies only; report contains proprietary info
Acknowledged Federal Support: **Y**

RPPR Final Report
as of 14-Mar-2023

Publication Type: Journal Article Peer Reviewed: Y **Publication Status:** 1-Published
Journal: Optics Letters
Publication Identifier Type: DOI Publication Identifier: 10.1364/OL.44.004199
Volume: 44 Issue: 17 First Page #: 4199
Date Submitted: 7/27/20 12:00AM Date Published: 8/1/19 4:00AM
Publication Location:
Article Title: Ultra-sensitive plasmonic sensing based on gold nanostrip arrays
Authors: T. Ronurpraful, N. Jerop, N. Noginova
Keywords: plasmic sensor
Abstract: The extra-narrow reflection feature in angular dependence of reflectivity of periodic gold nanostrip arrays presents interest for sensing application. We explore its behavior in a modified dielectric environment and characterize the capability for sensing small changes in the dielectric permittivity of the environment.
Distribution Statement: 2-Distribution Limited to U.S. Government agencies only; report contains proprietary info
Acknowledged Federal Support: **Y**

Publication Type: Journal Article Peer Reviewed: Y **Publication Status:** 1-Published
Journal: New Journal of Physics
Publication Identifier Type: DOI Publication Identifier: 10.1088/1367-2630/ab7d7c
Volume: 22 Issue: 4 First Page #: 043002
Date Submitted: 7/27/20 12:00AM Date Published: 4/1/20 4:00AM
Publication Location:
Article Title: Plasmon drag effect with sharp polarity switching
Authors: T Ronurpraful, D Keene, N Noginova
Keywords: plasmon drag effect
Abstract: The generation of significant photocurrents observed in plasmonic metasurfaces is interesting from a fundamental point of view and promising for applications in plasmon-based electronics and plasmonic sensors with compact electrical detection. We show that photoinduced voltages in strongly modulated plasmonic surfaces demonstrate a highly asymmetric angular dependence with polarity switching around the plasmon resonance conditions. The effects are tentatively attributed to coupling between localized and propagating plasmons.
Distribution Statement: 2-Distribution Limited to U.S. Government agencies only; report contains proprietary info
Acknowledged Federal Support: **Y**

Publication Type: Journal Article Peer Reviewed: Y **Publication Status:** 1-Published
Journal: Scientific Reports
Publication Identifier Type: DOI Publication Identifier: 10.1038/s41598-021-81128-4
Volume: 11 Issue: 1 First Page #:
Date Submitted: 8/9/21 12:00AM Date Published: 7/21/21 4:00AM
Publication Location:
Article Title: Nanoporous gold nanoleaf as tunable metamaterial
Authors: Sangeeta Rout, Zhen Qi, Monika M. Biener, Devon Courtwright, Jakeem C. Adrien, Ezekiel Mills, Mohar
Keywords: Metamaterials, Composite Materials
Abstract: We have studied optical properties of single-layer and multi-fold nanoporous gold leaf (NPGL) metamaterials and observed highly unusual transmission spectra composed of two well-resolved peaks. We explain this phenomenon in terms of a surface plasmon absorption band positioned on the top of a broader transmission band, the latter being characteristic of both homogeneous “solid” and inhomogeneous “diluted” Au films. The transmission spectra of NPGL metamaterials were shown to be controlled by external dielectric environments, e.g. water and applied voltage in an electrochemical cell. This paves the road to numerous functionalities of the studied tunable and active metamaterials, including control of spontaneous emission, energy transfer and many others.
Distribution Statement: 2-Distribution Limited to U.S. Government agencies only; report contains proprietary info
Acknowledged Federal Support: **Y**

RPPR Final Report
as of 14-Mar-2023

Publication Type: Journal Article Peer Reviewed: Y **Publication Status:** 1-Published
Journal: Journal of Nanophotonics
Publication Identifier Type: DOI Publication Identifier: 10.1117/1.JNP.15.026002
Volume: 15 Issue: 02 First Page #:
Date Submitted: 8/9/21 12:00AM Date Published: 5/1/21 8:00AM
Publication Location:
Article Title: Effect of flexural stress on fabrication and optical properties of a composite photonic material
Authors: Devon Courtwright, Sangeeta Rout, Jakeem Adrien, Mikhail A. Noginov
Keywords: Metamaterials, Composite Materials
Abstract: We spin coated thin films of PMMA polymer doped with HITC laser dye onto microscope cover slides under applied flexural stress and found the patterns of scattering (milkiness) to correlate with the spatial variation of the pressure pattern. We further deposited thin gold films on top of the HITC:PMMA films and measured highly unusual transmission spectra of Au collected from strongly deformed (stressed) local areas of the sample. These spectra, which strongly deferred from those of plain Au films deposited onto unstressed glass, could not be described by simple, e.g. Maxwell Garnett, effective media models, calling for a thorough theoretical study.
Distribution Statement: 2-Distribution Limited to U.S. Government agencies only; report contains proprietary info
Acknowledged Federal Support: **Y**

Publication Type: Journal Article Peer Reviewed: Y **Publication Status:** 1-Published
Journal: Nanomaterials
Publication Identifier Type: DOI Publication Identifier: 10.3390/nano10112135
Volume: 10 Issue: 11 First Page #: 2135
Date Submitted: 8/9/21 12:00AM Date Published: 10/1/20 4:00AM
Publication Location:
Article Title: Effect of Random Nanostructured Metallic Environments on Spontaneous Emission of HITC Dye
Authors: Sangeeta Rout, Zhen Qi, Ludvig S. Petrosyan, Tigran V. Shahbazyan, Monika M. Biener, Carl E. Bonne
Keywords: Au nanofoams; concentration quenching; emission kinetics; energy transfer
Abstract: We have studied emission kinetics of HITC laser dye on top of glass, smooth Au films, and randomly structured porous Au nanofoams. The observed concentration quenching of luminescence of highly concentrated dye on top of glass (energy transfer to acceptors) and the inhibition of the concentration quenching in vicinity of smooth Au films were in accord with our recent findings. Intriguingly, the emission kinetics recorded in different local spots of the Au nanofoam samples had a spread of the decay rates, which was large at low dye concentrations and became narrower with increase of the dye concentration. We infer that in different subvolumes of Au nanofoams, HITC molecules are coupled to the nanofoams weaker or stronger. The inhibition of the concentration quenching in Au nanofoams was stronger than on top of smooth Au films. This was true for all weakly and strongly coupled subvolumes contributing to the spread of the emission kinetics.
Distribution Statement: 2-Distribution Limited to U.S. Government agencies only; report contains proprietary info
Acknowledged Federal Support: **Y**

Publication Type: Journal Article Peer Reviewed: Y **Publication Status:** 1-Published
Journal: Applied Physics Letters
Publication Identifier Type: DOI Publication Identifier: 10.1063/5.0051901
Volume: 119 Issue: 3 First Page #: 031102
Date Submitted: 8/9/21 12:00AM Date Published: 7/1/21 4:00AM
Publication Location:
Article Title: Stimulated emission in vicinity of the critical angle
Authors: Joshua K. Asane, Md G. R. Chowdhury, Kanij M. Khabir, Viktor A. Podolskiy, Mikhail A. Noginov
Keywords: Stimulated emission, miniature lasers, critical angle
Abstract: We have demonstrated amplified spontaneous emission (ASE) propagating at the planar interface between two adjacent dielectrics with slightly different refractive indexes. This emission originates from the leaky mode, fueled by optical gain in the low-index dielectric, is outcoupled to the high-index dielectric in vicinity of the critical angle for total internal reflection. This led us to observation of spectacular concentric rings of ASE emission occurring above the low and soft stimulated emission threshold. The results of our study can be used to develop novel miniature low-threshold stimulated emission sources and photonic circuits operating at optical frequencies.
Distribution Statement: 2-Distribution Limited to U.S. Government agencies only; report contains proprietary info
Acknowledged Federal Support: **Y**

RPPR Final Report
as of 14-Mar-2023

Publication Type: Journal Article Peer Reviewed: Y **Publication Status:** 1-Published
Journal: Laser & Photonics Reviews
Publication Identifier Type: DOI Publication Identifier: 10.1002/lpor.202000250
Volume: 15 Issue: 3 First Page #: 2000250
Date Submitted: 8/9/21 12:00AM Date Published: 2/1/21 5:00AM
Publication Location:
Article Title: How do the Purcell factor the Q-factor and the beta factor affect the laser threshold
Authors: Jacob B. Khurgin, Mikhail A. Noginov
Keywords: Purcell factor, Q-factor, beta factor
Abstract: As lasers get more and more miniaturized and their dimensions become comparable to the wavelength, two interconnected phenomena take place: the fraction of spontaneous radiation going into a specific laser mode (?-factor) increases and can ultimately reach unity, while the radiative lifetime gets shortened by the Purcell factor Fp. Often it is assumed that increase of these two factors, along with the quality factor (Q-factor), almost invariably causes reduction of the lasing threshold. This assumption is tested on various photonic and plasmonic lasers, demonstrating that, while there is obvious correlation between the aforementioned factors and the laser threshold, the dependence is far from being straightforward and omnipresent. Depending on specific laser material and geometry, the threshold can decrease, increase, or stay unchanged when ?-factor, Q-factor, and Fp increase. For the most part, the reduction of threshold is achieved simply by reducing the laser volume and this volume
Distribution Statement: 2-Distribution Limited to U.S. Government agencies only; report contains proprietary info
Acknowledged Federal Support: **Y**

Publication Type: Journal Article Peer Reviewed: Y **Publication Status:** 1-Published
Journal: Journal of the Optical Society of America B
Publication Identifier Type: DOI Publication Identifier: 10.1364/JOSAB.399318
Volume: 37 Issue: 10 First Page #: 3108
Date Submitted: 8/9/21 12:00AM Date Published: 9/1/20 4:00AM
Publication Location:
Article Title: Concentration dependence of two-photon absorption in PMMA polymeric films doped with rhodamine laser dyes
Authors: J. K. Asane, M. A. Noginov
Keywords: Chi(3) nonlinearity; rhodamine laser dyes
Abstract: We have studied poly(methyl methacrylate) (PMMA) films doped with rhodamine 6G and rhodamine B laser dyes as potential nonlinear material components for nanophotonics. For both dyes, the optimal concentrations, at which the emission excited via the two-photon-absorption (TPA) process is maximized, have been determined. Despite relatively large values of TPA cross sections obtained in this study, the characteristic pumping densities needed to observe pronounced nonlinear effects substantially exceed the laser damage threshold for Au or alternative plasmonic materials. This makes the studied laser dyes unsuitable for some of the intended nanophotonics applications.
Distribution Statement: 2-Distribution Limited to U.S. Government agencies only; report contains proprietary info
Acknowledged Federal Support: **Y**

RPPR Final Report
as of 14-Mar-2023

Publication Type: Journal Article Peer Reviewed: Y **Publication Status:** 1-Published
Journal: Journal of the Optical Society of America B
Publication Identifier Type: DOI Publication Identifier: 10.1364/JOSAB.403612
Volume: 37 Issue: 11 First Page #: 3200
Date Submitted: 8/9/21 12:00AM Date Published: 10/1/20 4:00AM
Publication Location:
Article Title: Emission of R6G dye in Fabry–Perot cavities in weak and strong coupling regimes
Authors: Md Omar Faruk, Nelly Jerop, Mikhail A. Noginov
Keywords: Strong coupling; cavity dispersion
Abstract: We have studied spectra and angular distribution of emission in Fabry–Perot cavities formed by two silver mirrors separated by a layer of poly (methyl methacrylate) polymer doped with rhodamine 6G (R6G) dye in low (20 g=l) and high (200 g=l) concentrations. The frequency of emission radiated to a cavity mode was larger at large outcoupling angles—the “rainbow” effect.At the same time, the angle of the strongest emission was also determined by the cavity size: the larger the cavity, the larger the angle. The angular distribution of emission is commonly dominated by two symmetrical lobes (located at the intersection of the three-dimensional emission cone with a horizontal plane) pointing to the left and to the right of the normal to the sample.Despite the strong Stokes shift in R6G dye, the branch of the cavity dispersion curve obtained in the emission experiment is positioned above the one obtained in the reflection (extinction) experiment.
Distribution Statement: 2-Distribution Limited to U.S. Government agencies only; report contains proprietary info
Acknowledged Federal Support: **Y**

Publication Type: Journal Article Peer Reviewed: Y **Publication Status:** 1-Published
Journal: Journal of the Optical Society of America B
Publication Identifier Type: DOI Publication Identifier: 10.1364/JOSAB.409998
Volume: 38 Issue: 1 First Page #: 88
Date Submitted: 8/9/21 12:00AM Date Published: 12/1/20 5:00AM
Publication Location:
Article Title: Effect of metallic substrates and cavities on emission kinetics of dye-doped polymeric films
Authors: S. Koutsares, L. S. Petrosyan, S. Prayakarao, D. Courtwright, C. E. Bonner, T. V. Shahbazyan, M. A. N
Keywords: Energy transfer, concentration quenching, Fabry-Perot cavity
Abstract: We have studied emission kinetics in dye-doped polymeric films (HITC:PMMA), deposited on top of glass and silver and embedded in Fabry-Perot cavities (Metal-Insulator-Metal waveguides). For highly doped films on glass, we observed strong concentration quenching, as evidenced by a dramatic shortening of the emission kinetics, consistent with our previous studies. However, for the same dye-doped films on top of silver, slower emission kinetics were observed despite the high decay rates of individual dye molecules near the metallic surface. The concentration quenching rates in Fabry-Perot cavities were nearly identical to those of HITC:PMMA films deposited on top of silver. These findings are explained within a theoretical model for the inhibition of Förster Energy Transfer near a metallic surface. Furthermore, the emission kinetics of the dye-doped films on top of silver were approximately single exponential – consistent with the strong coupling of excited molecules with propagating SPPs
Distribution Statement: 2-Distribution Limited to U.S. Government agencies only; report contains proprietary info
Acknowledged Federal Support: **Y**

RPPR Final Report
as of 14-Mar-2023

Publication Type: Journal Article Peer Reviewed: Y **Publication Status:** 1-Published
Journal: Applied Magnetic Resonance
Publication Identifier Type: DOI Publication Identifier: 10.1007/s00723-021-01347-w
Volume: 52 Issue: 7 First Page #: 749
Date Submitted: 8/11/21 12:00AM Date Published: 6/1/21 4:00AM
Publication Location:
Article Title: Ferromagnetic Resonance in Permalloy Metasurfaces
Authors: N. Noginova, V. Gubanov, M. Shahabuddin, Yu. Gubanova, S. Nesbit, V. V. Demidov, V. A. Atsarkin, E.
Keywords: Ferromagnetic Resonance, Permalloy, Metasurfaces
Abstract: The transition from para- to ferromagnetic behavior in magnetic systems can be considered to be a part of a general problem of the transition from quantum (oneparticle) to classical (multiple-particle) behavior. Here we present a brief review of recent studies in electron magnetic resonance (EMR) and spin relaxation in situations which are at the borderline between paramagnetic and ferromagnetic cases. Most attention is paid to EMR in magnetic nanoparticles. It is shown that the giant spin model based on the quantum spin Hamiltonian can be successively applied for interpretation of the specific features observed in the experiment, such as a narrow spectral component and “forbidden” half-field resonances. Another example is the transformation of the level anticrossing typical for anisotropic EPR spectra of paramagnetic ions into the magnetic pseudoresonance (which manifests itself as a giant peak of radio-frequency absorption) observed in ferromagnets with axial anisotropy.
Distribution Statement: 2-Distribution Limited to U.S. Government agencies only; report contains proprietary info
Acknowledged Federal Support: **Y**

Publication Type: Journal Article Peer Reviewed: Y **Publication Status:** 1-Published
Journal: Applied Magnetic Resonance
Publication Identifier Type: DOI Publication Identifier: 10.1007/s00723-020-01213-1
Volume: 51 Issue: 11 First Page #: 1467
Date Submitted: 8/11/21 12:00AM Date Published: 8/1/20 4:00AM
Publication Location:
Article Title: Electron Spin Resonance on the Border Between Para- and Ferromagnetism: Quantum versus Classical
Authors: V. A. Atsarkin, N. Noginova
Keywords: Electron Spin Resonance, Paramagnetism, Ferromagnetism
Abstract: The transition from para- to ferromagnetic behavior in magnetic systems can be considered to be a part of a general problem of the transition from quantum (oneparticle) to classical (multiple-particle) behavior. Here we present a brief review of recent studies in electron magnetic resonance (EMR) and spin relaxation in situations which are at the borderline between paramagnetic and ferromagnetic cases. Most attention is paid to EMR in magnetic nanoparticles. It is shown that the giant spin model based on the quantum spin Hamiltonian can be successively applied for interpretation of the specific features observed in the experiment, such as a narrow spectral component and “forbidden” half-field resonances. Another example is the transformation of the level anticrossing typical for anisotropic EPR spectra of paramagnetic ions into the magnetic pseudoresonance (which manifests itself as a giant peak of radio-frequency absorption) observed in ferromagnets with axial anisotropy.
Distribution Statement: 2-Distribution Limited to U.S. Government agencies only; report contains proprietary info
Acknowledged Federal Support: **Y**

RPPR Final Report
as of 14-Mar-2023

Publication Type: Journal Article Peer Reviewed: Y **Publication Status:** 1-Published
Journal: Journal of the Optical Society of America B
Publication Identifier Type: DOI Publication Identifier: 10.1364/JOSAB.419818
Volume: 38 Issue: 6 First Page #: 2012
Date Submitted: 8/11/21 12:00AM Date Published: 6/1/21 4:00AM
Publication Location:
Article Title: Magnetically dependent plasmon drag in permalloy structures
Authors: Mohammad Shahabuddin, David W. Keene, Maxim Durach, Vladimir S. Posvyanskii, Vadim A. Atsarkin,
Keywords: Plasmon drag, permalloy
Abstract: Significant photovoltages are observed in permalloy grating-like structures in response to pulsed laser light illumination. Electrical signals are enhanced at plasmon resonance conditions and show a clear dependence on the magnetic field with a characteristic hysteresis. Estimations show that the effect could not be explained solely by laser-induced heating. Alternative mechanisms are discussed.
Distribution Statement: 2-Distribution Limited to U.S. Government agencies only; report contains proprietary info
Acknowledged Federal Support: **Y**

Publication Type: Journal Article Peer Reviewed: Y **Publication Status:** 1-Published
Journal: Journal of Physics D: Applied Physics
Publication Identifier Type: DOI Publication Identifier: 10.1088/1361-6463/abba93
Volume: 54 Issue: 3 First Page #: 035307
Date Submitted: 8/11/21 12:00AM Date Published: 1/1/21 5:00AM
Publication Location:
Article Title: Extreme sensitivity of plasmon drag to surface modification
Authors: T Ronurpraful, N Jerop, A Koech, K Thompson, N Noginova
Keywords: Plasmon drag, sensor
Abstract: Giant enhancement of photocurrents in plasmonic structures (plasmon drag effect) provides opportunities for compact electric monitoring of plasmonic effects, and thus is promising for plasmonic-based sensing applications. In the experiment, we measure photoinduced electric signals in flat and profile-modulated systems, and test their sensitivity to small changes of the local dielectric environment, such as a presence of Langmuir–Blodgett monolayers at the metal surface. We show that the addition of a stearic acid monolayer leading to a small shift in plasmon resonance conditions can be ultimately resolved with electrical measurements as the switching in the photovoltage polarity.
Distribution Statement: 2-Distribution Limited to U.S. Government agencies only; report contains proprietary info
Acknowledged Federal Support: **Y**

Publication Type: Journal Article Peer Reviewed: Y **Publication Status:** 1-Published
Journal: Scientific Reports
Publication Identifier Type: DOI Publication Identifier: 10.1038/s41598-022-23243-4
Volume: 12 Issue: 1 First Page #:
Date Submitted: 11/27/22 12:00AM Date Published: 11/1/22 4:00AM
Publication Location:
Article Title: Effect of metal/dielectric substrates on photopolymerization of BITh thin films
Authors: L. Hesami, C. Yang, E. Anwar, N. Noginova, M. A. Noginov
Keywords: Light-Matter Interaction, Photopolymerization
Abstract: We have studied effects of metal–dielectric substrates on photopolymerization of [2,2?-Bi-1H-indene] -1,1?-dione-3,3?-diyl diheptanoate (BITh) monomer. We synthetized BITh and spin-coated it onto a variety of dielectric, metallic, and metal–dielectric substrates. The films were exposed to radiation of a UV–Visible Xe lamp, causing photo-polymerization of monomer molecules. The magnitude and the rate of the photo-polymerization were monitored by measuring the strength of the?~?480 nm absorption band, which existed in the monomer but not in the polymer. Expectedly, the rate of photo-polymerization changed nearly linearly with the change of the pumping intensity. In contrast with our early study of photo-degradation of semiconducting polymer P3HT, the rate of photo-polymerization of BITh is getting modestly higher if the monomer film is deposited on top of silver separated from the monomer by a thin insulating MgF2 layer preventing a charge transfer.
Distribution Statement: 1-Approved for public release; distribution is unlimited.
Acknowledged Federal Support: **Y**

RPPR Final Report
as of 14-Mar-2023

Publication Type: Journal Article Peer Reviewed: Y **Publication Status:** 1-Published
Journal: Chirality
Publication Identifier Type: DOI Publication Identifier: 10.1002/chir.23509
Volume: 34 Issue: 12 First Page #: 1503
Date Submitted: 11/27/22 12:00AM Date Published: 10/1/22 4:00AM
Publication Location:
Article Title: Hydrothermal synthesis of chiral carbon dots
Authors: Anastasia Visheratina, Leila Hesami, Ashleigh K. Wilson, Nicole Baalbaki, Natalia Noginova, Mikhail A. I
Keywords: Chirality, quantum dots, carbon
Abstract: Nanocolloids that are cumulatively referred to as nanocarbons, attracted significant attention during the last decade because of facile synthesis methods, water solubility, tunable photoluminescence, easy surface modification, and high biocompatibility. Among the latest development in this reserach area are chiral nanocarbons exemplified by chiral carbon dots (CDots). They are expected to have applications in sensing, catalysis, imaging, and nanomedicine. However, the current methods of CDots synthesis show often contradictory chemical/optical properties and structural information that required a systematic study with careful structural evaluation. Here, we investigate and optimize chiroptical activity and photoluminescence of L- and D-CDots obtained by hydrothermal carbonization of L- and D-cysteine, respectively. Nuclear magnetic resonance spectroscopy demonstrates that they are formed via gradual dehydrogenation and condensation reactions of the starting amino acid.
Distribution Statement: 1-Approved for public release; distribution is unlimited.
Acknowledged Federal Support: **Y**

Publication Type: Journal Article Peer Reviewed: Y **Publication Status:** 1-Published
Journal: ACS Omega
Publication Identifier Type: DOI Publication Identifier: 10.1021/acsomega.1c03794
Volume: 6 Issue: 50 First Page #: 34294
Date Submitted: 11/27/22 12:00AM Date Published: 12/1/21 5:00AM
Publication Location:
Article Title: Probing Charge Transport Kinetics in a Plasmonic Environment with Cyclic Voltammetry
Authors: Mohammad Shahabuddin, Ashleigh K. Wilson, Ashah C. Koech, Natalia Noginova
Keywords: charge transport, plasmonic environment, electrochemical reaction
Abstract: Possible modifications in electrochemical reaction kinetics are explored in a nanostructured plasmonic environment with and without additional light illumination using a cyclic voltammetry (CV) method. In nanostructured gold, the effect of light on anodic and cathodic currents is much pronounced than that in a flat system. The electron-transfer rate shows a 3-fold increase under photoexcitation. The findings indicate a possibility of using plasmonic excitations for controlling electrochemical reactions.
Distribution Statement: 1-Approved for public release; distribution is unlimited.
Acknowledged Federal Support: **Y**

CONFERENCE PAPERS:

Publication Type: Conference Paper or Presentation **Publication Status:** 1-Published
Conference Name: CLEO: QELS_Fundamental Science
Date Received: 12-Sep-2019 Conference Date: 10-May-2019 Date Published: 10-May-2019
Conference Location: San Jose, California
Paper Title: Development of Near-Infrared Rare Earth Doped Organic Materials for Nanophotonics Applications
Authors: J. K. Asane, A. Bullock, M. Clemmons, N. Noginova, M. A. Noginov
Acknowledged Federal Support: **Y**

RPPR Final Report
as of 14-Mar-2023

Publication Type: Conference Paper or Presentation **Publication Status:** 1-Published
Conference Name: Conference on Lasers and Electro-Optics
Date Received: 12-Sep-2019 Conference Date: 10-May-2019 Date Published: 10-May-2019
Conference Location: San Jose, CA, USA
Paper Title: Light-Matter Interaction in Disordered Metal-Dielectric Environments
Authors: S. Rout, M. Biener, Z. Qi, C. E. Bonner, T. V. Shahbazyan, and M. A. Noginov
Acknowledged Federal Support: **Y**

Publication Type: Conference Paper or Presentation **Publication Status:** 1-Published
Conference Name: Conference on Lasers and Electro-Optics
Date Received: 11-Sep-2019 Conference Date: 10-May-2019 Date Published: 10-May-2019
Conference Location: San Jose, CA, US_A
Paper Title: Effect of Fabry-Perot Cavities on Concentration Quenching
Authors: S. Koutsares, S. Prayakarao, D. Courtwright, C. E. Bonner, and M. A. Noginov
Acknowledged Federal Support: **Y**

Publication Type: Conference Paper or Presentation **Publication Status:** 1-Published
Conference Name: Conference on Lasers and Electro-Optics
Date Received: 09-Aug-2021 Conference Date: 11-May-2020 Date Published:
Conference Location: Washington, DC
Paper Title: Control of Concentration Quenching with Metallic Substrates and Cavities
Authors: S. R. Koutsares, L. S. Petrosyan, D. Courtwright, S. Prayakarao, C. E. Bonner, T. V. Shahbazyan, M. A.
Acknowledged Federal Support: **Y**

Publication Type: Conference Paper or Presentation **Publication Status:** 1-Published
Conference Name: Conference on Lasers and Electro-Optics
Date Received: 26-Jul-2020 Conference Date: 11-May-2020 Date Published:
Conference Location: Washington, DC
Paper Title: Emission in Fabry-Perot Cavities in Weak and Strong Coupling Regimes
Authors: Md Omar Faruk, Nelly Jerop, Mikhail A. Noginov
Acknowledged Federal Support: **Y**

Publication Type: Conference Paper or Presentation **Publication Status:** 1-Published
Conference Name: Conference on Lasers and Electro-Optics
Date Received: 26-Jul-2020 Conference Date: 11-Sep-2019 Date Published:
Conference Location: Washigton, DC
Paper Title: Nanoporous Gold Nanoleaf as Tunable Metamaterial
Authors: S. Rout, Z. Qi, M. Biener, D. Courtwright, J. Adrien, M. Shahabuddin, C. E. Bonner, N. Noginova, M. A. I
Acknowledged Federal Support: **Y**

Publication Type: Conference Paper or Presentation **Publication Status:** 1-Published
Conference Name: Metamaterials, Metadevices, and Metasystems 2019
Date Received: 27-Jul-2020 Conference Date: 11-Aug-2019 Date Published:
Conference Location: San Diego, United States
Paper Title: Plasmon related electrical effects in strongly modulated metasurfaces
Authors: D. Keene. T. Ronurpraful, N. Nogniova
Acknowledged Federal Support: **Y**

Publication Type: Conference Paper or Presentation **Publication Status:** 1-Published
Conference Name: Conference on Lasers and Electro-Optics
Date Received: 27-Jul-2020 Conference Date: 11-May-2020 Date Published:
Conference Location: Washington, DC
Paper Title: Extreme sensitivity of plasmon drag to surface modification
Authors: T. Ronurpraful, N. Jerop, N. Noginova
Acknowledged Federal Support: **Y**

Publication Type: Conference Paper or Presentation **Publication Status:** 1-Published
Conference Name: Conference on Lasers and Electro-Optics
Date Received: 27-Jul-2020 Conference Date: 11-May-2020 Date Published:
Conference Location: Washington, DC
Paper Title: Magneto-dependent plasmon drag in permalloy structures
Authors: M. Shahabuddin, D. Keene, N. Noginova
Acknowledged Federal Support: **Y**

Publication Type: Conference Paper or Presentation **Publication Status:** 1-Published
Conference Name: CLEO Conference
Date Received: 10-Aug-2021 Conference Date: 09-May-2021 Date Published: 09-May-2021
Conference Location: Virtual
Paper Title: Effect of thickness of a dye-doped polymeric film on the concentration quenching of luminescence
Authors: Sangeeta Rout, S. R. Koutsares, D. Courtwright, E. Mills, A. Shorter, S. Prayakarao, C. E. Bonner, M. A
Acknowledged Federal Support: **Y**

Publication Type: Conference Paper or Presentation **Publication Status:** 1-Published
Conference Name: CLEO Conference
Date Received: 10-Aug-2021 Conference Date: 09-May-2021 Date Published:
Conference Location: Virtual
Paper Title: Stimulated Emission with Evanescent Gain in the Total Internal Reflection Geometry
Authors: J. K. Asane, Md G. R. Chowdhury, K. M. Khabir, V. A. Podolskiy, M. A. Noginov
Acknowledged Federal Support: **Y**

Publication Type: Conference Paper or Presentation **Publication Status:** 1-Published
Conference Name: Metamaterials, Metadevices, and Metasystems 2022
Date Received: 27-Nov-2022 Conference Date: 21-Aug-2022 Date Published: 03-Oct-2022
Conference Location: San Diego, United States
Paper Title: Effect of electrochromic polymer switching on surface plasmon polaritons
Authors: Ashleigh K Wilson, Paula Fortuno, Mohammad Shahabuddin, Natalia Noginova
Acknowledged Federal Support: **Y**

PATENTS:

Intellectual Property Type: Patent Date Received: **27-Nov-2022**
Patent Title: SYSTEM AND METHOD FOR PLASMONIC CONTROL OF SHORT PULSES IN OPTICAL FIBERS
Patent Abstract:
Patent Number: 10756503
Patent Country: USA
Application Date: 17-Jul-2018 Application Status: 3

RPPR Final Report
as of 14-Mar-2023

Date Issued: 25-Aug-2020

Intellectual Property Type: Patent Date Received: **27-Nov-2022**
Patent Title: SYSTEM AND METHOD FOR PLASMONIC CONTROL OF SHORT PULSES IN OPTICAL FIBERS
Patent Abstract:
Patent Number: US11374378B2
Patent Country: USA
Application Date: 21-Aug-2020 Application Status: 3
Date Issued: 28-Jun-2022

Partners

,

I certify that the information in the report is complete and accurate:
Signature: Mikhail A. Noginov
Signature Date: 12/13/22 6:53PM

Control of Organic Matter with Strong Coupling

W911NF1810472

Final Report

Sept. 29, 2018 – Sept. 28, 2022

P.I.: Mikhail A. Noginov (Norfolk State University)

Co-P.I.: Natalia Noginova (Norfolk State University)

Program Manager: Dr. Kenneth Caster (AFOSR)

Technical Report

Abstract

Scores of physical phenomena, including light emission, donor-acceptor energy transfer, wetting and chemical reactions, can be strongly modified in the vicinity of metamaterials (rationally designed metal-dielectric composites) and other non-local dielectric environments. They, arguably, occur in the weak coupling regime of light-matter interaction, when the rates of the processes are affected, while the energy states of the interacting systems remain intact. Despite the richness of physical phenomena enabled by the weak coupling, an even greater control of light-matter interactions can be achieved in the strong coupling regime (of e.g. excitons in molecular ensembles and resonant cavities), when the eigen-energies of interacting states differ significantly (by ~1 eV!) from those of individual not interacting constituents. We argue that such a strong change of the energy eigenvalues may constitute creation of a new hybridized matter, with greatly modified quantum mechanical wave-functions, spectroscopic properties, dispersion, surface potentials, electron transport and pathways of chemical reactions. Our studies of weak and strong coupling phenomena revealed that we just scratched the surface of the complex multi-faceted problem and, while providing for some answers, uncovered an even larger number of intriguing questions (below) to be answered in the this research program. (1) Where is the crossover of the classical and quantum regimes of a strong coupling? (2) Can two types of molecules form a new coherent state (coherent matter) enabled by their strong coupling with a cavity? (3) Why chemical reactions and the energy transfer are always inhibited on top of metal/dielectric substrates? Can rationally designed dielectric environments accelerate these processes? (4) Does the strong coupling exist in the absence of photons and can this effect be observed experimentally? (5) Can the strong coupling control magnetoresistivity in organic semiconductors? (6) Can a strong coupling occur in random inhomogeneous composite media? The understanding of these phenomena is to lead to development of advanced organic and polymeric materials for future U.S. Air Force applications. Student development was among the major goals of this project. While two graduate students were planned to be recruited and trained in the proposed research program, a much larger number of students, including underrepresented minorities, benefited from the project through participation in research and professional development activities.

Part 1

Sept. 29, 2018 – July 31, 2019.

Organization of the Part 1 Technical Report and the Record of Achievements

This research was partly inspired by the preliminary results obtained under the previous AFOSR grant (FA9550-14-1-0221). In the first year of this project (W911NF1810472), three such studies, initiated two years ago, have been finalized and published. Thus, in the paper "Effect of metal–dielectric substrates on chemiluminescence kinetics", we demonstratd the effect of strong coupling on photodegradation of the semiconducting polymer P3HT [1]. In the second publication, entitled "Effect of metal–dielectric substrates on chemiluminescence kinetics", we have shown that non-local metal-dielectric environments can control the rate of a chemiluminescence reaction [2]. In the third study,"Enhancement of Electrochromic Polymer Switching in Plasmonic Nanostructured Environment" , which was almost entirely supported by the this research grant, we have studied fast electrochromic switching of polyaniline deposited on nanostructured plasmonic gold substrates [3]. These three tasks are highlighted in Part I of this technical report. The two particular projects groupped together in Part II of this report include (i) Search for correlation between electrical conductivity of P3HT polymer and its coupling with the Fabry-Perot cavity [4] and (ii) The effect of a strong coupling involving the lowest excited state of a dye molecule on the spectroscopic properties of the second excited state [5]. In Part III of the report, we combined two of our recent studies of enhancement and control of spontaneous emission in dye-doped polymers with resonant (nanodisks [6]) and non-resonant cavities (metal-dielectric-metal waveguides [7]).

Major Publications

[1] V. N. Peters, Md Omar Faruk, J. Asane, R. Alexander, D. A. Peters, S. Prayakarao, S. Rout, M. A. Noginov, "Effect of Strong Coupling on Photodegradation of the Semiconducting Polymer P3HT", Optica 6, 318-325 (2019).

[2] V. N. Peters, C. Yang, S. Prayakarao, and M. A. Noginov, "Effect of metal–dielectric substrates on chemiluminescence kinetics", Journal of the Optical Society of America B, 36, E132-E138 (2019).

[3] M. Shahabuddin, T. McDowell, C. E. Bonner, N. Noginova, "Enhancement of Electrochromic Polymer Switching in Plasmonic Nanostructured Environment", ACS Applied Nano Materials 2, 1713-1719 (2019).

[4] Joshua Kwame Asane, Vanessa Nicole Peters, Rohan Alexander, Tylisia Wallace, D'Angelo Peters, Mikhail A. Noginov, "Study of electrical conductivity of the poly(3 hexylthiophene-2, 5-diyl) polymer in resonant Fabry–Perot cavities," J. Nanophoton. 13(2), 026007 (2019).

[5] E. K. Tanyi, E. Harrison, C. On, M. A. Noginov, "Coupling of the First and Second Excited States of R6G Dye with the Fabry–Perot Cavity", Physica Status Solidi B, 256 (3), 1800045 (2019).

[6] A. Vaskin, S. Mashhadi, M. Steinert, K. E. Chong, D. Keene, S. Nanz, A. Abass, E. Rusak, D.-Y. Choi, I. Fernandez-Corbaton, T. Pertsch, C. Rockstuhl, M. A. Noginov, Y. S. Kivshar, D. N. Neshev, N. Noginova, and I. Staude, "Manipulation of Magnetic Dipole Emission from Eu3+ with Mie-Resonant Dielectric Metasurfaces", Nano Lett. (2019).

[7] Srujana Prayakarao, Deionjalei Miller, Devon Courtwright, Carl E. Bonner, and Mikhail A. Noginov, "Non-resonant enhancement of spontaneous emission of HITC dye in metal-insulator-metal waveguides," J. Opt. Soc. Am. B 36, 2312-2316 (2019).

Conference Presentations

[1] J. K. Asane, A. Bullock, M. Clemmons, N. Noginova, and M. A. Noginov, "Development of Near-Infrared Rare Earth Doped Organic Materials for Nanophotonics Applications," in Conference on Lasers and Electro-Optics, OSA Technical Digest (Optical Society of America, 2019), paper FTh4M.6.

[2] S. Koutsares, S. Prayakarao, D. Courtwright, C. E. Bonner, and M. A. Noginov, "Effect of Fabry-Perot Cavities on Concentration Quenching," in Conference on Lasers and Electro-Optics, OSA Technical Digest (Optical Society of America, 2019), paper JTh2A.20.

[3] S. Rout, M. Biener, Z. Qi, C. E. Bonner, T. V. Shahbazyan, and M. A. Noginov, "Light-Matter Interaction in Disordered Metal-Dielectric Environments," in Conference on Lasers and Electro-Optics, OSA Technical Digest (Optical Society of America, 2019), paper FTu3D.4.

PART I

1. Effect of Strong Coupling on Photodegradation of the Semiconducting Polymer P3HT

Photonic structures are commonly designed to manipulate scattered or emitted light. However, in recent years, they were demonstrated to affect a variety of phenomena, including chemical reactions, which lie outside the traditional electrodynamics domain. In this work, we have studied the effect of a Fabry–Perot cavity on the chemical reaction of practical importance—photodegradation of the semiconducting polymer 2,5-poly(3-hexylthiophene) (P3HT), which is the material of choice in organic photovoltaics. Experimentally, Fabry–Perot cavities, composed of two silver mirrors and filled with P3HT polymer, were photoexposed over tens of hours, and the concentration of the remaining thiophene rings (composing P3HT) was studied as a function of time. It has been found that in the regime of strong coupling with the cavity, characterized by one of the largest values of the Rabi splitting reported in the literature (1.0 eV), the normalized rate of photodegradation is reduced threefold, substantially larger than in the weak coupling regime reported in our recent study. This result adds to the toolbox of strong coupling phenomena and paves the road towards long-range control of chemical reactions and catalysis.

2. Effect of metal–dielectric substrates on chemiluminescence kinetics

We studied chemiluminescence of rhodamine 6G (R6G) dye in a series of R6G:DNPO:PMMA films deposited onto a variety of metallic, metal–dielectric, and dielectric substrates. We found that chemiluminescence kinetics on top of Ag and Au films covered by an insulating MgF2 layer had longer decay times than those on top of purely dielectric substrates, MgF2 films on glass. We infer that Ag- and Au-based substrates with an insulating MgF2 layer on top affected the reaction rates by influencing polarization energies of reactants and surrounding molecular dipoles. At the same time, the chemiluminescence kinetics on top of Ag and Au surfaces (without an insulating MgF2 spacer) were substantially shorter than those on top of dielectric substrates, probably because of conventional chemical catalysis. The peak emission intensities on top of metallic substrates (with and without the MgF2 layer on top) were lower than those on top of purely dielectric substrates, likely due to inhibition of the energy transfer to acceptors (R6G dye molecules) known in the vicinity of metals. The further reduction of

chemiluminescence intensity on top of lamellar metal–dielectric stacks could be due to preferential emission of light inside the volume of the metamaterial rather than outside.

3. Origin of Fast Electrochromic Switching of Polyaniline Deposited on Plasmonic Gold

Electrochromic materials show a reversible color change upon reduction or oxidation of the material by application of a small voltage. Polyaniline (PANI) is a promising material due to its high conductivity, high contrast in coloration change, low operation voltages, and long-term stability without degradation as compared to other conducting polymers. However, slow color switching, with the response time typically on the order of seconds [1], limits its use in modern applications. Recent research [2] points to a very interesting possibility of controlling PANI switching with plasmonic nanostructures. In particular, incorporation of PANI into metalic nanoslit arrays enables control of color with slit dimensions and demonstrates faster electrochromic switching. However, effects of plasmonic environment on charge transport and color switching of PANI are not yet fully studied and understood. The various factors associated with plasmonic environment can play a role, including modification of the photonic mode density, hot electron emission, interface charging or a combination of several factors.

In this study, based on the preliminary results obtained under the previous AFOSR grant funding (FA9550-14-1-0221), we explore oxidation/reduction reactions in PANI in plasmonic environment and compare the effects observed in thin PANI films deposited on gold nanomesh structures with those deposited on flat gold, Fig 1(a,b). The gold nanomesh substrates are fabricated by depositing of gold (40 nm thick) onto porous anodic alumina membranes with 30 and 100 nm-size pores, which produces highly nanostructured surface, Fig 1(b), featuring multiple localized plasmon resonances (observed in the reflection spectrum as a broad dip around λ = ~ 630 nm). PANI films of 40 nm thick are deposited on the substrates by electrochemical method. In the experiment (Fig 1(c)), we study changes in coloration as a response to applied potential in the circular voltammetry (CV) setup, simultaneously recording both electric current and the optical reflectivity (at λ = 633 nm) as the function of the voltage. As one can see, the voltage-current dependences (Fig. 1 (c)) and color switching behavior are significantly different in the nanomesh and flat gold structures. The films on nanostructured gold demonstrate much steeper changes in reflection with the increase in voltage than those on the flat gold (see Fig. 1 (d)). An interesting feature of the nanomesh systems is a small reflectivity peak observed around 0.2 V, which is not present in the flat gold.

In order to better understand the reverse behavior in the reflectivity curves observed at small voltages in nanostructured systems, a handheld camera was used to capture the image of the electrochromic cell with PANI/flat gold and PANI/nanomesh electrodes during the CV experiment. As one can see in Fig. 2 (a), PANI/flat gold system demonstrates the gradual coloration switching which is well expected. The PANI film is transparent and yellow at small voltages, and gradually changes to blue and dark. In contrast, the coloration behavior in PANI/nanomesh system is significantly different. With increasing the applied voltage from the color of the system changes respectively from brownish to yellow, light yellow, and then to brownish again, then a slight increment of potential turns the cell color into deep green, blue, violet and dark, Fig 2 (d). This reverse coloration behavior observed at small voltages in PANI/nanomesh is confirmed with the reflectance spectra recorded in the UV-Vis spectrophotometer setup. With the applied potential the gradual and monotonous coloration changes and a corresponding decrease in the reflection is observed for the flat gold structures, and the non-monotonous behavior and drastic changes in the coloration is observed for PANI with gold nanomesh (Figs. 2 (c) and (f)).

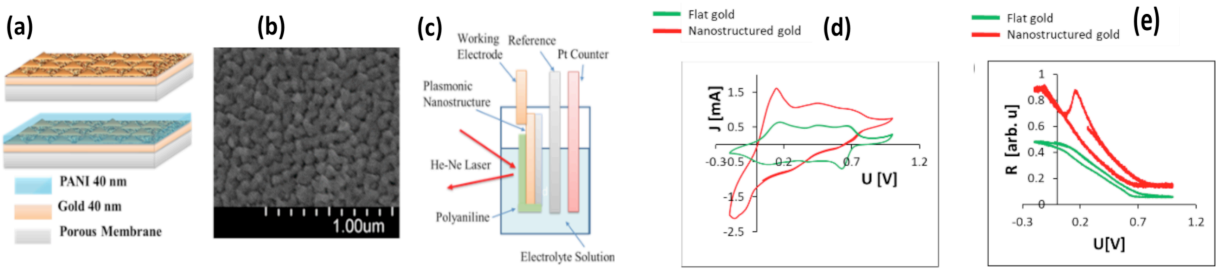

Fig. 1 (a) Schematic of sample; (b) SEM image of plasmonic nanostructure; (c) Experimental set up; (d) CV curves, (e) Reflectivity as the function of the voltage in flat and nanostructured samples.

Steeper color switching and saturation at moderate voltages observed in the nanostructured gold correlate with the results of Ref [2], where acceleration and strong contrast of PANI switching were observed in plasmonic cavities. Our results indicate that the modification of electrochemical switching is a general effect associated with plasmonic environment. Strongly asymmetric CV curves and unusual coloration behavior at low voltages observed in PANI/nanomesh systems is an intriguing finding. We believe that such a behavior can be related to the interface effects. According to [3, 4, 5] PANI is a p-type semiconductor with the work-function of 4.42 to 4.78 eV, which would form the Schottky contact with metal if its work function is lower than that. While in gold the work function is of 5.3 eV [6], in nanostructured gold it can be significantly lower. Values of 3.6 eV and 3.4 eV were reported in gold nanoparticles [7]. In this case, the barrier and a depletion layer in PANI are expected to form, slowing down the switching at low voltages and accelerating the switching at above threshold voltages. The possibility to control the interface effects and coloration behavior with nanostructuring can open new applications for photochromic polymers in electronics and optoelectronics. In addition, charging of the plasmonic nanofeatures can be controlled with an optical excitation at the frequency range of plasmon resonances [8]. The experiments with an additional optical illumination are underway.

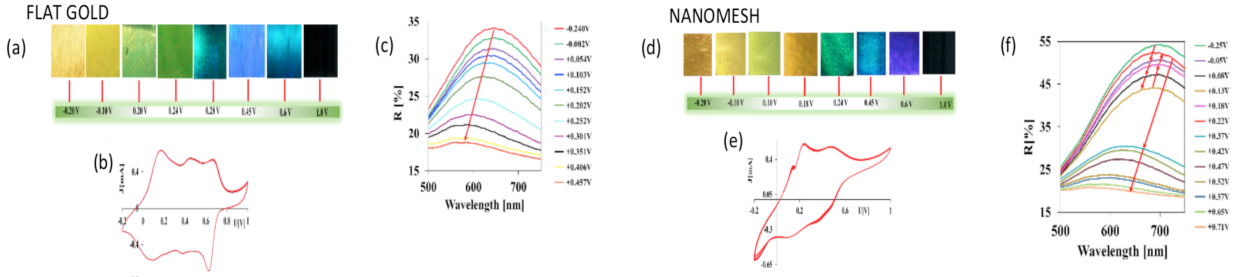

Fig. 2. Electrochromic experiment in (a-c) PANI/flat gold and (d-f) PANI/nanomesh systems. Change of coloration with applied potential (a, d); Corresponding CV curves (b, e) and; Reflection spectra at different voltages (c, f).

In conclusion, electrochromic polyaniline deposited on a gold nanomesh demonstrates high contrast colors, which can be electrochemically switched with applied potential. The switching behavior in nanostructured systems is significantly different than in PANI/flat gold structures, featuring the onset of steep changes in the coloration with increasing voltage above 0.15- 0.2 V, a presence of an additional peak in the voltage-current curves and reverse coloration behavior at small voltages. The effects are tentatively attributed to the interface effects. Further experiments will clarify the mechanism.

[1] Graham-Rowe, D. “Electronic paper rewrites the rulebook for display.” Nature Photonics 1, 248–251 (2007).

[2] Xu, T.; Walter, E. C.; Agrawal, A.; Bohn, C.; Velmurugan, J.; Zhu, W.; Lezec, H. J.; Talin, A. A. “High-Contrast and Fast Electrochromic Switching Enabled by Plasmonics.” Nature Communication, 7, 10479 (2016).

[3] Yakuphanoglu, F.; Senkal, B. F. “Electric and Thermoelectric Properties of Polyaniline Organic Semiconductor and Electrical Characterization of Al/PANI MIS Diode.” J. Phys. Chem. C, 111, 1840-1846 (2007).

[4] Chen, S. A.; Fang, Y.; Lee, H. T. “Polyacrylic Acid-Doped Polyaniline as p-type Semiconductor in Schottky Barrier Electronic Device.” Synthetic Metals, 55-57, 4082-4086 (1993).

[5] Bera, A.; Deb, K.; Kathirvel, V.; Bera, T.; Thapa, R.; Saha, B. “Flexible Diode of Polyaniline/ITO Heterojunction on PET Substrate.” Appl. Surf. Sci., 418, 264-269 (2017).

[6] Sachtler, W. M. H.; Dorgelo, G. J. H.; Holscher, A. A. “The Work Function of Gold.” Surf. Sci., 5, 221-229 (1966).

[7] Zhang, Y.; Pluchery, O.; Caillard, L.; Humblot, A. F. L.; Casale, S.; Chabal, Y. J.; Salmeron, M. “Sensing the Charge State of Single Gold Nanoparticles via Work Function Measurements.” ACS Nano lett., 15, 51-55 (2015).

[8] Sheldon, M. T.; Groep, J. V.; Brown, A. M.; Polman, A.; Atwater, H. A. “Plasmoelectric Potentials in Metal Nanostructures.” Science, 346, 6211, 828-831 (2014).

PART II

4. Study of electrical conductivity of the poly(3 hexylthiophene-2, 5-diyl) polymer (P3HT) in resonant Fabry-Perot cavities

1. Introduction. Recently, organic semiconducting polymers have been at the center of intense industrial and academic research, due to their ability to create flexible and inexpensive devices that can be processed on a large scale. Such devices are to be used in thin-film transistors, photoelectrical cells, light emitting diodes, photovoltaics, plasmonic devices, photoelectrical cells and many more electronic applications [1-6]. However, the widespread adoption of these materials into electronic systems is hindered by the very low charge carrier mobility, which is associated with large disorder in organic materials, as compared to conversional inorganic semiconductors.[7]

Light-matter interaction enters the strong coupling regime when the photon exchange rate between exciton and electromagnetic modes becomes faster than the decay and/or decoherence rates of either constituent.[8] Strong coupling leads to the formation of two hybridized light-matter polaritonic states, P+ and P, separated by the energy gap known as the Rabi splitting, Fig.1. In quantum electrodynamics, the Rabi splitting (for a single quantum emitter) is proportional to $(1+n_{ph})^{1/2}$, where n_{ph} is the number of photons in the mode. This means that even in the dark, there always exists a finite Rabi splitting attributed to the interaction with vacuum fluctuations.

Light-matter interaction in the strong coupling regime offers exciting possibilities for exploring a broad range of physical phenomena, including Bose-Einstein condensation in organic and inorganic semiconductors [9], modification of chemical reactivities [10] and surface potentials [11], Fano resonances [12], Förster energy transfer [13], spontaneous [14] and stimulated [15] emission, and van der Waals interactions [16]. Strong coupling of e.g. molecular ensembles with electromagnetic

modes can be achieved by utilizing surface plasmon resonances or confined electromagnetic environments, such as cavities. A typical example of a strongly coupled system is a Fabry-Perot (micro) cavity (composed of two parallel metallic mirrors), which is resonant with an electronic transition in a dye-doped polymer or an organic semiconductor filling the cavity. Large molecular concentrations and collective dipole moments lead to gigantic Rabi splitting (as large as 1.12 eV [17]), which are comparable with energy eigenvalues of not coupled constituents taken separately. The latter light-matter interaction is said to occur in the ultra-strong coupling regime.

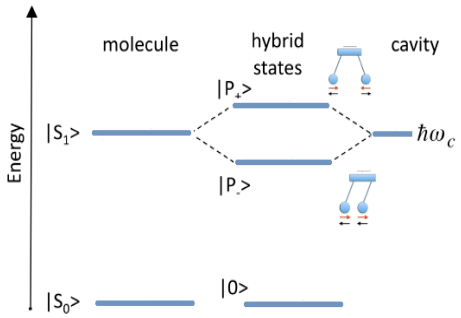

Fig. 1. The simplified energy diagram showing the interaction of a HOMO-LUMO (S_0–S_1) transition of a molecule resonant with a cavity mode $\hbar\omega_c$, where ω_c is the resonant oscillation frequency of the cavity. Strong coupling leads to the formation of two hybrid light–matter (polaritonic) states (P- and P_+) separated by the Rabi splitting energy $\hbar\Omega_R$. 0 represents the ground state.[18]

According to Ref. [7], large ensembles (~10^5) of organic molecules can be strongly coupled to plasmonic modes, resulting in an increase of electrical conductivity (similarly to enhancement of the energy transfer in the strong coupling regime predicted in Refs. [19, 20]). We asked the question whether this phenomenon is universal and whether it should be expected in other strongly coupled systems involving organic molecules and semiconducting polymers.

In the present study, we searched for the effect of strong coupling (with Fabry-Perot cavities) on electrical conductivity of Poly(3-hexylthiophene-2,5-diyl) polymer (P3HT). Despite the remarkably strong coupling (Rabi splitting ~1.0 eV), no correlation between the strong coupling and the electrical conductivity has been found. The only effect on the electrical conductivity was (tentatively) from increase of the order in thick P3HT films.

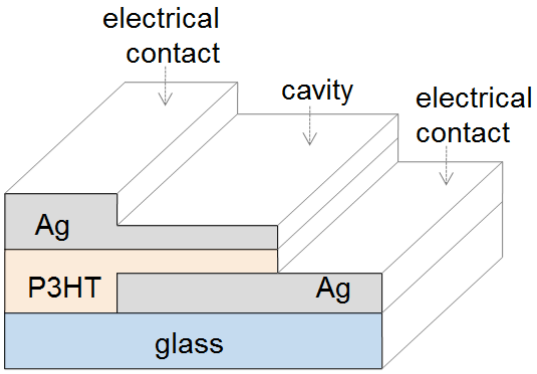

Fig. 2. Schematics of the Fabry-Perot cavity: bottom layer Ag ~ 200 nm and the top semi-transparent Ag layer ~ 40 nm sandwiching polymeric P3HT films of different thicknesses.

2. Experimental Samples and Measurements

2.1 Sample fabrication. We designed and experimentally fabricated multiple resonant Fabry-Perot cavities by sandwiching 2,5-poly(3-hexylthiophene) (P3HT) semiconducting polymeric films of different thickness between thick bottom silver layer (deposited onto a glass substrate) and a thin semi-transparent top silver layer, Fig. 2. The metallic Ag films were deposited on clean glass substrates using thermal evaporator (Edwards coating, Auto306) and all film thicknesses were measured with the Bruker DektakXT profilometer. The polymeric solutions were prepared from high purity, 99.995%, P3HT flakes (with molecular weight ~ 40 kD and head-to-tail regioregularity >99%, obtained from Sigma Aldrich), dissolved in ACS grade chloroform from Fisher Scientific.

2.2 Numerical modeling of resonant cavities. Numerical solutions to Maxwell equations were obtained using the commercial finite element method (FEM) solver, COMSOL Multiphysics. The spectra of real and imaginary parts of the dielectric permittivity of Ag were obtained from Ref. [21], and those of the P3HT polymer were adopted from Ref. [22]. The reflectance spectra of Fabry-Perot cavities of difference sizes filled with P3HT were calculated and the energy

positions of the dips in the reflectance spectra were plotted against the cavity thickness d, forming two branches of the dispersion curve with Rabi splitting, Fig. 3.

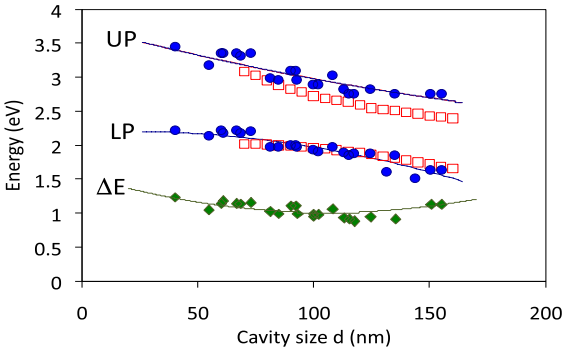

Fig. 3. Dependence of the spectral positions of the reflectance dips on the cavity size *d*. UP is the upper polariton branch, LP is the lower polariton branch, and DE=UP-LP is the difference between them. Red open squares – calculation, blue closed circles and green filled diamonds – experiment, solid lines – guides for eyes.

2.3 Optical studies. The reflectance spectra of the experimental samples were measured in the integrated sphere of the Lambda 900 spectrophotometer. Two minima in the reflectance spectra, manifesting the strong coupling, have been observed in most of the samples studied. The corresponding experimental dispersion curve, characterized by one of the largest Rabi splittings reported in the literature, 1.0 eV, was in a good agreement with that calculated numerically, Fig. 3.

The absorbance spectra taken in the series of P3HT films of different thickness (deposited on glass) reveal known in the literature structure of the P3HT absorption band, featuring maxima and shoulders at 520 nm, 550 nm and 600 nm in thicker films, while the absorbance bands of thinner P3HT films were nearly featureless, Fig. 4. This suggests that thick films have higher degree of crystallinity than thin films [23].

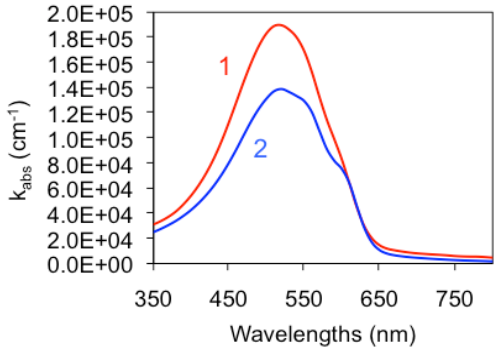

Fig. 4. Absorption spectra indicating increase of crystallinity with increase of the thickness of P3HT films deposited onto glass substrates; trace 1: film thickness ~ 76 nm; trace 2: film thickness ~ 255 nm.

2.4 Electrical studies. The current-voltage (I-V) response of the cavity samples, measured in a straightforward setup involving dc voltage supply from Xantrex, voltmeter and ammeter (both 34405A Multimeters from Agilent), was found to be linear or ohmic in nature, Fig. 5.

Alternatively, the dc resistance of P3HT cavity samples, R, was routinely measured using the digital multimeter (model 34405A from Agilent) switched to the ohmmeter mode. The resistance of Ag films and other electrical conduits, measured in the schematics of Fig. 2 without P3HT layer, was properly taken into account. The electrical conductivity of the samples studied was calculated from the Pouillet's relation, $\sigma_{dc}=L/(RA_c)$, where σ_{dc} is the dc conductivity, A_c is the cross-sectional area of the P3HT cavity, and L is the thickness of the P3HT layer.

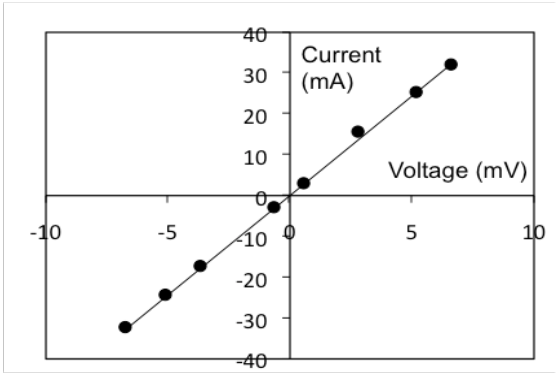

Fig. 5. Typical I-V curve of the Fabry-Perot cavity filled with the P3HT polymer.

In our experiments, we used two nominally identical batches of P3HT (from Sigma Aldrich). The results of their electrical conductivity studies are summarized in Figs. 6a and 6b. We have found that: (i) In both series of samples, the measured values of electrical conductivity fell within the range of data reported in the literature,

between 10^{-4} S/cm and 10^{-9} S/cm.[24-29] (ii) There is no any obvious correlation between the size dependence of the electrical conductivity and the behavior of the dispersion curve. In particular, no anomaly in the electrical conductivity is observed at the cavity size equal to ~100 nm, when the energy gap between the upper and the lower polariton branches is the smallest (Fig. 3, green diamonds) and the interaction of the coupled constituents is the strongest. (iii) The only observable trend was the increase of electrical conductivity with the increase of the cavity size, Fig. 6. As electrical conductivity is expected to increase with an increase in the polymer's crystallinity 30, the latter phenomenon can tentatively explain our experimental results.

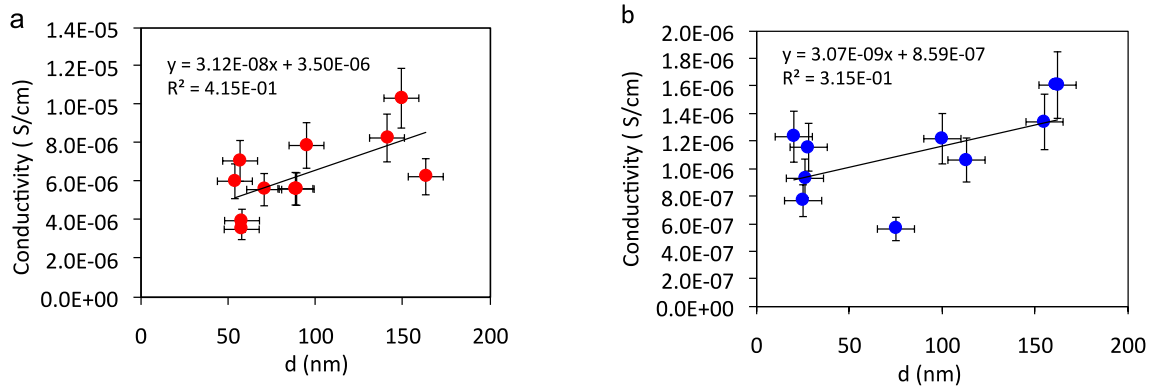

Fig. 6. Electrical conductivity as a function of the thickness of the P3HT layers, measured in samples fabricated from two batches of the P3HT polymer. Linear trendlines are guides for eyes.

3. Summary. We have studied electrical conductivity of P3HT polymeric films, which were stronger or weaker coupled to Fabry-Perot cavities. Despite the observation of a gigantic strong coupling evidenced by the Rabi splitting of 1.0 eV, no obvious correlation was found between the strong coupling and the electrical conductivity. The latter was (presumably) primarily affected by an increase of the polymer's crystallinity in thick P3HT films. On the other hand, since the upper and the lower polariton branches of the dispersion curve (as well as the difference between them) were nearly flat and featureless, Fig. 3, observation of any sharp singularities in thickness-dependent electrical conductivity could not be expected. At the same time, somewhat surprisingly, ~20% "sagging" of the DE curve in Fig. 3 did not result in any noticeable effect on electrical conductivity either. We conclude that the effect of strong coupling on electrical conductivity of molecular ensembles, reported in Ref. [7], is not universal and not readily observed in every strongly coupled system.

In the recent paper [31], published after the submission of the present manuscript, enhancement of electrical (dark) conductivity as well as photoconductivity was reported in P3HT deposited onto resonant plasmonic array of nanoholes in Ag film, similar to that used in Ref. [7].

1 J. Zhao, Z. Chi, Z. Yang, X. Chen, M. S. Arnold, Y. Zhang, J. Xu, Z. Chi and M. P. Aldreda, "Recent developments of truly stretchable thin film electronic and optoelectronic devices", Nanoscale, 10, 5764 (2018).

2 L.-L. Chua, J. Zaumseil, J.-F. Chang, E. C.-W. Ou, P. K.-H. Ho, H. Sirringhaus, and R. H. Friend, "General observation of n-type field-effect behaviour in organic semiconductors" Nature 434, 194 (2005).

3 K. M. Coakley and M.D. McGehee, “Conjugated Polymer Photovoltaic Cells”, Chem. Mater. 16, 4533 (2004).

4 I. McCulloch, R. S. Ashraf, L. Biniek, H. Bronstein, C. Combe, J. E. Donaghey, D. I. James, C. B. Nielsen, B. C. Schroeder, and W. Zhang, “Design of semiconducting indacenodithiophene polymers for high performance transistors and solar cells”, Acc. Chem. Res, 45, 714 (2012).

5 B. S. Ong, Y. Wu, P. Liu, and S. Gardner, “High-Performance Semiconducting Polythiophenes for Organic Thin-Film Transistors”, J. Am. Chem. Soc. 126, 3378–3379 (2004).

6 Y. R. Leroux, J. C. Lacroix, K. I. Chane-Ching, C. Fave, N. Félidj, G. Lévi, J. Aubard, J. R. Krenn, and A. Hohenau, “Conducting polymer electrochemical switching as an easy means for designing active plasmonic devices”, J. Am. Chem. Soc. 127, 16022 (2005).

7 E. Orgiu, J. George, J. A. Hutchison, E. Devaux, J. F. Dayen, B. Doudin, F. Stellacci, C. Genet, J. Schachenmayer, C. Genes, G. Pupillo, P. Samorì & T. W. Ebbesen; “Conductivity in organic semiconductors hybridized with the vacuum field”, Nature Materials 14, 1123–1129 (2015).

8. Törmä and W. Barnes; “Strong coupling between surface plasmon polaritons and emitters” Rep. Prog. Phys. 78, 013901 (2015).

9 D. W. Snoke, and J. Keeling; “The new era of polariton condensates”, Physics Today 70, 10, 54 (2017).

10 P. Vasa and C. Lienau; “Plasmonic Cavity Coupling”, ACS Photonics 5, 2 (2018).

11 J. A. Hutchison, A. Liscio, T. Schwartz, A. Canaguier-Durand, C. Genet, V. Palermo, P. Samorì, and T. W. Ebbesen, “Tuning the work-function via strong coupling”, Adv. Mater. 25, 2481(2013).

12 T. J. Arruda, A. S. Martinez, and F. A. Pinheiro, “Unconventional Fano effect and off-resonance field enhancement in plasmonic coated spheres”, Phys. Rev. A, 87, 043841 (2013).

13 T. Tumkur, J. Kitur, C. E. Bonner, A. Poddubny, E. E. Narimanov, and M. A. Noginov, “Control of Förster energy transfer in the vicinity of metallic surfaces and hyperbolic metamaterials”, Faraday Discussions, Royal Society of Chemistry, 178, 395 (2015).

14 Z. Jacob, J.-Y. Kim, G. V. Naik, A. Boltasseva, E. E. Narimanov, V. M. Shalaev, “Engineering photonic density of states using metamaterials” Appl Phys B, 100, 215 (2010).

15 J. K. Kitur, L. Gu, T. Tumkur, C. E. Bonner and M. A. Noginov, “Stimulated emission of surface plasmons on top of metamaterials with hyperbolic dispersion”, ACS Photonics 2, 1019 (2015).

16 S. A Maier, Plasmonics: Fundamentals and Applications (2007).

17 S. Gambino, M. Mazzeo, A. Genco, O. Di Stefano, S. Savasta, S. Patanè, D. Ballarini, F. Mangione, G. Lerario, D. Sanvitto, G. Gigli, “Exploring Light–Matter Interaction Phenomena under Ultrastrong Coupling Regime”, ACS Photonics, 1, 1042 (2014).

18 J.A. Hutchison, T. Schwartz, C. Genet, E. Devaux, and T.W. Ebbesen, “Modifying chemical landscapes by coupling to vacuum fields”, Angew. Chemie - Int. Ed. 51, 1592 (2012).

19 J. Feist and F. J. Garcia-Vidal, “Extraordinary Exciton Conductance Induced by Strong Coupling”, Phys. Rev. Lett. 114, 196402 (2015).

20 C. Gonzalez-Ballestero, J. Feist, E. Moreno, and F. J. Garcia-Vidal, “Harvesting excitons through plasmonic strong coupling”, Phys. Rev. B 92, 121402(R) (2015).

21 P. B. Johnson and R. W. Christy, “Optical Constants of the Noble Metals”, Phys. Rev. B 6, 4370 (1972).

22 V. N. Peters, T. U. Tumkur, G. Zhu, M. A. Noginov, “Control of a chemical reaction (photodegradation of the p3ht polymer) with nonlocal dielectric environments”, Sci. Rep. 5, 14620 (2015).

23 K. Sakamakib, K. Akagib, H. Shirakawab, H. Kyotani, “Relationship between crystallinity and electrical conductivity of highly conducting polyacetylene film”, Syn. Met. 84, 365 (1997).

24 J. Obrzut and K. A. Page, “Electrical conductivity and relaxation in poly(3-hexylthiophene)”, Phys. Rev. B, 80, 195211 (2009).

25 B. K. Kuila and A. K. Nandi, “Physical, mechanical, and conductivity properties of poly (3-hexylthiophene) - montmorillonite clay nanocomposites produced by the solvent casting method”, Macromolecules 37, 8577 (2004).

26 A. J. Mozer, N. S. Sariciftci, A. Pivrikas, R. Österbacka, G. Juška, L. Brassat and H. Bässler, “Charge carrier mobility in regioregular poly(3-hexylthiophene) probed by transient conductivity techniques: A comparative study”, Phys. Rev. B, 71, 035214 (2005).

27 J. Cui, D.E. Martínez-Tong, A. Sanz, T.A. Ezquerra, E. Rebollar, and A. Nogales, “Relaxation and Conductivity in P3HT/PC71BM Blends As Revealed by Dielectric Spectroscopy”, Macromolecules 49, 2709 (2016).

28 J. Hynynen, D. Kiefer, L. Yu, R. Kroon, R. Munir, A. Amassian, M. Kemerink, and C. Müller, “Enhanced Electrical Conductivity of Molecularly p-Doped Poly(3-hexylthiophene) through Understanding the Correlation with Solid-State Order”, Macromolecules 50, 8140 (2017).

29 W. Meng, R. Ge, Z. Li, J. Tong, T. Liu, Q. Zhao, S. Xiong, F. Jiang, L. Mao, and Y. Zhou, “Conductivity Enhancement of PEDOT:PSS Films via Phosphoric Acid Treatment for Flexible All-Plastic Solar Cells”, ACS Appl. Mater. Interfaces 7, 14089 (2015).

30 V. Saini, Z. Li, S. Bourdo, E. Dervishi, Y. Xu, X. Ma, V. P. Kunets, G. J. Salamo, T. Viswanathan, A. R. Biris, D. Saini, and A. S. Biris, “Electrical, Optical, and Morphological Properties of P3HT-MWNT Nanocomposites Prepared by in Situ Polymerization”, J. Phys. Chem. C 113, 8023 (2009).

31 K. Nagarajan, J. George, A. Thomas, E. Devaux, T. Chervy, Azzini, C. Ganet, T.W. Ebbesen “Conductivity and Photoconductivity of a p-type Organic Semiconductor under Ultra-Strong Coupling”. ChemRxiv Preprint (2018).

5. Coupling of the First and Second Excited States of R6G Dye with the Fabry–Perot Cavity

Strong coupling of an ensemble of highly concentrated dye molecules with a resonant Fabry-Perot cavity results in the formation of energy-split polaritonic states drawing on the properties of interacting light and matter. [1,2] If the resonance frequency in the molecule (e.g. absorption line) and that of the cavity, taken separately, match each other, the spectrum of the combined strongly coupled system will feature two bands, one above, and one below the original (uncoupled) frequency. So far, most of strong coupling phenomena were studied in an approximation of a simple system involving the lowest excited state of an excitonic medium and one resonance in a plasmonic system or a cavity. [3,4] However, molecules have multiple excited states and Fabry-Perot cavities can support multiple resonances. The strong coupling in such realistic, although relatively complex, systems raises many intriguing questions. (i) For example, if a cavity is strongly coupled to one transition of a molecule and changes its energy substantially, will this affect eigen-energies of other molecular states, which are not coupled to the cavity? (ii) In metallic Fabry-Perot cavities, absorption transitions can be supported not only by an excitonic medium but also by a constituent metal. Does the coupling of the cavity with the constituent metal exist and can it be observed experimentally? (iii) Can the coupling affect

energy eigenstates of interacting systems without causing a splitting of the dispersion curves, and should such coupling be characterized as “strong”? These questions motivated the present study reported below.

We have fabricated several cavities formed by a highly reflective 200 nm thick Ag (or Al) mirror deposited on glass, a layer of poly(methyl)methacrylate (PMMA) polymer heavily doped with rhodamine 6G (R6G) molecules (in concentration 4.46 x 10^{-2} mol/L), and a semi-transparent ~30 nm Ag (or Al) mirror on top. The cavity resonance was tuned by varying the thickness, d of the R6G:PMMA film. Similar dye-doped polymeric films deposited on glass were used as control samples.

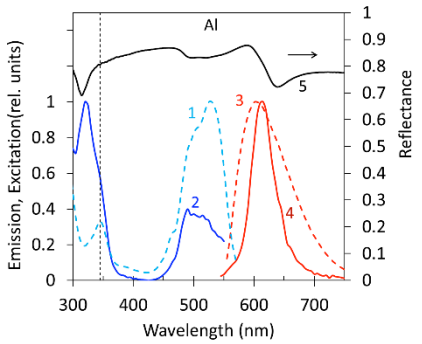

Fig. 1. Experimental reflectance, emission and excitation spectra measured in the *d*=124 nm Al cavity and the control sample (R6G:PMMA film on glass). Traces 1, 2 – excitation spectra; traces 3, 4 – emission spectra; traces 5- reflectance spectra. Traces 1 and 3 are measured on top of glass and traces 2 ,4, 5 – in the cavity.

Experimentally, we have studied reflectance, emission, and excitation spectra of the cavities and the control samples. Rhodamine 6G dye features multiple singlet-singlet electronic transitions accompanied by vibrionic transitions. The S0→S1 transition has the maximum at ~530 nm and a shoulder at ~490 nm. The absorption transition terminating at the second excited state, S0→S2, has the maximum at ~345 nm, and several other excited states lie at shorter wavelengths. The emission spectrum at the S1→S0 transition does not depend on the excitation wavelength and has a maximum at 595 nm (on a glass substrate).

In the small Al cavity (d=124 nm), only the fundamental mode (“λ/2” standing wave) was in resonance with the R6G transition (S0→S1), resulting in the strong coupling manifested by the splitting of the dip of the reflectance spectrum (Fig. 1, trace 5) and the shifts of the S0→S1 excitation and S1→S0 emission spectral bands (Fig. 1, traces 1-4, λ>0.45 μm). At the same time, no noticeable shift was observed in the spectral position of the S0→S2 excitation band, which was not in resonance with the cavity (Fig. 1, traces 1 and 2, λ~0.35 mm). Therefore, we conclude that strong coupling of the Fabry-Perot cavity with the S0→S1 molecular transition does not noticeably affect the energy of the S0→S2 transition. This is one of the central observations of this study.

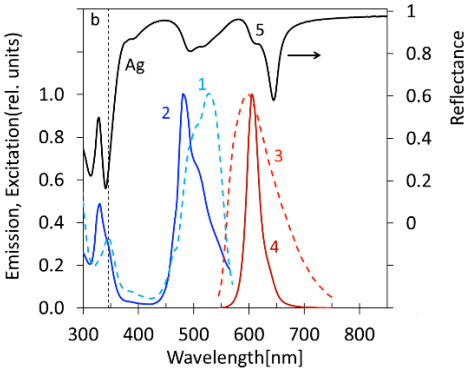

Fig. 2. Experimental reflectance, emission and excitation spectra measured in the *d*=182 nm Ag cavity and the control sample (R6G:PMMA film on glass). Traces 1, 2 – excitation spectra; traces 3, 4 – emission spectra; traces 5- reflectance spectra. Traces 1 and 3 are measured on top of glass and traces 2,4, 5 – in the cavity.

The fundamental mode (“λ/2” resonance) of the large (d=182 nm) Ag cavity is strongly coupled with the R6G S0→S1 transition as well, as evidenced by the energy splitting and the spectral shifts in Fig. 2 at λ>0.45 mm. However, the most intriguing spectral feature of Fig. 2 is a couple of sharp dips in the reflection spectrum at λ≤0.35 mm. These dips can be theoretically predicted in the cavity filled with undoped polymer (Fig. 2a) and are not related to the presence of dye. Instead, they are attributed to the strong coupling of the second cavity resonance (“λ” standing wave) with two material’s resonances at ~342 nm and ~317 nm. These resonances, located in the vicinity of the wavelength, at which the real part of dielectric permittivity of Ag is equal to zero ε’=0, and seen in the reflectance spectrum of bulk Ag and the spectrum of the imaginary part of the dielectric

permittivity of silver e", can be due to a combination of the bound and free electron transitions. This is the second important observation of this study.

The R6G dye absorption at the S0→S2 transition, which lies in the ~345 nm spectral range (in the R6G:PMMA film on glass), is not sufficiently strong to noticeably affect the reflection spectrum of the cavity. However, the excitation (and expectedly the absorption) spectrum at this transition is blue shifted due to the interaction with the cavity, which, in turn, is coupled with Ag metal material resonances, Fig. 2b, traces 1 and 2, λ<0.4 mm). Note that a blue shift of an excitation spectrum is characteristic of a cavity-exciton coupling (see Figs. 1b and 2b, λ>0.4 mm). The three examples above highlight the results of a thorough study of the reflectance, excitation and emission spectra in multi-resonant coupled systems – Ag and Al Fabry-Perot cavities and highly doped R6G:PMMA films. The comprehensive results, trends and conclusions will be presented at the conference.

[1] P. Törmä, W. Barnes, "Strong coupling between surface plasmon polaritons and emitters: a review" Rep. Prog. Phys. 2015, 78, 013901.

[2] T. Schwartz, J. A. Hutchison, C. Genet, T. W. Ebbesen, "Reversible Switching of Ultrastrong Light-Molecule Coupling," PRL 2011, 106, 196405.

[3] B. Luk'yanchuk, N. I. Zheludev, S. A. Maier, N. J. Halas, P. Nordlander, H. Giessen, C.T. Chong, Nature Materials 2010, 9, 707–715.

[4] A. Sobhani, A. Manjavacas, Y. Cao, M. J. McClain, F. J. García de Abajo, P. Nordlander, N. J. ACS Photonics 2017, 4, 2102–2110.

PART III

6. Manipulation of Magnetic Dipole Emission from Eu^{3+} with Mie-Resonant Dielectric Metasurfaces

Mie-resonant high-index dielectric nanoparticles have been suggested as a viable platform for enhancing both electric and magnetic dipole transitions of fluorescent emitters. While the enhancement of the electric dipole transitions by such dielectric nanoparticles has been demonstrated experimentally, the case of magnetic-dipole transi- tions remains largerly unexplored. Here we study the enhancement of spontaneous emission of Eu^{3+} ions, featuring both electric (at 610 nm) and magnetic-dominated (at 590 nm) dipole transitions, by a metasurface composed of Mie-resonant silicon nanocylinders. By fabricating a set of metasurfaces featuring a variation of the nanocylinder radius, we sweep the relevant Mie-type resonances of the metasurfaces over the spectral range of the electric and magnetic dipole transitions. After covering the meta- surfaces with a layer of an Eu^{3+} doped polymer, we observe an enhancement of the Eu^{3+} emission associated with the electric and magnetic-dominated dipole transitions. Importantly, the enhancement factor depends systematically on the type of the transition and the nanocylinder radius. Our results demonstrate that the branching ratio of emission via the electric or magnetic transition channel can be modified by a carefully designed dielectric metasurface. Importantly, for carefully chosen nanocylinder radius the magnetic contribution to the emission can be enhanced more strongly than the electric contribution. We confirm our observations by numerical simulations based on two different approaches.

7. Non-resonant enhancement of spontaneous emission of HITC dye in metal-insulator-metal waveguides

We have experimentally studied the non-resonant enhancement of spontaneous emission of HITC laser dye in metal-insulator-metal (MIM) waveguides (also referred to as Fabry–Perot

cavities). We have found that in the cavities, whose size was too small to support a fundamental or any higher order resonance, the emission decay rate increased, by nearly an order of magnitude, with reduction of the cavity size. At the same time, the emission intensity increased when the cavity size was reduced from ~200 to ~30 nm and dropped sharply when the cavity was smaller than ~30 nm. This emission enhancement, consistent with the perpendicular orientation of the emitting dipole with respect to the mirrors, is in a good agreement with the theoretical predictions known from the literature.

Part 2

Aug. 1, 2019 – July 31, 2020.

ABSTRACT AND CONTENTS

The main goal of this project is to study how physical and chemical proprties of organic matter can be controlled in strong and weak light-matter interaction regimes. In Section 1 of this report, we will discuss control of (i) spontaneous emission and (ii) energy transfer in rationally designed metal-dielectric environments (cavities and substrates) [1P,2P,1C-5C]. The effects of light-matter interaction on miniature plasmonic and photonic lasers are discussed in Section 2 [3P,6C] . Relevant to this study, intriguing and not well understood effects of the plasmon drag – generation of macroscopic currents enabled by and strongly coupled with surface plasmons – will be discussed in Section 3 [4P,5P,7C,8C]. Finally, the development of new metamaterials [6P] and devices [7P] (sensors) is reported in Section 4.

This Technical Report is organized as follows.

PUBLICATIONS

[1P] Srujana Prayakarao, Samantha R. Koutsares, Carl E. Bonner, and Mikhail A. Noginov, "Effect of nonlocal metal–dielectric environments on concentration quenching of HITC dye", JOSA B, 36, 3579-3587 (2019). https://doi.org/10.1364/JOSAB.36.003579

[2P] Vanessa N. Peters, Srujana Prayakarao, Samantha R. Koutsares, Carl E. Bonner, and Mikhail A. Noginov, "Control of Physical and Chemical Processes with Nonlocal Metal− Dielectric Environments", ACS Photonics 6, 3039−3056 (2019). DOI: 10.1021/acsphotonics.9b00734

[3P] E. K. Tanyi, S. Mashhadi, C. On, Md. O. Faruk, E. Harrison, N. Noginova, and M. A. Noginov, "Plasmonic laser with distributed feedback", Appl. Phys. Lett. 115, 151103 (2019). https://doi.org/10.1063/1.5117875

[4P] T. Ronurpraful, D. Keene, N. Noginova, "Plasmon drag effect with sharp polarity switching," New Journal of Physics. 22 (4) 043002 (2020), http://doi:10.1088/1367-2630/ab7d7c

[5P] D. Keene. T. Ronurpraful, N. Nogniova, "Plasmon related electrical effects in strongly modulated metasurfaces,". Proc. SPIE, Metamaterials, Metadevices, and Metasystems. 11080 45 (2019). http://doi:10.1117/12.2532069

[6P] S. R. Koutsares, E. K. Tanyi, S. J. Daniel, R. S. Savelev, M. Rahmani, D. Neshev, I. V. Shadrivov, and M. A. Noginov "Low-loss volume modes in a lamellar hyperbolic metamaterial slab", JOSA B, 37, 1065-1072 (2020).

[7P] T. Ronurpraful, N. Jerop, N. Noginova, "Ultra-sensitive plasmonic sensing based on gold nanostrip arrays," Optics Letters. 44 (17). 4199, (2019). http://doi:10.1364/OL.44.004199

CONFERENCE PRESENTATIONS

[1C] M. A. Noginov, S. Prayakarao, S. R. Koutsares, S. Rout, D. Courtwright, C. E. Bonner, "Effects of inhomogeneous metal-dielectric environments on spontaneous emission and energy transfer" *SPIE Optics & Photonics*, Aug. 11-15, 2019, San Diego, CA, paper 11091- 4 ***(invited)***.

[2C] S. R. Koutsares, L. S. Petrosyan, D. Courtwright, S. Prayakarao, C. E. Bonner, T. V. Shahbazyan, M. A. Noginov, Control of Concentration Quenching with Metallic Substrates and Cavities", in *Conference on Lasers and Electro-Optics*, OSA Technical Digest (Optical Society of America, 2020), paper FM1D.4.

[3C] D. Courtwright, S. Koutsares, S. Prayakarao, C. Bonner, Mikhail A. Noginov, "Effect of non-local metal-dielectric environments on concentration quenching and spontaneous emission" *SPIE Optics & Photonics*, Aug. 11-15, 2019, San Diego, CA, paper 11080-105.

[4C] S. Koutsares, S. Prayakarao, D. Courtwright, C. E. Bonner, M. A. Noginov, L. S. Petrosyan and T. V. Shahbazyan, "Effect of Fabry-Perot Cavities on Concentration Quenching", Progress in Nanotechnology, 2019 NSF Nanoscale Science and Engineering Grantees Conference, December 9-10, 2019, The Westin Alexandria - Alexandria, VA.

[5C] Md Omar Faruk, Nelly Jerop, Mikhail A. Noginov, "Emission in Fabry-Perot Cavities in Weak and Strong Coupling Regimes", in *Conference on Lasers and Electro-Optics*, OSA Technical Digest (Optical Society of America, 2020), paper JW2D.6.

[6C] J. B. Khurgin, M. A. Noginov, "Miniature lasers: what does and what does not matter?" *SPIE Optics & Photonics*, Aug. 11-15, 2019, San Diego, CA, paper 11080-7 ***(invited)***.

[7C] T. Ronurpraful, N. Jerop, N Noginova, "Extreme sensitivity of plasmon drag to surface modification," in *Conference on Lasers and Electro-Optics*, OSA Technical Digest (Optical Society of America, 2020), paper FM4Q.8.

[8C] M. Shahabuddin, D. Keene, N. Noginova, “Magneto-dependent plasmon drag in permalloy structures,” in *Conference on Lasers and Electro-Optics*, OSA Technical Digest (Optical Society of America, 2020), paper JTu2D.14.

8. S. Rout, Z. Qi, M. Biener, D. Courtwright, J. Adrien, M. Shahabuddin, C. E. Bonner, N. Noginova, and M. A. Noginov, “Nanoporous Gold Nanoleaf as Tunable Metamaterial”, in *Conference on Lasers and Electro-Optics*, OSA Technical Digest (Optical Society of America, 2020), paper JTh2C.7.

TECHNICAL REPORT

SECTION 1. CONTROL OF SPONTANEOUS EMISSION AND ENERGY TRANSFER IN RATIONALLY DESIGNED METAL-DIELECTRIC ENVIRONMENTS

1.1 Control of Concentration Quenching with Metallic Substrates and Cavities [1P,2P,1C-4C]

[In collaboration with Shahbazyan group, Jackson State University]

Close proximity to metallic surfaces, lamellar metal-dielectric metamaterials and other nanostructures can strongly affect many physical phenomena, including spontaneous emission and Förster energy transfer. In multiple recent studies, Förster transfer was claimed to be enhanced [1], inhibited [2] or not affected [3] by non-local metal-dielectric environments. This unsettled controversy motivated the present study.

In the recent works, we have shown that (i) Förster energy transfer (or the related concentration quenching of luminescence) is inhibited in the vicinity of metallic surfaces and lamellar hyperbolic metamaterials [2,4] and (ii) the rate and intensity of spontaneous emission can be strongly enhanced in thin metal-insulator-metal (MIM) waveguides (or Fabry-Perot cavities) [5]. In this study, focused on the effect of Fabry-Perot cavities on the energy transfer (which was found to be very different from that in Ref. [1]), we report on several important observations that shed light on the underlying physics of a broader range of related phenomena.

Our experimental samples were films of dye-doped polymer HITC:PMMA deposited on glass and Ag substrates or sandwiched between two Ag films to form a Fabry-Perot cavity. The HITC:PMMA film thicknesses ranged from d=12 nm to d=340 nm, and the dye concentrations (in solid state) were equal to c=2 g/l and c=30 g/l. In the kinetics measurements, the samples were excited at λ=795 nm with ~150 fs pulses of a Ti:sapphire laser and the emission was detected with a VIS/IR streak camera. In our data analysis, we first treated all kinetics as single-exponential and determined effective decay rates γ. In the second step, we studied the deviation of emission kinetics from exponential functions and analyzed it in terms of "convexity" factors ζ, proportional to the second derivative of the kinetics plotted in semi-logarithmic coordinates. The major results and their analysis are summarized below.

1. Dye-Doped Films Deposited on Glass In agreement with Ref. [4], the emission kinetics shorten at high dye concentration (c=30 g/l), indicating concentration quenching – energy transfer to quenching centers. Such quenching was very modest at low dye concentration (c=2 g/l).

Since some donor molecules have quenching centers (acceptors) nearby and others do not, the energy transfer emission kinetics of ensembles of donors deviate from single exponential functions. Correspondingly, the convexity factors ζ measured at high dye concentration were greater than those at the low dye concentration.

A modest decrease of γ was observed with the reduction in the film thickness d. In thin films, donors are surrounded by smaller numbers of acceptors, which leads to a reduction in the energy transfer and concentration quenching.

The convexity factors ζ slightly increase as film distances d reduce. As film thickness decreases, the energy transfer transitions from the 3D regime to the 2D regime. Correspondingly, $\propto \exp(-\sqrt{t/\tau})$ emission kinetics [6] (with smaller ζ) change to $\propto \exp(-\sqrt[3]{t/\tau})$ kinetics [7] (with larger ζ). Note that this and the previous explanations are plausible when the film thickness is comparable to the Förster radius ≤10 nm and become less likely at d≥10 nm.

2. Highly Doped HITC:PMMA Films (c=30 g/l) Deposited on Silver At large film thicknesses d, the emission decay rates γ and convexity factors ζ are almost the same as those measured on top of glass. This is expected, since at large distance from the interface, the effect of metal is small [4].

The difference between the decay rates on top of glass and on top of silver increases with the reduction in the film thickness *d*. Such slowing down of the emission kinetics on top of Ag and the corresponding reduction of concentration quenching (Fig. 1, trace 1) is consistent with Ref. [4]. A strong reduction in convexity ζ is observed on top of silver at *d* ranging between ~100 nm and ~200 nm. Accordingly, the emission kinetics, plotted in semi-logarithmic coordinates, look nearly linear. This suggests that donors transfer their energy to acceptors in a synchronized manner. Strong coupling of excited molecules with propagating surface plasmons and with each other (*via* coupling to plasmons), can be a possible explanation of this effect (in analogy with coherent spontaneous emission of dye molecules strongly coupled with plasmonic substrates [8,9]). An increase of both emission decay rates γ and convexity factors ζ were observed at small film thicknesses, $d \leq 50$ nm. Both effects can be due to the expected luminescence quenching in close vicinity to metal [10] (energy transfer to metal or lossy waves).

3. Highly Doped HITC:PMMA Films (c=30 g/l) in Fabry-Perot Cavities The decay rates γ of highly concentrated dye (c=30 g/l) in cavities (Fig. 1, trace 2) are the sums of the spontaneous emission rates γ_{sp}, which are, presumably, independent of *c*, and the energy transfer (concentration quenching) rates γ_{et}, $\gamma=\gamma_{sp}+\gamma_{et}$. The latter were obtained by subtracting the spontaneous emission rates γ_{sp} measured in similar cavities in Ref. [5] (Fig. 1, trace 3) from the experimental decay rates γ measured in this study (Fig 1, trace 2). Intriguingly, the result of this subtraction (Fig. 1, blue circles) closely follows the decay rates measured on top of silver (Fig. 1, trace 1). Therefore, the effect of a cavity on the concentration quenching does not extend beyond the mere effect of the silver substrate (the bottom Ag layer), and the semi-transparent silver mirror on the top makes almost no difference. This result is strikingly different from that of Ref. [1], claiming enhancement of the energy transfer in cavities. On the other hand, strongly different contributions to the concentration quenching of the top and bottom Ag films are in line with Ref. [11], claiming that frequency shifts of absorbers or emitters in the vicinity of a metallic surface strongly depend on its thickness. The convexity factors ζ in cavities were slightly smaller than those on top of glass.

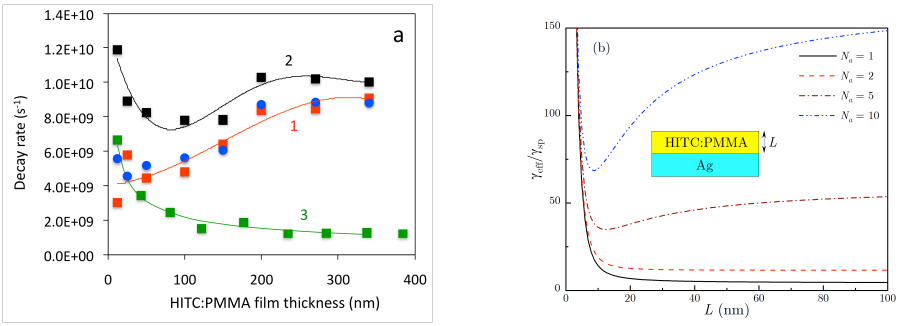

Fig. 1. (a) Trace 1 and red squares: dependence of the emission decay rate on the thickness of the HITC:PMMA film on top of Ag at dye concentration 30 g/l. Trace 2 and black squares: same as above in Fabry-Perot cavities. Trace 3 and green squares: same as above at low dye concentration 3 g/l [5]. Blue circles: Trace 3 subtracted from Trace 2. (b) Normalized effective decay rate is plotted against HITC:PMMA film thickness for several acceptor concentrations.

4. Non-Exponential Spontaneous Emission in Vicinity of Air/Dielectric Interface The convexity of the emission kinetics did not originate solely from the energy transfer. Thus, the calculated spontaneous emission kinetics (in absence of any energy transfer) deviated from exponential functions due to gradients of the photonic density of states (PDOS) in the vicinity of the air/dielectric interface [12]. However, the calculated ζ factors were much smaller than those measured in any experimental samples studied in this work. Therefore, the effect of PDOS on the shapes of spontaneous emission kinetics existed but was small.

5. Theoretical Model [T. Shahbazyan, L. Petrosyan] These finding were explained within a theoretical model that incorporates a reduction of the Förster radius in inhomogeneous and absorptive environment, which leads to a reduction of the Förster decay rate relative to the spontaneous decay rate of an isolated donor. For high dye concentrations, the calculated effective decay rate exhibits a clear minimum at intermediate distances where the suppression of concentration quenching is not fully compensated by an increase of the metal quenching.

[1] P. Andrew, W. L. Barnes, Science., 290, 785-788 (2000).

[2] T. Tumkur, J. Kitur, C. Bonner, A. Poddubny, E. Narimanov and M. Noginov, Faraday Discussions,178, 395-412 (2015).

[3] C. Blum et al., Phys. Rev. Lett. 109, 203601 (2012).

[4] S. Prayakarao, S. R. Koutsares, C. E. Bonner, and M. A. Noginov, JOSA B, 36, 3579-3587 (2019).

[5] S. Prayakarao, D. Miller, D. Courtwright, C. E. Bonner, and M. A. Noginov, J. Opt. Soc. Am. B 36, 2312-2316 (2019).

[6] V. M. Agranovich, M. D. Galanin, *Electronic Excitation Energy Transfer in Condensed Matter*, North-Holland: Amsterdam (1982).

[7] F. Reil, U. Hohenester, J. R. Krenn, and A. Leitner, Nano Lett. 8 , 4128-4133 (2008).

[8] S. Aberra Guebrou, C. Symonds, E. Homeyer, et al., Phys Rev. Lett., 108, 066401 (2012).

[9] L. Shi, T. K. Hakala, H. T. Rekola, J.-P. Martikainen, R. J. Moerland, and P. Törmä, Phys. Rev. Lett., 112, 153002 (2014).
[10] J. R. Lakowicz, Anal Biochem. 337, 171–194 (2005).

[11] R. R. Chance, A. Prock, R. Silbey, Phys. Rev. A, 12, (1975).

[12] E. Snoeks, A. Lagendijk, and A. Polman, Phys. Rev. Lett., 74 2459-2462 (1995).

1.2 Emission in dye-doped Fabry-Perot Cavities in Weak and Strong Coupling Regimes [5C]

We have studied frequency, angular, and polarization dependence of emission in Fabry-Perot cavities formed by two parallel silver mirrors separated by a layer of polymer (PMMA) doped with Rhodamine R6G (R6G) laser dye in low (c=20 g/l) and high (c=200 g/l) concentrations. The cavity sizes d were sufficiently large for the cavity branch of the dispersion curve to be positioned below the horizontal exciton branch, Figs. 1 a-d.

The frequency of emission originating from the cavity branch of the dispersion curve was larger at large outcoupling angles – the “rainbow” effect, Figs. 1a and 1c. Furthermore, the angle (and the frequency) of the strongest emission were determined by the cavity size: the larger the cavity, the larger is the angle – another realization of the rainbow effect, Fig 1d.

The angular distribution of emission (measured in a horizontal plane) is commonly dominated by two symmetrical lobes pointing to the left and to the right of the normal to the sample.

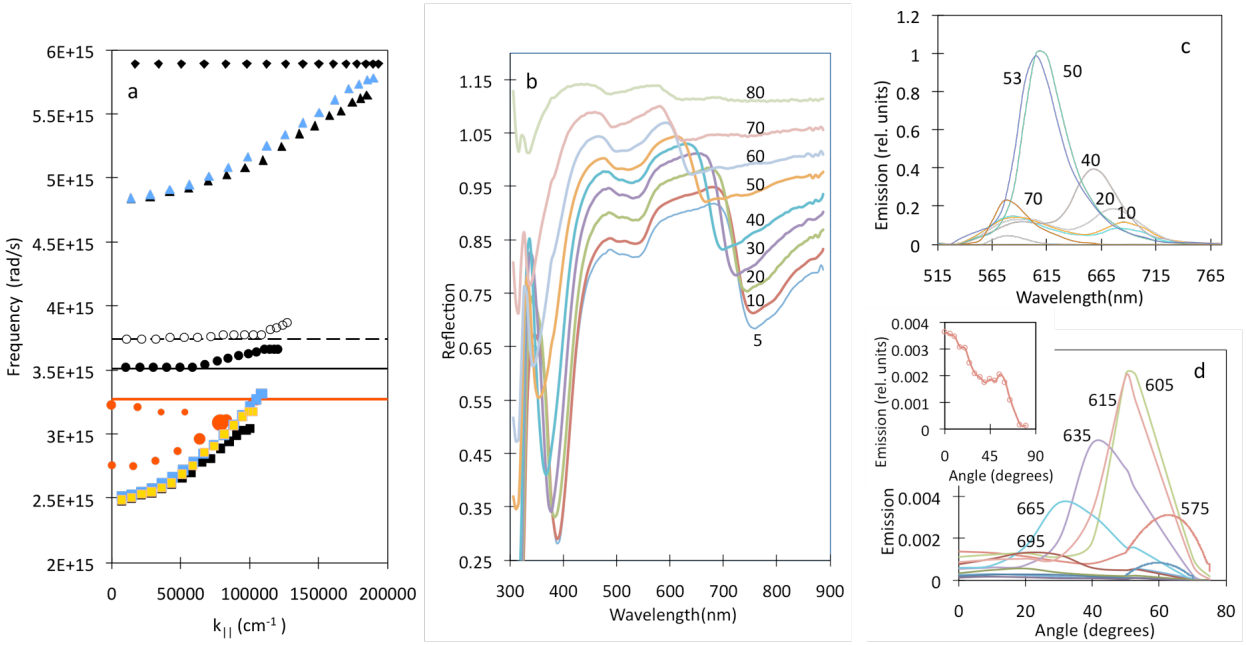

Figure 1. REFLECTION SPECTRA, EMISSION SPECTRA AND DISPERSION CURVES IN A FABRY-PEROT CAVITY WITH R6G DYE. (a) Dispersion curves of the d=205 nm cavity at the dye concentration c=200 g/l. Black characters – dispersion curves derived from the s polarized reflection measurements; blue characters – fitting the experimental dispersion curves using the transfer matrix calculator; yellow squares – dispersion of an undoped cavity calculated analytically. Black horizontal lines: absorption maximum (solid line) and absorption shoulder (dashed line) of R6G:PMMA deposited on glass. Red circles: "cavity emission" and "exciton emission" branches of the dispersion curve (in s polarization). The sizes of the red circles are proportional to the emission intensities. The lower, "cavity emission" branch demonstrates the "rainbow" effect. Red horizontal line: emission maximum of R6G:PMMA deposited on glass. (b) Reflection spectra recorded, in s polarization, at multiple incidence angles (written next to the traces). (c) Emission spectra recorded, in s polarization, at multiple detection angles (demonstrating the "rainbow" effect). (d) Angular emission profiles recorded, in s polarization, at multiple wavelengths (demonstrating the "rainbow" effect). Inset: angular dependence of emission originating from the exciton emission branch in a smaller cavity (d=185 nm, c=200 g/l).

Intriguingly, despite the strong Stokes shift in R6G dye, causing the emission frequency to be smaller than the absorption frequency, the branch of the cavity dispersion curve obtained in the emission experiment has higher energy than the one obtained in the reflection experiment, Fig. 1a. This effect is not fully understood. At the same time, the emission originating from the exciton branch of the dispersion curve has very broad angular distribution with the maximum at $\theta=0^{o}$.

The signatures of strong cavity-exciton coupling were observed at high dye concentration (c=200 g/l), but not at low concentration (c=20 g/l). The effect of the strong coupling on the cavity's emission is exemplified by a dramatic difference in the angular distribution of emission in d≈200 nm cavities with high dye concentration (c=200 g/l, strong coupling) and low dye concentration (c=20 g/l, weak coupling).

Most importantly, we demonstrated the possibility to control the ground state concentration, the coupling strength, and the dye emission spectra with Q-switched laser pumping, Fig. 2. More theoretical and experimental studies are required to fully explore this intriguing phenomenon.

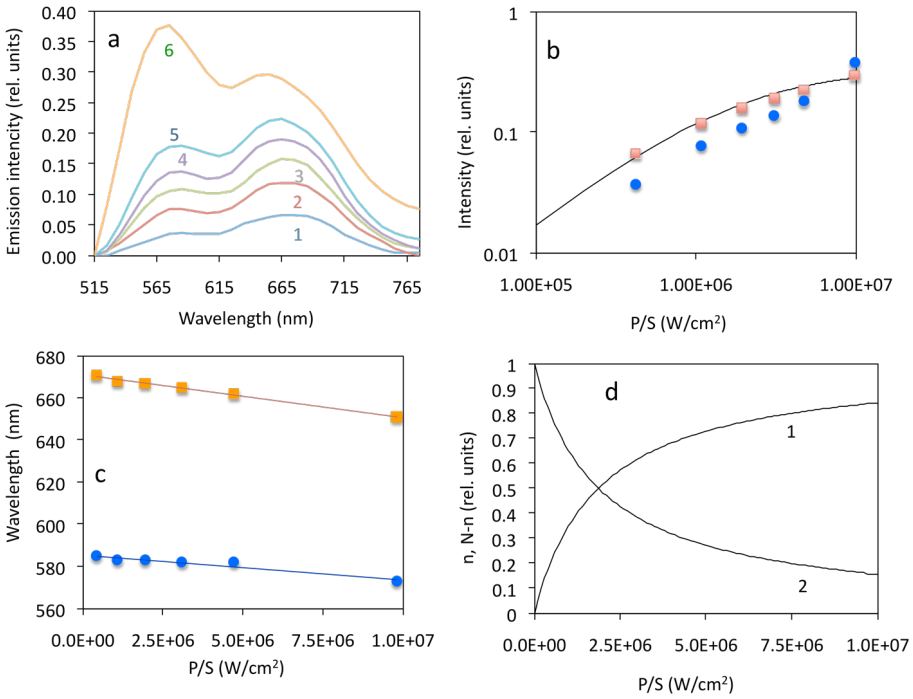

Figure 2. CONTROL OF STRONG COUPLING WITH PUMPING INTENSITY. (a) Emission spectra of the Fabry-Perot cavity (d=205 nm, c=200 g/l) measured in p polarization at different peak pumping intensities: 4.2×10^5 W/cm^2 (trace 1), 1.1×10^6 W/cm^2 (trace 2), 1.9×10^6 W/cm^2 (trace 3), 3.1×10^6 W/cm^2 (trace 4), 4.7×10^6 W/cm^2 (trace 5), 9.8×10^6 W/cm^2 (trace 6). The spectra demonstrate the saturation of the emission intensity and its spectral shift with increase of the pumping power. (b) Pumping power dependence of the emission intensity originating from the lower "cavity emission" branch of the dispersion curve (orange squares) and the upper "exciton emission" branch of the dispersion curve (blue circles). Solid line is the fitting with the analytical model. (c) Wavelengths positions of the emission maxima at different pumping intensities. Orange squares: "cavity emission" branch, blue circles: "exciton emission" branch. (d) Saturation of the population of the excited state n, trace 1, and depopulation of the ground state (N-n), trace 2, calculated using analytical model.

SECTION 2. LIGHT-MATTER INTERACTIONS IN MINIATURE PLASMONIC AND PHOTONIC LASERS

2.1 Surface Emitting Plasmonic Laser with Distributed Feedback [3P]

[In collaboration with Menon group, CUNY]

Plasmonic lasers are of great interest to scientists and engineers due to their small size, which can be of the order of ~10 nm [1], and potential applications ranging from telecommunication and nanocircuitry to sensors and biomedical imaging. Lasers based on propagating surface plasmons (also known as surface plasmon polaritons, SPPs), although less compact, have advantages over their localized plasmon counterparts (spasers) because of a much smaller threshold gain. Many such lasers, operating with and without intentional feedback, have been discussed in the literature. The most relevant to the present study, is the plasmonic laser with the distributed feedback (DFB) reported in Ref. [2]. In Ref. [2], the laser beam was outcoupled from the end of the DFB strip, in the plane of the grating, which required fabrication of the high-quality edge of the sample. In our work, we took one step further and demonstrated a low-threshold DFB laser emitting from the whole pumped area at the angle ~30^o relative to the normal of the surface.

In a plasmonic DFB laser, the forward and backward surface waves propagating in a periodic array of elements (which can be implemented *via* periodic modulation of the refractive index or the system's geometry), are coupled to each other if the vacuum wavelength λ_0 is equal to: [3]

$$\lambda_0 = 2n_{sw}\Lambda/m \quad \Leftrightarrow \quad n_{sw}k_0 = \frac{m}{2}G, \tag{1}$$

where n_{sw} is the effective refractive index of the (plasmonic) surface wave, Λ is the period of the grating, G is the corresponding wavenumber, k_0 is the photon wavenumber in vacuum and m (the Bragg's order) is an integer number. The surface plasmon (or SPP) wave with the wavenumber $n_{sw}k_0$ propagating perpendicular to the grooves of the grating can be decoupled at the angle, q_0 given by the equation

$$k_0 \sin(\theta_0) = n_{sw}k_0 - G, \tag{2}$$

where + and – signs in front of the terms $n_{sw}k_0$ and G were chosen to correspond to our experiment described below. Combining Eqs. 1 and 2 one gets

$$\sin(\theta_0) = \left(\frac{m}{2} - 1\right)\frac{G}{k_0} \text{ and} \tag{3}$$

$$n_{sw} = \frac{m}{2}\frac{G}{k_0}. \tag{4}$$

These equations will be used at the analysis of the DFB laser.

Sample description

Our experimental sample consisted of the (1) S-1805 positive photoresist grating, deposited on top of glass using the holographic lithography technique (325 nm HeCd laser, period Λ=583 nm), (2) ~60 nm layer of Ag deposited on top of the photoresist grating, and (3) 3.0 μm thick layer of the PMMA polymer doped with the R6G laser dye in concentration 6.0×10^{-2} mol/L (in solid state), Fig. 1a. The sample was pumped with ~10 ns pulses of the frequency doubled Q-switched Nd:YAG laser at λ=532 nm. The laser beam was lightly focused to the spot with the area 0.06 cm^2. The sample's emission was collected with an optical bundle and directed to the input slit of a monochromator. The signal was detected with the photomultiplier tube (PMT), attached to the monochromator's output slit and processed using a combination of the boxcar integrator and lock-in amplifier.

The series of emission spectra taken at several gradually increasing pumping energies, in the direction normal to the sample's surface (Fig. 1b), shows transformation from the spontaneous emission, with the maximum at λ~585 nm, to the predominantly stimulated emission, which is manifested by the growth of the λ=601 nm peak. This emission is nearly polarization independent and its relatively large spectral width is consistent with the stimulated emission without intentional feedback (or amplified spontaneous emission, ASE), which can originate from both (i) SPPs scattered by unintentional defects or (ii) the volume of the dye-doped polymer.

At the same time, we have observed two narrow laser beams propagating at the angle θ_0~30°, on both sides of the sample's surface. Their well-defined slightly elongated spots had yellowish color that were distinctly different from the orange ASE background, Fig. 1c. The corresponding spectral line was ~1 nm wide and had a maximum at 585.5 nm – nearly 15 nm away from the maximum of the ASE band, Fig. 1b. This emission was purely TM polarized (compare Fig. 1c and Fig. 1d), which is consistent with its surface plasmon origin. By recording a series of emission spectra corresponding to different pumping powers, we were able to plot the input-output curve (inset of Fig. 1b) and evaluate the threshold pumping density, 1.2 mJ/cm^2, which was very close to that of the broad-band stimulated emission recorded in the normal direction and nearly six times smaller than the threshold pumping density reported in the DFB plasmonic laser in Ref. [2]. The arching lines seen on the screen next to the laser spot (Figs. 1c and 1d) are due to diffraction of the partly coherent ASE emission by the grating – the phenomenon, whose detailed study will be reported elsewhere. The well-defined laser beam and the narrow spectral line (whose spectral position is close to, although not identical to the maximum of the gain band and ASE) are indicative of the stimulated emission with a feedback. Furthermore, the distinct polarization dependence of the laser intensity is consistent with its surface plasmon origin.

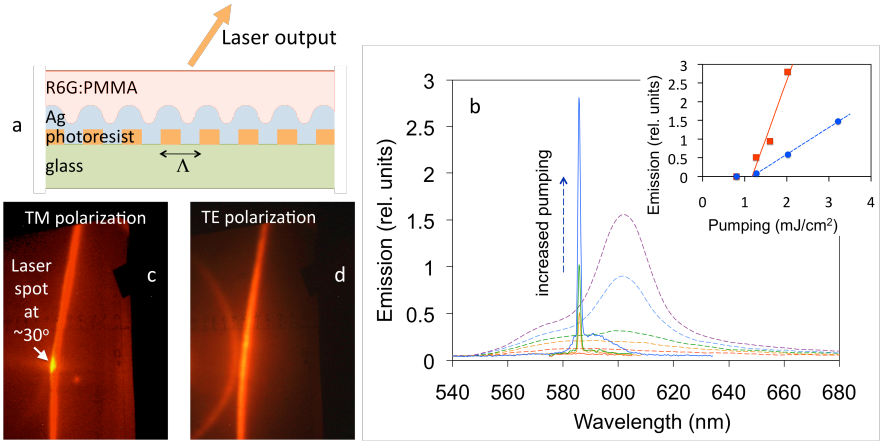

Fig. 1. (a) Schematics of the plasmonic laser. (b) The series of emission spectra recorded at several pumping energies recorded at the position of the laser spot (solid lines) and at the direction normal to the grating surface (dashed lines). Inset: Corresponding input-output curves measured at the laser spot (red squares) and at the normal direction (blue circles). (c) Laser spot on the white screen, recorded in TM polarization at ~30° from the normal to the sample. (d) Photograph of the same screen in TE polarization does not show any laser spot.

Substituting experimental values of G, k_0 and θ_0 to Eq. 3, we have determined m=3.00, which is very close to integer 3. Assuming that the surface wave is a SPP, we find from Eq. 4, n_{sw}=1.50. However, at λ_0=585.5 nm, the refractive index of the SPP wave is equal to $n_{sw} = \sqrt{\varepsilon_m \varepsilon_d / (\varepsilon_m + \varepsilon_d)}$ =1.62. (Here ε_m is the dielectric permittivity of Ag [4] and ε_d is that of the dye doped PMMA [5]. The latter modest discrepancy can be explained by the fact that the values of dielectric permittivities in our experimental sample slightly deviate from those known in the literature. Alternatively, the surface wave might not be a pure SPP but rather a hybrid SPP-related mode supported by a waveguide formed by Ag grating on one side and the polymer/air interface on the other side. The detailed discussion and analysis of the demonstrated laser will be presented at the conference.

[1] M. A. Noginov et al., "Demonstration of a spaser-based nanolaser," Nature **460**, 1110-1112 (2009).

[2] E. K. Keshmarzi, R. N. Tait, P. Berrini, "Surface plasmon distributed feedback lasers", PQE-2017, Jan, 8-13, 2017, Snowbird, Utah, USA.

[3] O. Svelto, *Principles of Lasers* (Springer, 2010).

[4] P. B. Johnson and R. W. Christy, "Optical Constants of the Noble Metals," Physical Review B **6** (12), 4370--4379 (1972).

[5] N. Sultanova, S. Kasarova and I. Nikolov. "Dispersion properties of optical polymers," Acta Physica Polonica A **116**, 585-587 (2009).

2.2 How do the Purcell factor the Q-factor and the beta factor affect the laser threshold? [6C]

[In collaboration with J. B. Khurgin, Johns Hopkins Univ.]

As lasers get more and more miniaturized and their dimensions become comparable to the wavelength, two interconnected phenomena take place: the fraction of spontaneous radiation going into a specific laser mode (β-factor) increases and can ultimately reach unity, while the radiative lifetime gets shortened by the Purcell factor F_p. Often it is assumed that increase of these two factors, along with the quality factor (Q-factor), almost invariably causes reduction of the lasing threshold. We test this assumption on various photonic and plasmonic lasers, and show that, while there is obvious correlation between the

aforementioned factors and the laser threshold, the dependence is far from being straightforward and omnipresent. Depending on specific laser material and geometry, the threshold can decrease, increase, or stay unchanged when β-factor, Q-factor, and F_p increase. For the most part, the reduction of threshold is achieved simply by reducing the laser volume and this volume reduction can concurrently cause the increase in β-factor and/or Purcell factor, but it would be imprudent to say that the increase in either of these factors is the cause of threshold reduction.

SECTION 3. PLASMON DRAG

[Noginova group]

3.1 Plasmon drag effect with sharp polarity switching [4P]

The generation of significant photocurrents observed in plasmonic metasurfaces is interesting from a fundamental point of view and promising for applications in plasmon-based electronics and plasmonic sensors with compact electrical detection. We show that photoinduced voltages in strongly modulated plasmonic surfaces demonstrate a highly asymmetric angular dependence with polarity switching around the plasmon resonance conditions. The effects are tentatively attributed to coupling between localized and propagating plasmons.

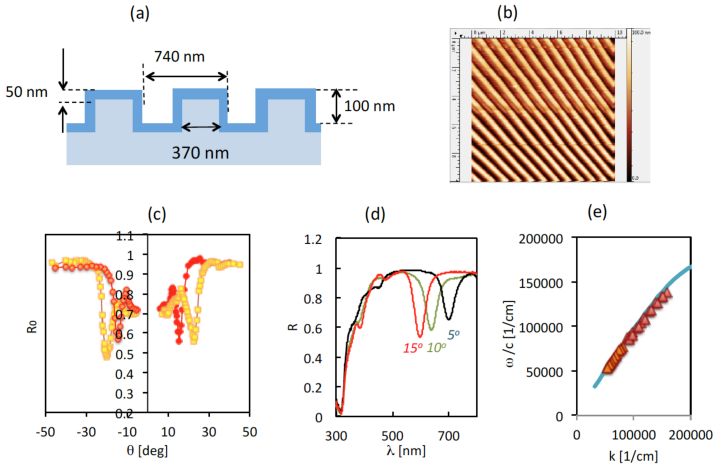

Fig. 1. (a) Schematics and (b) AFM image of Ag/DVD structures; (c) Reflectivity *vs* angle for λ = 585 nm (yellow) and 632.8 nm (red); (d) Reflection spectra at p polarization and various orientations as indicated; (e) SPP dispersion relationship, Ag/DVD (points) and estimation for flat films, Eq. 2 (solid trace).

3.2 Plasmon related electrical effects in strongly modulated metasurfaces [5P]

Photogeneration of significant electrical voltages observed in plasmonic metasurfaces is promising for applications in plasmon-based electronics and plasmonic sensors with compact electrical detection. In order to better understand the role of the surface geometry, we study photoinduced electrical effects in profile-modulated plasmonic surfaces. Photoinduced voltages in strongly modulated plasmonic surfaces demonstrate highly asymmetric angular dependence with polarity switching at the plasmon resonance conditions. The effects are attributed to coupling between localized and propagating plasmons and discussed in the frame of the electromagnetic momentum loss approach.

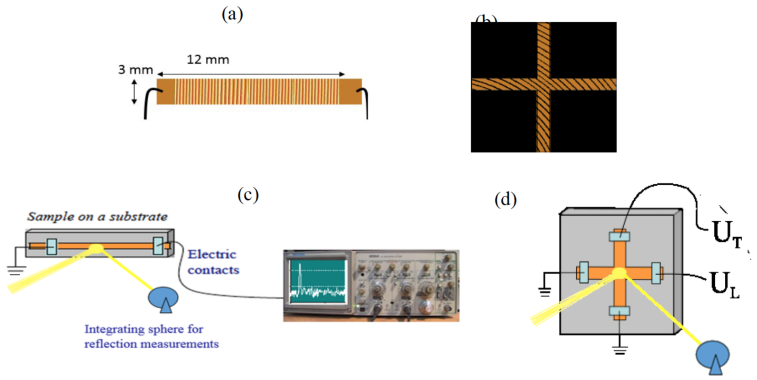

(a) and (b) Schematics of the experimental samples. (c) and (d) Experimental setup and geometry of the sample orientations.

3.3 Extreme sensitivity of plasmon drag to surface modification [7C]

Plasmon-induced photocurrents in 1D profile modulated structures switch their polarity in the presence of an additional monolayer at the metal-dielectric interface. The effect presents opportunities for compact plasmonic sensors with electrical detection.

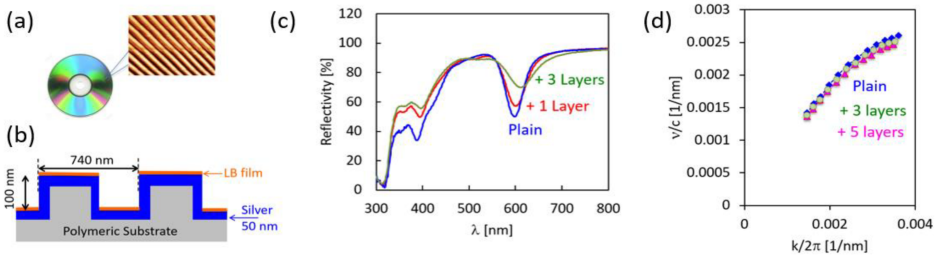

Fig. 1. (a) Nanostructured substrate (AFM image) is derived from Verbatim DVD-R; (b) Schematic of the sample with mono- or multilayer film deposited with LB method; (c) Reflectivity spectra at p-polarization before (plain) and after deposition of LB films; (d) Dispersion curves for 1-d order SPP with different number of layers

3.4 Magneto-dependent plasmon drag in permalloy structures [8C]

Plasmon-enhanced photovoltages in 1D profile-modulated permalloy films strongly depend on magnetic field, with a characteristic hysteresis. The effect is discussed in terms of the anomalous Nernst effect.

SECTION 4. DEVELOPMENT OF METAMATERIALS AND DEVICES

4.1 Low-loss volume modes in a lamellar hyperbolic metamaterial slab [6P]

[In collaboration with Australian National University and ITMO (Russia)]

We have studied, theoretically and experimentally, coupling to propagating volume (or bulk) modes in a lamellar Ag/MgF_2 hyperbolic metamaterial.

In the metamaterial comprised of 20 pairs of Ag(25nm)/MgF_2(35nm) layers (Fig. 1), the propagation length of the fundamental bulk mode was predicted to be equal to L=44 μm, and even longer propagation lengths are expected at larger numbers of layers. These long propagation lengths, which are of high technological importance to photonic circuits and stimulated emission at the nanoscale, motivated our studies.

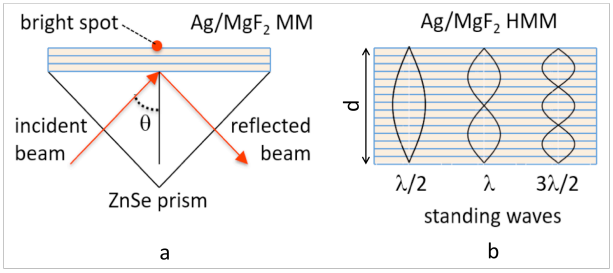

Fig 1. (a) Schematics of the experimental sample: alternating 25 nm Ag and 35 nm MgF_2 layers deposited onto a high-index ZnSe prism. (b) First three standing wave modes supported by the lamellar metamaterial slab.

Consistent with the modes' low loss and large propagation lengths, is the highly efficient light penetration (down to the back wall of the metamaterial's slab) through tens of Ag layers, whose cumulative thickness can be as large as 500 nm (Fig. 2).

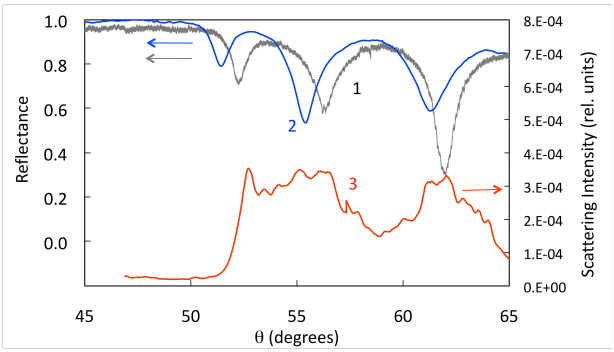

Fig. 2. Trace 1: Experimental reflectance profile in the sample (fabricated using thermal vapor deposition technique) consisting of 10 pairs of Ag/MgF_2 layers. Trace 2: Same for the sample with 20 pairs of Ag/MgF_2 layers. Trace 3: Intensity of the bright spot visible on the back side of the sample (collected using CCD camera).

The modes' refractive indices are strongly affected by theroughness of Ag layers, which had to be taken into account in order to obtain a good agreement between the theory and the experiment. The high sensitivity of the volume modes to the surface roughness can be a detrimental factor in device applications.

4.2 Ultra-sensitive plasmonic sensing based on gold nanostrip arrays [7P]

[Noginova group]

The extra-narrow reflection feature in angular dependence of reflectivity of periodic gold nanostrip arrays presents interest for sensing application. We explore its behavior in a modified dielectric environment and characterize the capability for sensing small changes in the dielectric permit tivity of the environment.

Gold nanostrip arrays demonstrate an extrasharp feature in reflection, which, depending on environment, can be observed as a sharp maximum or sharp drop in the an- gular profile of reflectivity. This feature is likely originated from the interaction of the collective plasmonic mode and diffraction. We experimentally demonstrate the opportunity to resolve small changes in the dielectric permittivity of the environment and estimate the characteristic parameters for this sensing approach. Since this feature is associated with plasmonic excitations, which are confined to the surface, it is promising for applications where small volumes of the testing material are used.

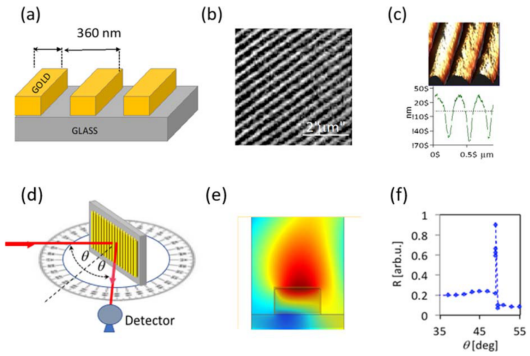

Fig. 1. (a) Schematics of the gold strip array; (b) SEM image; (c) AFM image (top) and corresponding profile (bottom); (d) measurement setup; (e) H-field at the plasmon resonance conditions at air–gold interface; (f) angular dependence of the reflected intensity in air.

Part 3

Aug. 1, 2020 – July 31, 2021.

ABSTRACT

The main goal of this project is to study how physical and chemical properties of organic matter can be controlled in strong and weak light-matter interaction regimes. In the first two years, the studied metal-dielectric environments were homogeneous plane films and lamellar stacks. At this time, we report the effects of random nanostructured environments on the light-matter coupling, emission, energy transfer, and rates of electrochemical reactions. In Section 1 of this report, we describe fabrication and studies of optical properties of two tunable composite materials: (i) nanoporous gold leaves [1P,1C] and (ii) flexture-controlled composite Au/dye/polymer films [2P]. In Section 2, we report the effects of nanoporous gold foams on light-matter coupling and concentration quenching (Förster energy transfer) [3P,2C-4C]. The effects of randomly nanostructured metallic coatings on rates of electrochemical reactions [5C] are discussed in Section 3. Development of miniature lasers is one of the important goals of the light-matter interaction research, reported in Section 4. Toward this end, we demonstrared all-dielectric thin film laser operating in the vicinity of the critical angle [4P,6C] and have published the tutorial paper explaining the effects of the Purcell factor, the mode volume, and the quality factor on the efficiency of microscale and nanoscale lasers [5P]. The research aimed at effects of metal-dielecrtic environments on two-photon absorption (TPA) in laser dyes is discussed in Section 5 [6P]. Several other publications and presentations acknowleging the grant [7P-12P,7C-10C] are not discussed for brevity.

CONTENTS

The Technical Report is organized as follows.

PUBLICATIONS

[1P] Sangeeta Rout, Zhen Qi, Monika M Biener, Devon Courtwright, Jakeem C Adrien, Ezekiel Mills, Mohammad Shahabuddin, Natalia Noginova, Mikhail A Noginov, "Nanoporous gold nanoleaf as tunable metamaterial", Scientific Reports, 11, 1795 (2021). https://doi.org/10.1038/s41598-021-81128-4

[2P] D. Courtwright, S. Rout, J. Adrien, M. A Noginov, "Effect of flexural stress on fabrication and optical properties of a composite photonic material", Journal of Nanophotonics 15, 026002 (2021). https://doi.org/10.1117/1.JNP.15.026002

[3P] Sangeeta Rout, Zhen Qi, Ludvig S. Petrosyan, Tigran V. Shahbazyan, Monika M. Biener, Carl E. Bonner and Mikhail A. Noginov, "Effect of Random Nanostructured Metallic Environments on Spontaneous Emission of HITC Dye", Nanomaterials, 10, 2135 (2020). doi:10.3390/nano10112135.

[4P] Joshua K. Asane, Md G. R. Chowdhury, Kanij M. Khabir, Viktor A. Podolskiy, and Mikhail A. Noginov, "Stimulated emission in vicinity of the critical angle", Appl. Phys. Lett. 119, 031102 (2021); doi: 10.1063/5.0051901.

[5P] J. B. Khurgin, M. A. Noginov, "How Do the Purcell Factor, the Q-Factor, and the Beta Factor Affect the Laser Threshold?, Laser & Photonics Reviews, 2000250 (2021). https://doi.org/10.1002/lpor.202000250

[6P] J. K. Asane, M. A. Noginov, "Concentration dependence of two-photon absorption in PMMA polymeric films doped with rhodamine laser dyes", JOSA B, 37, 3108-3115 (2020). https://doi.org/10.1364/JOSAB.399318

[7P] Md Omar Faruk, Nelly Jerop, Mikhail A. Noginov, "Emission of R6G dye in Fabry–Perot cavities in weak and strong coupling regimes", JOSA B, 37, 3200-3212 (2020). https://doi.org/10.1364/JOSAB.403612

[8P] S. Koutsares, L. S. Petrosyan, S. Prayakarao, D. Courtwright, C. E. Bonner, T. V. Shahbazyan, M. A. Noginov, "Effect of metallic substrates and cavities on emission kinetics of dye-doped polymeric films", JOSA B 38, 88-94 (2021). https://doi.org/10.1364/JOSAB.409998

[9P] T. RonurPraful, N Jerop, A Koech, K Thompson, N Noginova, "Extreme sensitivity of plasmon drag to surface modification, " J. Phys. D: Appl. Phys. 54 035307 (2021).

[10P] V. A. Atsarkin, N. Noginova, "Electron Spin Resonance on the Border Between Para-and Ferromagnetism: Quantum versus Classical," Appl. Magn. Res. 51, 1467–1480(2020) (2020)

[11P] M Shahabuddin, DW Keene, M Durach, VS Posvyanskii, VA Atsarkin and N. Noginova "Magnetically dependent plasmon drag in permalloy structures, "JOSA B 38 (6), 2012-2018 (2021).

[12P] N. Noginova, V. Gubanov, M. Shahabuddin, Yu. Gubanova, S. Nesbit, V. V. Demidov, V. A. Atsarkin, E. N. Beginin, A. V. Sadovnikov, "Ferromagnetic Resonance in Permalloy Metasurfaces", Applied Magnetic Resonance **52**, 749–758 (2021).

CONFERENCE PRESENTATIONS

[1C] S. Rout, Z. Qi, M. Biener, D. Courtwright, J. Adrien, M. Shahabuddin, C. E. Bonner Jr., N. Noginova, M. A. Noginov, "Tunable optical properties of nanoporous gold leaf metamaterials," Proc. SPIE 11460, Metamaterials, Metadevices, and Metasystems 2020, 1146023 (20 August 2020); https://doi.org/10.1117/12.2571003

[2C] Vanessa N. Peters, Srujana Prayakarao, Samantha R. Koutsares, Sangeeta Rout, Carl E. Bonner and Mikhail A. Noginov, "Control of Physical Phenomena with Nonlocal Metal−Dielectric Environments" Metanano, online conference https://metanano.itmo.ru, Sept. 14-18, 2020 (***keynote***).

[3C] M. A. Noginov, “Control of emission and energy transfer with nonlocal metal-dielectric environments”, The Triangle Hard Matter Workshop hosted by Duke Materials Initiative, online conference, December 8, 2020 (***invited***).

[4C] Mikhail A. Noginov, “Control of Physical Phenomena with Nonlocal Metal-Dielectric Environments”, Strong Coupling with Organic Molecules (SCOM) virtual conference, April 26 – April 28, 2021 (original intended location: Gothenbirg, Sweden), *invited*.

[5C] A. Wilson, M. Shahabuddin, Md. Rab, J. Grace, N . Noginova, "Probing charge kinetics in plasmonic environment with cycllic voltammetery, " Material Research Society Meeting, April 2021.

[6C] Joshua Asane, Md Golam Chowdhury, Kanij Khabir, Viktor Podolskiy, Mikhail Noginov, ”Stimulated Emission With Evanescent Gain in the Total Internal Reflection Geometry”, CLEO Conference (virtual), May 9 – May 14, 2021, paper JW1A.128.

[7C] Sangeeta Rout, S. Koutsares, D. Courtwright, E. Mills, A. Shorter, S. Prayakarao, C. Bonner, Mikhail Noginov, “Effect of Thickness of a Dye-Doped Polymeric Film on the Concentration Quenching of Luminescence”, CLEO Conference (virtual), May 9 – May 14, 2021, paper JW1A.96.

[8C] T. Ronurpraful, N. Jerop, A. Koech, K. Thompson, and N. Noginova, “Electrical detection of surface modification in plasmonic metasurfaces”, SPIE-Metamaterials, Metadevices, and Metasystems 2020, 2020.

[9C] D. Keene, M. Shahabuddin, T. Ronurpraful, M. Durach and Noginova, N., Plasmon-related electric effects in various plasmonic materials. Bulletin of the American Physical Society, March 2021 #S41.00007.

[10C] J. Munga, T. Ronurpraful, D. Keene, Md. Rab, N. Jerop, F. Bett, M. Durach and N. Noginova, Enhancement of electric and magnetic emission in lLangmuir blodgett films and sandwich structures with Eu3+ ions. Bulletin of the American Physical Society, March 2021.

TECHNICAL REPORT

SECTION 1. RANDOM NANOSTRUCTURED METAL-DIELECTRIC COMPOSITE MATERIALS

1.1. Nanoporous gold nanoleaf as tunable metamaterial [1P,1C]

Abstract: We have studied optical properties of single and multi-fold nanoporous gold leaf metamaterials and demonstrated that they can be controlled with applied voltage and dielectric environment [1P,1C].

Complex metal-dielectric environments, including metamaterials, plasmonic structures, and Fabry-Perot cavities, have been demonstrated to control scores of phenomena including spontaneous and stimulated emission, Förster energy transfer, van der Waals interactions, and chemical reactions. At this time, we report studies and real-time control of optical properties of nanoporous gold leaves (NPGLs) – unique centimeter-size and ~100 nm thick multilayered (meta) materials.

The NPGL samples have been prepared from one layer of 12 K gold leaf through dealloying in 10 ml of concentrated HNO_3 (68%, ACS, VWR) solution at room temperature for one hour. Different thicknesses of the fabricated samples, ranging from 84 nm to 943 nm, were achieved by folding one layer of the gold leaf once (two layers), twice (four layers), and three times (eight layers). The dealloying parameters for all samples studied were nominally the same, resulting in pore diameters (in different samples) ranging from 20±3 nm to 27±3 nm. The NPG leaf was rinsed thoroughly in DI water for at least three times after the dealloying process before being transferred onto glass substrates. Finally, the fabricated samples were dried in air before taking any measurements. The scanning electron microscope (SEM) image of a single-layer Au nanoleaf sample is depicted in Fig. 1a.

The results of the transmittance measurements are summarized in Fig. 1b. The reference sample, 90 nm thick gold film deposited on glass, had the transmission maximum at 505 nm, near to epsilon-near-zero (ENZ) point for Au. At the same time, Au nanoleaf samples had two transmission peaks. The first had its maximum almost at the same wavelength as the transmission peak in a smooth Au film, while the second was shifted to longer wavelengths (up to 605 nm). The characteristic “wiggles” could be seen in the reflection spectra of the nanoleaf samples at the wavelengths corresponding to both transmission maxima. (Note that qualitatively similar double peak transmission spectra were obtained when Au films were deposited on nanoporous alumina membranes. However, the effect was not universal and the spectra of gold-coated polymers with micro-bubbles were quite different [2P].)

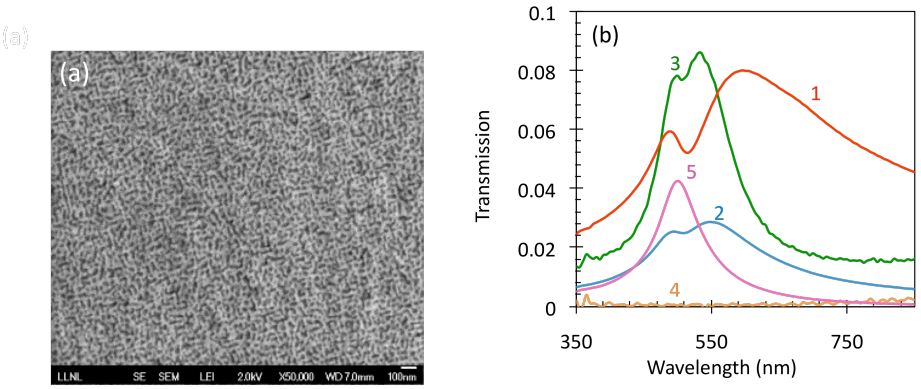

Figure 1. (a) SEM image of the single-layer Au nanoleaf sample. (b) Transmission spectra of a single-layer (trace 1), two-layers (trace 2), four-layers (multiplied by 100, trace 3) and eight-layers (multiplied by 100, trace 4) NPGLs. Control sample: 90 nm Au film (trace 5).

With increase of the number of layers, the width of the long-wavelength transmission peak got reduced and its spectral position was shifted to shorter wavelengths. This could be the effect of (i) the overall thickness of NPGL layers or (ii) the (coincidental) effect of the sizes of voids or ligaments, which were slightly different in different samples. (More studies are needed to differentiate between the two possible causes of the spectral shifts.) The absorbance [A=-log(T)] calculated for both transmission maxima, grew almost linear with the thickness of (single-layer or multi-layer) nanoleaf samples, in a good agreement with the Beer's law. This result is not trivial, since strong diffusion (and deviation from the Beer's law) could be expected in the highly scattering samples.

When Au nanoleaf was placed in water, its long-wavelength absorption peak moved slightly (by ~10 nm) to shorter wavelengths, while the short-wavelength peak practically did not change its spectral position. This result is in qualitative agreement with Ref. [1]. However, the spectral shift in our studies is smaller than that reported in [1]. Different behavior of the short-wavelength and long-wavelength transmission peaks suggests that they have different nature.

To tune the optical properties of NPGL, we placed the sample in a two-electrode electrochemical cell. Gold nanoleaf, with attached copper tape conduit, served as a working electrode, while the a platinum wire played a role of a counter electrode. Following [2], the electrolyte was 0.7 M solution of NaF in water. The applied voltage, varied between -2V and +2V, caused changes in both strength (~10%) and the wavelength position ($\Delta\lambda$~20 nm) of the long-wavelength transmission peak. These changes in the optical spectra were, presumably, due to change in the charge density [2]. However, in contrast to [2], larger spectral changes in our experiment were observed when negative (rather than positive) voltage was applied to the gold leaf.

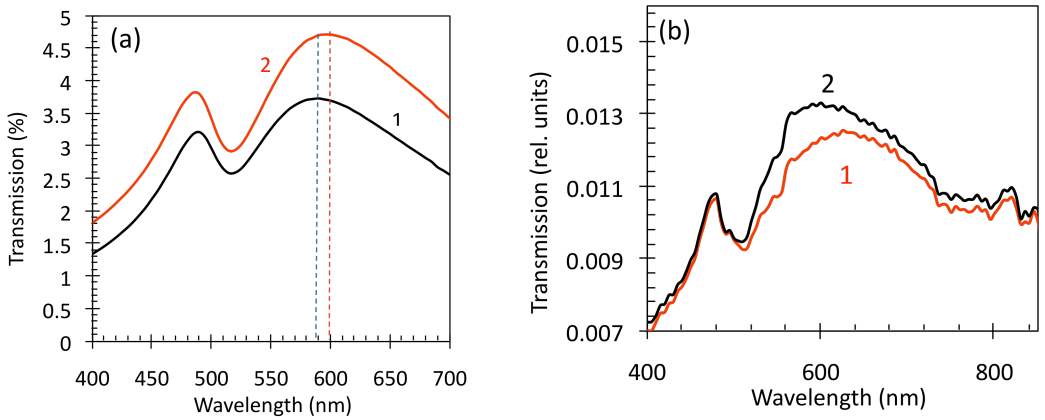

Figure 2. (a) Transmission spectra of the Au nanoleaf in air (trace 1) and water (trace 2). (b) Transmission spectra of Au nanoleaf in electrochemical cell at applied positive voltage (+1.5V, trace 1) and negative voltage (-2V, trace 2).

In Ref. [3], it has been shown that the vicinity of metallic (Ag) films or lamellar metal/dielectric structures helps to reduce the rate of concentration quenching of the HITC laser dye. In our preliminary studies, we have found that Au nanoleafs inhibit concentration quenching even stronger than smooth gold films do. Real-time control of the dye emission with active and tunable Au nanoleaf metamaterials is the subject of future studies.

To summarize, we have studied optical properties of single and multi-fold nanoporous gold leafs and demonstrated that they can be controlled with applied voltage as well as dielectric environment. The experimental results, their analytical modeling and tentative explanation will be discussed in more detail at the conference.

[1] X. Lang, L. Qian, P. Guan, J. Zi, and M Chen, "Localized surface plasmon resonance of nanoporous gold", Appl. Phys. Lett., 98, 093701 (2011).

[2] D. Jalas, L. Shao, R. Canchi, et al. "Electrochemical tuning of the optical properties of nanoporous gold", Sci Rep 7, 44139 (2017).

[3] S. Prayakarao, S. R. Koutsares, C. E. Bonner, and M. A. Noginov, “Effect of nonlocal metal–dielectric environments on concentration quenching of HITC dye”, JOSA B, 36, 3579-3587 (2019).

1.2 Effect of flexural stress on fabrication and optical properties of a composite photonic material [2P]

Abstract: We spin coated thin films of PMMA polymer doped with HITC laser dye onto microscope cover slides under applied flexural stress and found the patterns of scattering (milkiness) to correlate with the spatial variation of the pressure pattern. We further deposited thin gold films on top of the HITC:PMMA films and measured highly unusual transmission spectra of Au collected from strongly deformed (stressed) local areas of the sample. These spectra, which strongly deferred from those of plain Au films deposited onto unstressed glass, could not be described by simple, e.g. Maxwell Garnett, effective media models, calling for a thorough theoretical study.

In sample preparation, poly(methyl) methacrylate (PMMA) polymer (with an average molecular weight 120,000) was dissolved in a dichloromethane (DCM) solvent, in concentration 116 g/l, and sonicated, at room temperature, for a total of 90 minutes. A laser dye, 2-[7-(1,3-Dihydro-1,3,3-trimethyl-2H-indol-2-ylidene)-1,3,5-heptatrienyl]-1,3,3-trimethyl-3H-indolium iodide (HITC), was added to the polymer solution for better visibility, as discussed below, in the concentration 30 g/l (in solid state). The solution was then spin coated onto 0.2 mm thick glass cover slips from VWR, using a 6800 Spin Coater from Specialty Coating Systems with an applied vacuum pressure of approximately 2 psi (according to the manufacturer’s specifications). The spin coating was performed at 555 RPM for 3 seconds, followed by 5000 RPM for 25 seconds, and finally at 7500 RPM for 16 seconds. By using the relatively high concentration of PMMA in DCM, the films were intentionally made scattering (milky) to provide for visibility of the patterns discussed below, Fig. 1a.

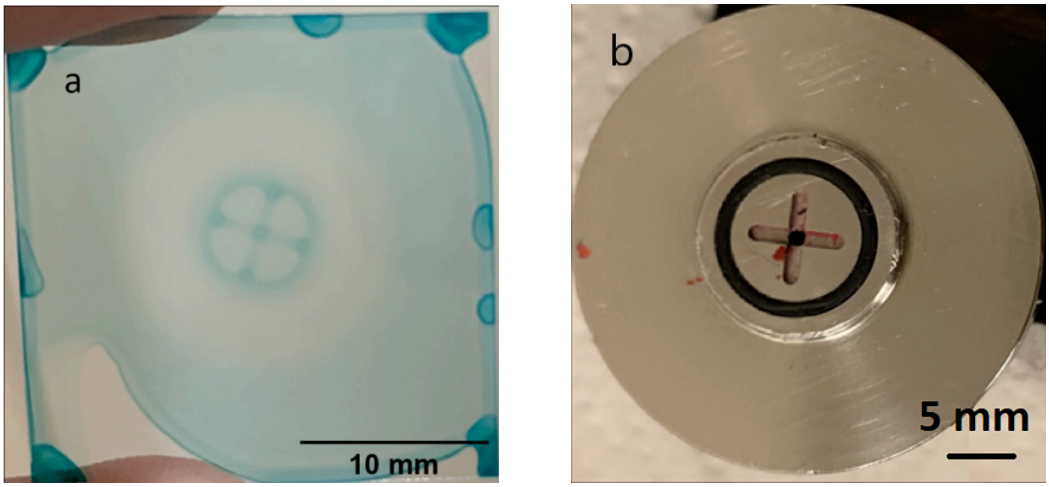

Figure 1. (a) HITC:PMMA film deposited onto 25x25 mm glass slip at applied flexural stress (vacuum suction). (b) Photograph of the chuck holding the sample, showing the hole for the vacuum suction, two slits forming a cross, elevated metallic ring and the rubber o-ring (black).

The chuck of the spin coater, holding the sample by applied vacuum, had a small hole in the center for a vacuum suction, o-ring for keeping the vacuum, and two slits (forming a cross) for a uniform distribution of the vacuum, Fig. 1b. As we see below, the latter functionality was not highly efficient and the stress applied to the sample by vacuum (strictly speaking, by atmospheric pressure) was highly non-uniform. As the vacuum was turned on, the glass slip bent, forming a bowl shape. Subsequently, the PMMA film was deposited onto a curved surface. In the end of the spinning cycle, when the rotation stopped, the vacuum was broken and the glass substrate with the deposited HITC:PMMA film popped up, becoming plane again.

Almost instantaneously, an intense greenish-bluish image of the cross and the ring appeared and become clearly visible (the greenish-bluish coloration was characteristic of HITC dye and was never observed in PMMA films without dye), Fig. 1a. This observation, suggesting that the flexural stress provided by vacuum is strongly inhomogeneous at the 1 mm scale, is one of the most intriguing results of this study. The thickness of the HITC:PMMA film measured (using DekTak XT stylus profilometer from Bruker) in the arm of the cross, 120 nm ±10%, was similar, within the experimental error, to that measured outside or the cross. We infer that the intense coloration of the cross and the ring were due to smaller amount of scattering in the respective local areas, determined by local non-uniformity of the flexure stress. (An alternative explanation accounting for a segregation of the dye molecules and their higher concentrations in the positions of the cross and the ring appears to be less likely.)

We then deposited thin Au films (using a Nano 36 thermal evaporator from Kurt J. Lesker) on top of HITC:PMMA films, with the images of the cross and the ring described above (Fig. 1a), photographed them (Fig. 2), and took their transmission and reflection spectra (using a Lambda 900 spectrophotometer, PerkinElmer) from the local areas corresponding to the arms of the cross and the spots outside of the ring and the cross (Fig. 3). The size of the light spot on the sample was 3.6 mm x 1.3 mm in the transmission experiments and 8 mm x 1.2 mm in the reflection experiments.

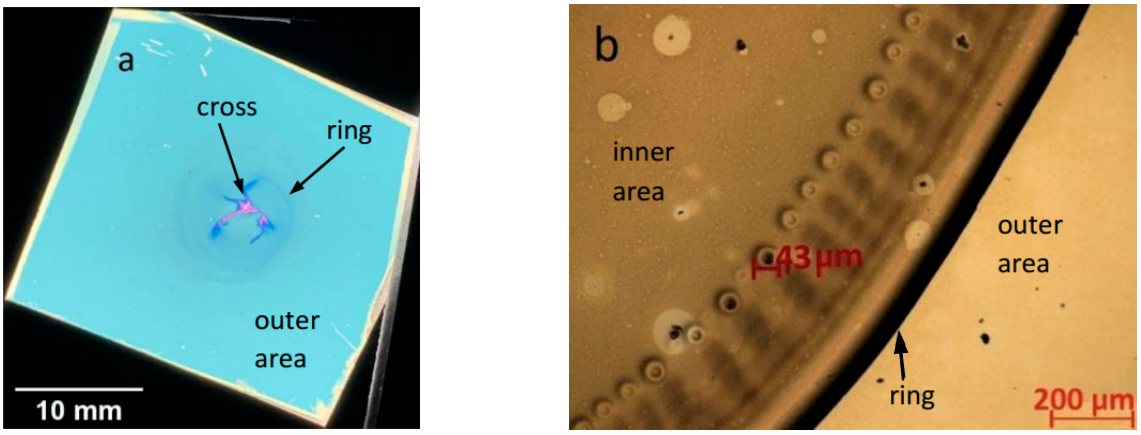

Figure 2. (a) Photograph of the glass slip sample with deposited HITC:PMMA and Au films, taken in the transmission mode. The greenish-bluish coloration dominating the area of the sample is characteristic of “regular” unstressed Au films, the deformed cross is pink and blue, while the ring surrounding the cross is grayish-bluish. (b) Photograph of the ring taken in the reflection mode. The 43 µm “crater” is one of many “open sphere” features created in the ring area in the course of fabrication.

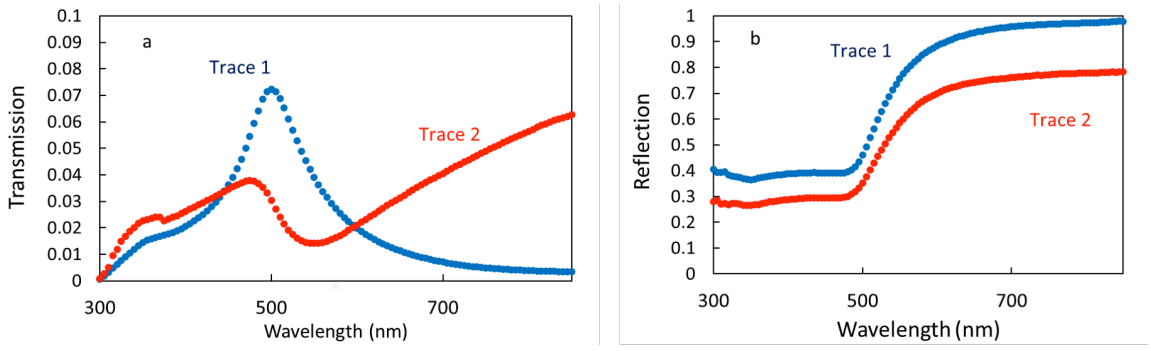

Figure 3. Transmission (a) and reflection (b) spectra of the HITC:PMMA films measured outside of the ring (trace 1) and in the position of the cross’ arm (trace 2).

Outside of the cross and the ring, the transmitted light was greenish-bluish (Fig. 2a), characteristic of thin Au films, and the transmission spectrum featured the well known peak at 500 nm, trace 1 in Fig. 3a. By comparing the experimental transmission spectrum with the one calculated using the on-line transfer

matrix solver, we evaluated the thickness of the gold film to be equal to 61 nm, while the thickness determined using the profilometer was ~40 nm. The characteristic reflection spectra of the "outer" area (outside of the ring) were typical of thin Au films, trace 1 in Fig. 3b.

At the same time, the transmission of the local areas with the patterned cross was strikingly different from that described above. Thus, in the arms of the cross, the transmitted light was pink and dark blue, see Fig. 2a. The corresponding transmission spectrum had the maximum at $\lambda \approx 470$ nm, the minimum at $\lambda \approx 550$ nm, and the growth (with increase of the wavelength) at $\lambda \geq 550$ nm, trace 2 in Fig. 3a. (In this particular measurement, the size of the focused light spot, 3.6 mm x 1.3 mm, was commeasurable with the arm of the cross, ~3 mm x 1 mm.) The corresponding reflection spectrum was not much different from that measured outside of the cross and the ring (Fig. 3b, trace 2), possibly because the size of the light spot in the reflection measurements (~8 mm x 1.2 mm) was significantly larger than the size of the cross' arm and most of the reflected light was coming from the low-stressed area. Microphotographs of the gold-coated samples showed neat rows of ~10 μm cavities or craters, Fig. 2b. However, the morphology features determining the color and the spectra of the transmitted light must be much smaller.

The dip in transmission at $\lambda \approx 550$ nm followed by the transmission's growth at the longer wavelengths is characteristic of gold nanospheres embedded into a dielectric matrix. Therefore, we attempted to fit the transmission and reflection spectra of the HITC:PMMA:Au films using the Maxwell Garnett model (for Au nanospheres in the HITC:PMMA matrix). We further used the known analytical formulas to calculate the reflection and transmission spectra of a three-layered structure, such as glass/HITC:PMMA:Au/air (assuming the thickness of the Au film to be 61 nm). Although a qualitative (but not quantitative) agreement between the experimental transmission spectra of the cross and those calculated at Au filling factors $f \leq 0.3$ can be seen, even a qualitative agreement ceases to exist, for the same filling factors, if the experimental and the calculated reflection spectra are compared to each other. On the other hand, a modest agreement between the experimental and the calculated transmission spectra of the composite material can be found at Au filling factor $f \geq 0.8$, far beyond the range of applicability of the Maxwell Garnett model, when the experimental and the calculated transmission spectra have nothing in common.

We, thus, conclude that the transmission and the reflection spectra of HITC:PMMA:Au composites cannot be described in term of the Maxwell Garnett model. We further ran the calculations for an "inverted" Maxwell Garnett model (for HITC:PMMA "bubbles" in a gold matrix) and the agreement between the experiment and the calculation was not any better. Application of more complicated effective media theories, such as Bruggeman model, Bergman-Milton model, *etc.*, is the subject of a separate study to be published elsewhere.

To summarize, we have demonstrated that optical properties of HITC:PMMA:Au composite materials can be strongly altered by flexural stress applied to thin glass substrates during the spin coating. While the pattern of the stress distribution was seen in scattering of HITC:PMMA films without any metal, the gold film, deposited on top of the stressed polymeric film, changed the color of the transmitted light from greenish-bluish to pink or dark blue. Particularly intriguing and important result of this study is the high spatial resolution of the stress pattern determining the composite's optical properties and dispersion, which can find application in controlling incident light and spontaneous emission.

SECTION 2. EFFECT OF RANDOM NANOSTRUCTURED METALLIC ENVIRONMENTS ON SPONTANEOUS EMISSION OF HITC DYE [3P,2C-4C]

[In collaboration with Shahbazyan group, Jackson State University]

Abstract: We have studied emission kinetics of HITC laser dye on top of glass, smooth Au films, and randomly structured porous Au nanofoams. The observed concentration quenching of luminescence of highly concentrated dye on top of glass (energy transfer to acceptors) and the inhibition of the concentration quenching in vicinity of smooth Au films were in accord with our recent findings. Intriguingly, the emission kinetics recorded in different local spots of the Au nanofoam samples had a spread of the decay rates, which was large at low dye concentrations and became narrower with increase of the dye concentration. We infer that in different subvolumes of Au nanofoams, HITC

molecules are coupled to the nanofoams weaker or stronger. The inhibition of the concentration quenching in Au nanofoams was stronger than on top of smooth Au films. This was true for all weakly and strongly coupled subvolumes contributing to the spread of the emission kinetics. The experimental observations were explained using theoretical model accounting for change in the Förster radius caused by the strong energy transfer to metal.

1. Experimental Samples

The metallic and dielectric host matrixes and substrates in our study included (i) nanostructured Au nanofoams, Figure 1, (ii) Au films deposited on glass, and (iii) glass (control samples). The HITC:PMMA dye-doped polymers, spin coated onto the substrates above, were 80 ± 10 nm thick and had the concentrations of HITC (2-[7-(1,3-dihydro-1,3,3-trimethyl-2H-indol-2-ylidene)-1,3,5-heptatrienyl]-1,3,3-trimethyl-3H-indoliumiodide) dye ranging between 3.2 g/L and 36.5 g/L in solid state. (1 g/L of HITC in poly (methyl methacrylate) PMMA is equivalent to 0.00186 mol/L and 1.23×10^{18} cm^{-3}).

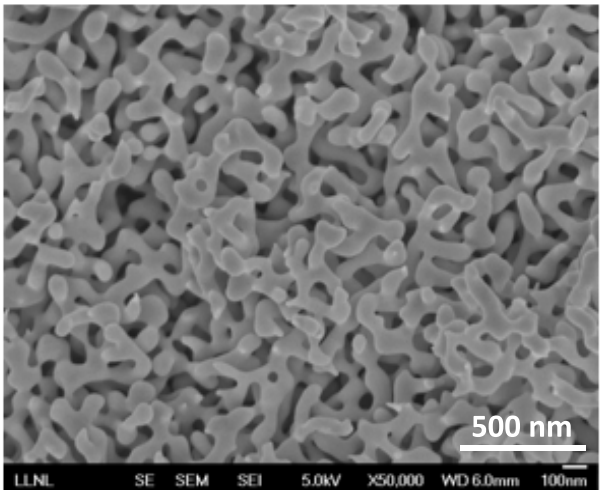

Figure 1. Scanning Electron Microscope (SEM) image of the Au nanofoam.

2. Spectroscopic Properties

As it was shown in our recent study, the absorption and excitation bands of HITC:PMMA films on glass have the maxima at 762 nm, and the emission band (the mirror image of the absorption band) has its maximum at 772 nm, Figure 2. The emission bands in HITC:PMMA films deposited on top of Au had a slight blue shift, which was much smaller than the emission bandwidth. The absorption spectra were taken using the spectrophotometer Lambda 900 (from PerkinElmer, USA) and the emission and excitation spectra were taken using the spectrofluorimeter (Fluorolog 3 from Horbia). Similar results were obtained in the present study, in which the same instruments were used in absorption, reflection and emission measurements.

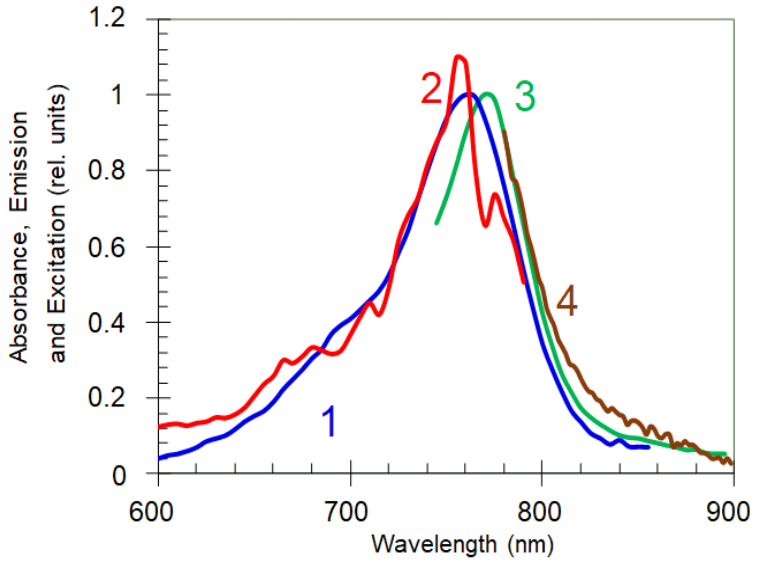

Figure 2. Absorption (trace 1), excitation (trace 2) and cw emission (trace 3) spectra of HITC:PMMA film on the glass substrate at the dye concentration equal to 8.5 g/L. Trace 4: emission spectrum at short-pulse pumping.

3. Emission Kinetics Measurements

In the emission kinetics measurements, the samples were excited at λ = 795 nm with ~150 fs pulses of the mode locked Ti:sapphire laser, Mira 900 (from Coherent, CA, USA). The diameter of the laser spot on the sample was ~2.5 mm and the average power (at 76 MHz repetition rate) was ~60 mW. The emission kinetics were recorded using the visible and near-infrared Streak Camera (Model C5680 from Hamamatsu, Japan). The measured width of the laser pulse, determined by the jitter of the laser and wide-open entrance slit of the streak camera was ~100 ps. A combination of the interference and long pass filters was used to block the laser light and transmit the HITC emission at λ ≥ 850 nm. Please note that some short-pulsed light (presumably laser light) leaked through the filters if the samples were scattering, e.g., Au nanofoams with or without dye, but not if smooth Au or glass substrates were used. To make sure that the scattered light did not interfere with our studies of the HITC emission, the kinetics were analyzed starting from 150 ps after the maximum of the laser pulse (after the scattered light was over).

4. Emission Kinetics in HITC:PMMA Films Deposited on Glass

The HITC emission kinetics in the samples with low dye concentrations ($n \leq 3.2$ g/L), deposited on glass were nearly single exponential (Figure 3a). However, they noticeably shortened and deviated from exponential functions at larger values of n, see Figure 3b ($n = 36.5$ g/L). This is the characteristic signature of a concentration quenching (energy transfer to acceptors). The effective emission decay rates, obtained by fitting experimental emission kinetics with single exponential functions, can be adequately fitted with the formula $(A + W) + \gamma n^2$ (Figure 4), where A and W are the rates of intra-central radiative and non-radiative decay and γn^2 is the energy transfer rate (see fitted values $A + W$ and γn^2 in Figure 5). The latter quadratic polynomial behavior is consistent with two possible scenarios: (i) quenching centers involve pairs of aggregated dye molecules and the energy transfer to quenching centers is direct or (ii) the concentration of quenching centers is proportional to the concentration of dye molecules, but the energy transfer is migration-assisted.

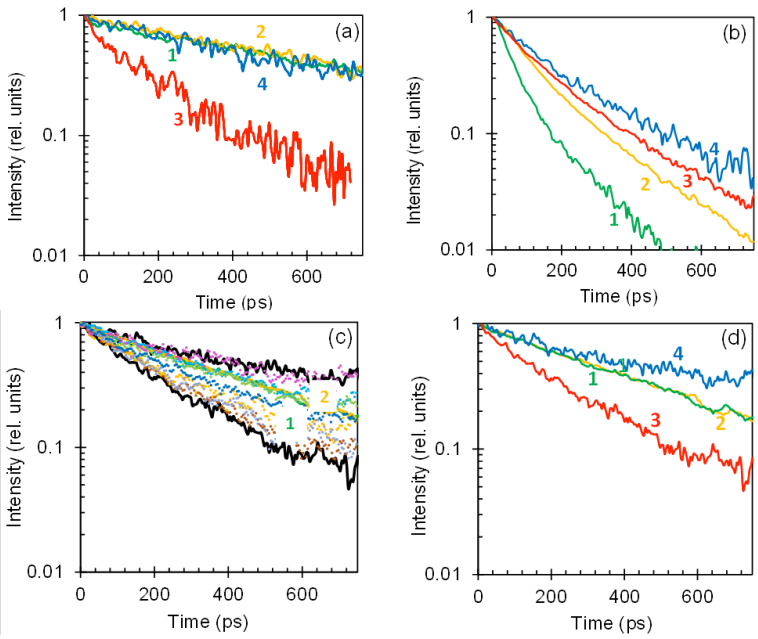

Figure 3. (a) Emission kinetics of HITC:PMMA at the low dye concentration equal to n = 3.2 g/L measured on top of glass (green trace 1), smooth thermally deposited Au film (yellow trace 2), and Au nanofoams: red trace 3 corresponds to the lower boundary of the emission kinetics spread, while the blue trace 4 corresponds to the upper boundary of the emission kinetics spread. (b) Same for the high dye concentration n = 36.5 g/L. (c) Emission kinetics of HITC:PMMA (n = 12.7 g/L) recorded in different local spots of the dye-doped Au nanofoam samples. Traces 1 and 2 are the emission kinetics of the n = 12.7 g/L HITC dye on top of glass and smooth Au substrates, respectively. (d) Same as 3a and 3b at the dye concentration n = 12.7 g/L.

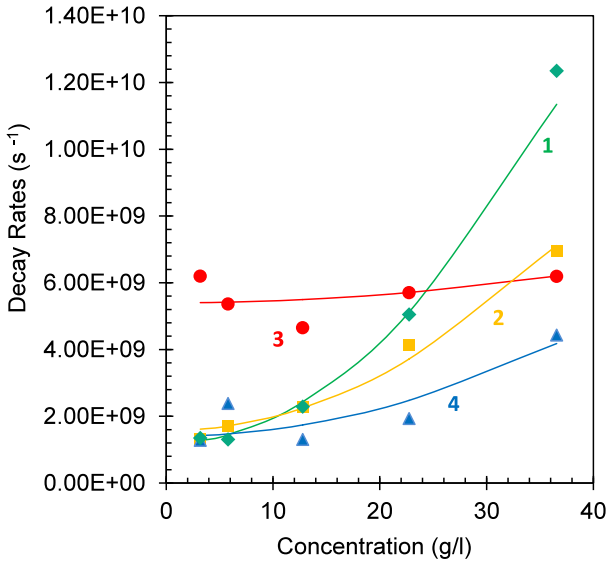

Figure 4. Emission decay rates in HITC:PMMA films at different dye concentrations on top of glass (trace 1), smooth thermally deposited Au film (trace 2), sub-volumes of the Au foams characterized by short emission kinetics (trace 3), and sub-volumes of the Au foams characterized by long emission kinetics (trace 4). Solid lines are the fits with the formula $(A + W) + \gamma n^2$. The spread of emission kinetics is a random process. This may explain larger error bars and poorer fit of the data points forming trace 3.

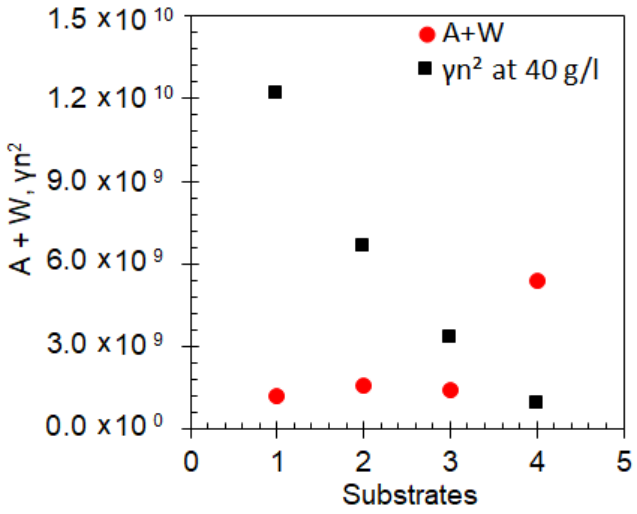

Figure 5. The values $A + W$ (red circles) and γn^2 (at n = 40 g/L, black squares) obtained from fitting of the datasets in Figure 4. (1) glass substrate, (2) smooth Au film substrates, (3) Au nanofoam (upper boundary of the emission kinetics spread), (4) Au nanofoam (lower boundary of the emission kinetics spread). The error bars are comparable to the sizes of the characters.

5. Emission Kinetics in HITC:PMMA Films Deposited on Smooth Au Films

As with HITC:PMMA films deposited on glass, the HITC emission kinetics measured on top of smooth thermally deposited Au films were relatively long and nearly single exponential at small dye concentrations (n = 3.2 g/L), Figure 3a. However, they shortened and deviated from exponential functions at large values of n (n = 36.5 g/L), Figure 3b. The latter shortening was not as strong as that on top of glass substrates, manifesting inhibition of the concentration quenching in vicinity of gold. The extracted value $A + W$ was nearly the same as on top of glass, while the value γn^2 was nearly two times smaller, Figure 5. This is the first important result of this study.

The ratios of the decay rates in HITC:PMMA films on top of Au and on top of glass are depicted in Figure 6. One can see that at large dye concentrations, $n \geq 20$ g/L, the ratio is smaller than unity, due to inhibition of the concentration quenching. On the other hand, at low dye concentrations ($n \leq 20$ g/L), when the concentration quenching is modest or small, the emission kinetics of HITC on smooth Au films, expectedly, become faster than those on glass (due to energy transfer to metal). In agreement with the Theoretical Modeling [3P], at the film thickness equal to 80 nm, this effect is modest, ~15%, comparable to the error bar in this particular experiment, Figure 6. Therefore, there is no contradiction, within the experimental error bar, between the results of Figures 5 and 6.

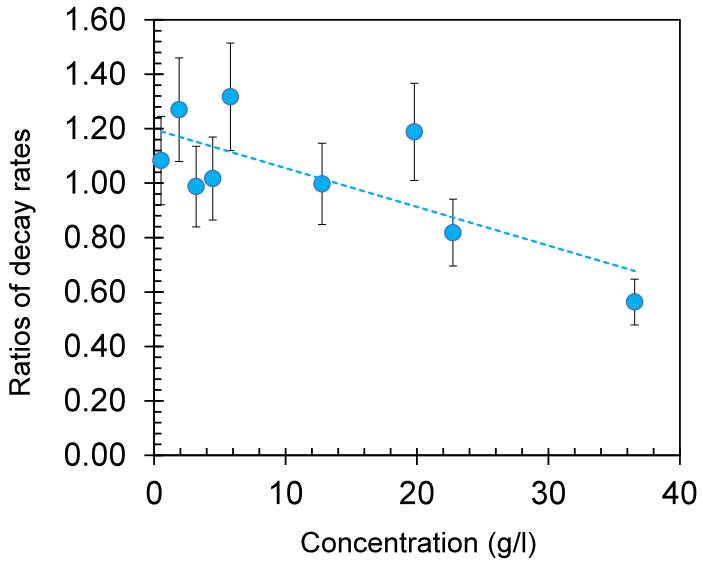

Figure 6. The ratios of the emission decay rates measured on top of smooth thermally deposited Au films and on top of glass, plotted as the function of the dye concentration. The dashed line is the linear fit of the data points - guide for eye.

In another particular experiment, we measured emission intensities I_0 right after the pumping pulse, before any noticeable decay of the excited state concentration could take place. (In this measurement, we made sure that no parasitic scattered laser light got mixed with the emission signal.) These initial intensities are proportional to the product of the Einstein coefficient A and the concentration of excited molecules n^*. (The latter was assumed to be proportional to the fraction of the pumping absorbed.) The scatter of the data points was large, partly because the samples with different dye concentrations were measured in different days and the precise optical alignment was not preserved from measurement to measurement. To reduce the data scatter, the initial emission intensities I_0 measured in dye doped films on top of Au films were divided by those on top of glass (taken in the same day), Figure 7. The increase of the latter ratios with increase of the dye concentration is in qualitative agreement with the reduction of the concentration quenching in vicinity of metal. However, although the emission decay rates and the initial emission intensities are related quantities, they are not directly proportional to each other (the former depends on the non-radiative decay rate and the latter does not).

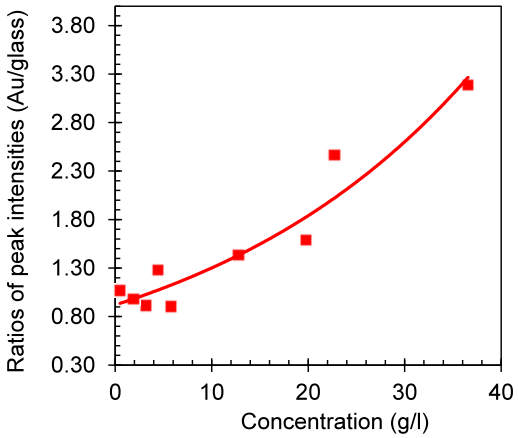

Figure 7. Ratios of the maximal emission intensities in HITC:PMMA films deposited on smooth Au films and on glass. The solid line is the fit of the data points with the second order polynomial - guide for eye.

The demonstrated inhibition of the concentration quenching in vicinity to gold is qualitatively similar to that in HITC:PMMA films on top of silver. This phenomenon is highly intriguing, since the common perception is that the molecular emission is quenched in vicinity of a metal, because of the energy transfer to a

metal. On the contrary, the experimentally observed behavior is opposite: *reduction* of the emission kinetics rate in vicinity of metal. This seeming controversy is explained in Ref. [3P].

6. Emission of HITC:PMMA Films Spin Coated onto Au Nanofoam Samples

In the series of experiments discussed in this section, HITC:PMMA/DCM solutions were spin coated onto Au nanofoams described above (DCM, dichloromethane, is the solvent). In these samples, the dye, whose spatial distribution was difficult to quantify, predominantly penetrated into the nanofoam's volume. The presence of HITC dye was barely seen at λ~770 nm in the reflection spectra of dye-impregnated nanofoams, n = 36.5 g/L (Figure 8, trace 2), as compared to nanofoams without dye (Figure 8, trace 1). At the same time, the presence of dye was clearly seen in the reflection spectrum of the HITC:PMMA film (n = 36.5 g/L, 80 nm) deposited on smooth Au film (Figure 8, trace 4), as compared to the reflection spectrum of a pristine Au film without dye (Figure 8, trace 3). (Similar observations have been made at multiple dye concentrations.)

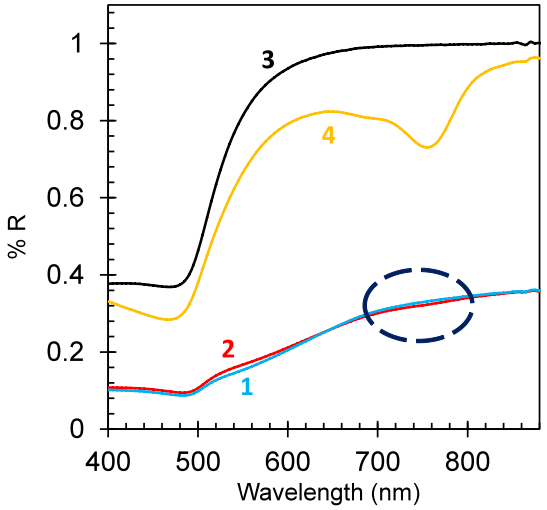

Figure 8. Reflectance spectra of the Au nanofoam without dye (trace 1) and with HITC:PMMA (n = 36.5 g/L) (trace 2). Reflection spectra of smooth gold film without dye (trace 3) and with HITC:PMMA (n = 36.5 g/L) (trace 4). The ellipse shows the area, where the dip in the reflection spectrum of Au nanofoam, caused by the absorption of the HITC dye, is expected.

The emission decay kinetics in the dye-doped Au nanofoam samples were *highly inhomogeneous.* This is one of the most important results of this study. Thus, emission kinetics measured in different locations on the sample could have strongly different rates. The spread of the emission kinetics in the 12.7 g/L sample is depicted in Figure 3c. The black traces in Figure 3c approximately correspond to the upper (slow decay) and the lower (fast decay) boundaries of the emission kinetics spread. The characteristic lateral scale of the emission non-uniformity (the effective sizes of domains with more or less homogeneous kinetics) was ~1 mm. Such spatial non-uniformity was never observed on top of glass or smooth Au films.

At *small dye concentration, n = 3.2 g/L*, the HITC:PMMA emission kinetics on top of glass and smooth Au films are almost identical (Figure 3a), the concentration quenching is weak, and the effect of a smooth gold substrate on the dye emission is relatively small (Figure 6). In the Au nanofoam sample, the kinetics corresponding to the upper boundary of the emission kinetics spread are the same as those on top of smooth gold and glass. At the same time, the kinetics corresponding to the lower boundary of the spread have significantly shorter (nearly threefold) decay times. We infer that in different subvolumes of the Au nanofoam, HITC molecules are coupled to the nanofoam weaker or stronger. Correspondingly, unquenched emission kinetics are due to HITC molecules modestly or weakly coupled to the Au nanofoam, while the shortened emission kinetics are due to the dye molecules, which are strongly coupled to and quenched by the Au nanofoam. (Here by *strong coupling* we do not mean the light-matter interaction resulting in the Rabi splitting).

To determine whether increase of the decay rates of the dye molecules coupled to Au nanofoams was due to enhancement of spontaneous emission A or non-radiative decay W, we analyzed multiple emission kinetics corresponding to the kinetics spread (similar to those in Figure 3c) and plotted the initial emission intensities I (~A) against the emission rates $A + W$, Figure 9. (At n = 3.2 g/L, the concentration quenching γn^2 was negligibly small.) The reduction of A ($\sim I$) with increase of $A + W$ suggests that the increase of the decay-time is due to increase of W rather than A (or, if both A and W are increased, the increase of W is larger than the increase of A). This behavior is consistent with the theoretical prediction [31].

At intermediate dye concentration, n = 12.7 g/L, the emission kinetics of dye on glass and on smooth Au films are close to each other (Figure 3d), although, they are shorter than those in the n = 3.2 g/L sample (Figure 3a). This signifies modest concentration quenching, whose inhibition is balanced by the energy transfer to metal. The latter emission kinetics are close to the upper (slower) boundary of the kinetics spread in Au nanofoams (which is narrower than that at low dye concentration) and much above the lower (fast) boundary of the kinetics spread, Figure 3d.

At high dye concentration, n = 36.5 g/L, the concentration quenching on top of glass and its inhibition in vicinity of a smooth Au film are strong. Correspondingly, the emission kinetics of dye on top of smooth gold are significantly different from those on glass, Figure 3b. In Au nanofoams, the spread of the emission kinetics becomes small and both upper and lower boundaries of the spread lie above the emission kinetics on glass and smooth gold, see Figures 3b and 4. The latter observation suggests that *the inhibition of the concentration quenching in Au nanofoams (in both strongly and modestly coupled subvolumes) is stronger than that on top of smooth Au films*. This important result of our study is discussed in detail below.

The decay rates corresponding to the upper (slow decay) boundary of the emission kinetics spread and their fitting with the formula $(A + W) + \gamma n^2$ are depicted in Figure 4 (blue triangles). The corresponding fitted values $A + W$ and γn^2 are shown in Figure 5. The determined value $A + W$ is close to those on top of glass and smooth Au films. Correspondingly, the emission kinetics on glass, smooth Au film and Au nanofoam (slow decay boundary of the kinetics spread) are nearly the same at small dye concentrations, when the concentration quenching is negligibly small, Figure 3a. The determined value γn^2 is nearly twice smaller than that in smooth Au samples. Therefore, at high dye concentrations, the emission kinetics in Au nanofoams are slower than those in smooth Au samples, Figure 3b. This proves that Au nanofoams inhibit concentration quenching much stronger than smooth Au films do, as discussed above. This experimental result can be explained by large surface area of Au nanofoams and relatively small molecule-to-metal distances in nanofoam samples [3P].

The decay rates corresponding to the low (fast decay) boundary of the emission kinetics spread have a strong concentration-independent contribution, presumably originating from the strong coupling of dye molecules with metal and the energy transfer to metal. The fitting of the decay rates with the formula $(A + W) + \gamma n^2$ and the extracted values $(A + W)$ and γn^2 are depicted in Figures 4 and 5. Noteworthy is the very large value $A + W$, which is four times larger than the analogous values in the other samples studied, Figure 5. This decay mechanism is so strong that it inhibits the concentration quenching almost completely (see Theoretical Modeling). Therefore, the slope of the corresponding trace in Figure 4 is very small, in agreement with Ref. [3P], and the decay rate at high concentration is nearly the same as that at low concentration. As the decay rates corresponding to the upper (slow decay) boundary of the emission kinetics spread increase with the growth of the dye concentration and the decay rates corresponding to the lower (fast decay) boundary of the emission kinetics spread practically do not, the spread of the emission kinetics is getting smaller with increased concentration. This is another important result of this study.

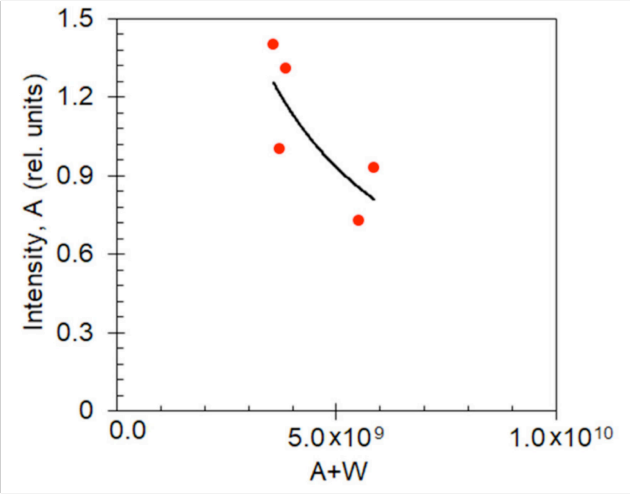

Figure 9. Maximal emission intensities (~*A*) plotted against the emission decay rates *(A + W)* measured in multiple local spots of the Au nanofoam sample at HITC concentration equal to *n* = 3.2 g/L. The solid line is the fit of the data points with the second order polynomial - guide for eye.

7. Summary

To summarize, in this work, we studied emission kinetics of HITC laser dye, embedded in the PMMA polymeric matrix, on top of smooth Au films and in random nanostructured metal-dielectric environments (Au nanofoams). The HITC:PMMA films deposited onto glass substrates served as control samples.

The concentration quenching of luminescence of highly concentrated dye on top of glass substrates is explained in terms of the energy transfer to acceptors formed by (i) pairs of dye molecules (at direct donor-acceptor energy transfer) or (ii) single dye molecules interacting with the host polymeric matrix (at migration-assisted energy transfer).

The concentration quenching is inhibited on top of smooth Au films, in agreement with the previous studies, where similar effects were observed on top of Ag films and Ag-based lamellar metal-dielectric metamaterials.

The emission kinetics recorded in different local spots of the Au nanofoam samples had very large spreads, which was never observed on top of smooth gold substrates. We infer that in different subvolumes of the Au nanofoam, HITC molecules are coupled to the nanofoam weaker or stronger.

The spread of the emission kinetics was particularly large at small dye concentrations *n*. It became smaller with increase of *n*, as the result of the interplay between the energy transfer to metal and the concentration quenching.

The inhibition of the concentration quenching was stronger in Au foams (in both strongly coupled subvolumes and weakly coupled subvolumes) than on top of smooth Au films. The most likely explanations of this difference include (i) large surface area and (ii) small molecule-to-metal distances in Au nanofoam samples.

The inhibition of concentration quenching in smooth Au film and Au nanofoam samples was explained using a theoretical model that is based on reduction of the Förster radius in the presence of strong energy transfer to the metal [3P].

In this study, we attributed most of the experimental observations to metal/dielectric environments influencing the dye molecules. The effects of purely dielectric environments on the emission kinetics of HITC dye is the subject of the further study to be published elsewhere.

SECTION 3. THE EFFECTS OF RANDOMLY NANOSTRUCTURED METALLIC COATINGS ON RATES OF ELECTROCHEMICAL REACTIONS [5C]

(Probing charge transport kinetics in plasmonic environment with cyclic voltammetry)

In the experiment, we consider an oxidation-reduction reaction of hexacyanoferrite [iron (II) state] to hexacyanoferrate [iron (III) state] in the $K_3[Fe(CN)_6]$/ KNO_3 aqueous media, and investigate how the vicinity to a nanostructured metallic surface affects this single electron-transfer process and modifies the charge transport kinetics. Using the cyclic voltammetry (CV) method we perform a comparative study of the reaction using two different electrodes: flat gold and gold nanomesh, and, in addition, explore possible effects of laser light illumination. The CV data is used to analyze the kinetics of the reaction, specifically the heterogeneous electron transfer rate (HET), which characterizes the electron transfer between electroactive species and an electrode surface.

Flat and gold nanomesh substrates are prepared by thermal deposition of gold (40 nm thick) onto precleaned glass substrates and nanoporous anodic aluminum oxide (AAO) substrates precoated with a 3 nm thick Cr adhesion layer. The deposition of gold onto AAO substrate produces highly nanostructured surfaces with 40 nm periodic pores. The CV experiments are performed without and with additional light illumination, referred as “in dark” and “in light” respectively. The additional illumination is provided by a diode laser with the wavelength 590 nm and 100 mW power. Light is focused on of the submersed area of the working electrode, which is our sample under study (gold nanomesh or flat gold depending on a particular run).

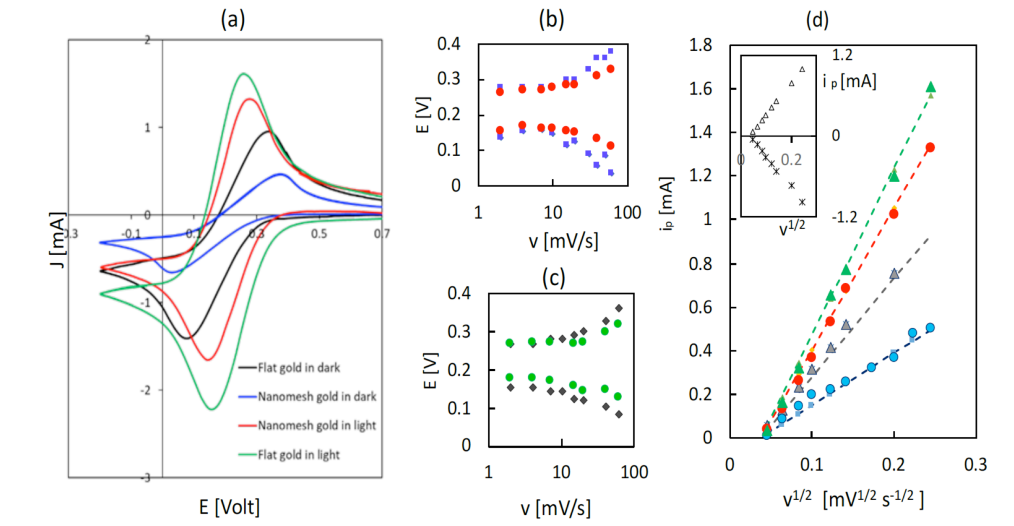

Figure 1. (a) Cyclic voltammogram obtained using flat gold (in light and dark field) and nanomesh gold (in light and dark field) as working electrode. Scan rate shown for each electrode 60mV/s. (b) Oxidation reduction peak potential in flat gold *vs* v sweep rate in light and dark; (c) same in nanomesh; (d) Anodic peak current *vs* $v^{1/2}$, experiment (points) and fitting (dashed traces). Inset: Anodic (triangles) and cathodic (stars) currents in flat gold in dark.

The effects of nanostructured environment and light are clearly seen in Figure 1. Under light illumination peak currents are higher than those in dark, and the change in the CV curves is stronger in nanostructured gold than that in flat (compare green and black traces for flat gold with blue and red for the nanostructure). Positions of the oxidation and reduction peaks change as well: the peak separation, *DE.* becomes lower. The effects of light are apparently more pronounced in the nanostructured system than in flat gold.

The further analysis of the experimental data involves the Randles-Sevcik’s equation [1] in application to the peak current magnitude and the Nicholson method [2] for estimations of the charge transfer rate. The peak currents show diffusion-related characteristic dependence on the scanning rate (~$av^{1/2}$, Fig. 1 (d)). The light-induced changes are much stronger in the nanostructured system than in flat gold

$$\frac{\alpha_{light}^{flat}}{\alpha_{dark}^{flat}} = 1.62 \pm 0.1\ ; \qquad (1a)$$

$$\frac{\alpha_{light}^{nano}}{\alpha_{dark}^{nano}} = 2.71 \pm 0.1. \quad (1b)$$

The analysis of the charge transfer rate, $k0$ with the Nicholson method shows that in both systems photoexcitation leads to significant growth of the rates. However, the photoinduced changes in HET rates are of the same order for both systems. They can be estimated as

$$\frac{k^{0}{}_{light}^{flat}}{k^{0}{}_{dark}^{flat}} = 3.1 \pm 0.1 \quad \text{in the flat system} \quad (2a)$$

$$\frac{k^{0}{}_{light}^{nano}}{k^{0}{}_{dark}^{nano}} = 3.2 \pm 0.2 \quad \text{in the nanomesh system} \quad (2b)$$

Which mechanisms are responsible for modification of chemical reactions in nanostructured and plasmonic environment is the subject of many scientific discussions. Different models are discussed involving generation of hot electrons [3], modification of surface charges [4], significant local electric effects [5] associated with high optical fields and high gradients of optical fields and photoinduced heating [6]. The photoinduced heating is expected to result in acceleration of diffusion and increased HET rates. We roughly estimate possible heating in our experimental conditions, considering the predominant channel of the heat transfer from the illuminated spot (~5x5 mm^2) to the solution (with the thermal conductivity of 0.6 W/mK), and then to the cuvette walls (2 cm away). The estimations yield, $DT \leq 6.5^0$ in the experiment with flat gold and up to threefold higher in nanomesh. Such changes seem to be too small to provide a significant impact, in particular to the diffusion coefficients.

In conclusion, the cyclic voltammetry method is employed to study possible modifications in the electrochemical reaction in nanostructured plasmonic environment with and without light illumination in the plasmon resonance range. The CV curves are strongly altered under the light illumination, and the effect of light on the magnitude of the currents is much stronger in the nanostructured system than that in flat fold. The analysis of the charge transfer rate with the Nicholson method shows that in both systems photoexcitation leads to significant growth of the HET rates.

1. N. Elgrishi, K. J. Rountree, B. D. McCarthy, E. S. Rountree, T. T. Eisenhart, and J. L. Dempsey, "A Practical Beginner's Guide to Cyclic Voltammetry," J. Chem. Ed. **95**, 197-206 (2018)
2. R. S. Nicholson, "Theory and Application of Cyclic Voltammetry for Measurement of Electrode Reaction Kinetics," Anal. Chem. **37** (11), 1351-1355 (1965)
3. Y. Zhang, S.i He, W. Guo, Y. Hu, J. Huang, J. R. Mulcahy, and W. D. Wei, "Surface-Plasmon-Driven Hot Electron Photochemistry," Chem. Rev. **118** 2927–2954 (2018)
4. M. Shahabuddin, T, McDowell, C, E. Bonner, and N, Noginova, "Enhancement of Electrochromic Polymer Switching in Plasmonic Nanostructured Environment," ACS Appl. Nano Mat. **2** (3), 1713-1719 (2019)
5. Van de Groep, J., Sheldon, M., Atwater, H. et al, "Thermodynamic theory of the plasmoelectric effect, " Sci Rep **6**, 23283 (2016).
6. Y. Dubi, I. W. Unbc and Y. Sivan "Thermal effects – an alternative mechanism for plasmon-assisted photocatalysis", Chem. Sci. **11**, 5017 (2020).

SECTION 4. COUPLING IN MINIATURE LASERS

4.1 Stimulated emission in vicinity of the critical angle [4P,6C]

[In collaboration with Podolskiy group at UMass Lowell]

Abstract: We demonstrated amplified spontaneous emission (ASE) enabled by evanescent gain at an interface between two adjacent dielectrics. The ASE wave is outcoupled to the high-index medium at the critical angle, enabling observation of spectacular emission rings.

To keep up with the Moore's law [1], future electronics will need nanocircuits operating at the optical frequency [2]. This demand inspires the development of nanocircuit components with gain, such as plasmonic nanolasers and spasers. While plasmonic lasers may have subwavelength dimensions, they suffer from inherent optical loss in metal. Therefore, the development of miniature metal-free lasers with the functionality of plasmonic lasers but without plasmonic absorption would be a major breakthrough in the development of photonic circuitry.

One of the first demonstrated plasmonic lasers was enabled by a surface wave propagating at the boundary between Ag film and dye-doped polymer with optical gain [3]. In the present work, we study (i) whether a guided wave can propagate at the interface between two dielectric layers (one of them with gain) and (ii) whether this mode can support low-loss stimulated emission.

Our samples were polymeric films (PMMA) doped with rhodamine 6G (R6G) dye (gain medium) deposited onto glass substrates (Fig. 1, Panel 1). The film thickness ranged between 1.68 μm and 4.15 μm, and the dye concentrations ranged between c=5 g/l and c=400 g/l (in solid state). At λ=575 nm, (which was close to the wavelength of maximal emission of R6G, λ=563 nm), the refractive indexes of glass and (undoped) PMMA are n_{glass}=1.5239 [4] and n_{PMMA}=1.4912 [5], respectively.

Relevant configurations, in which optical gain was harvested *via* evanescent fields extending to adjacent amplifying low index media were studied by several authors [6-9] and shown to have the total internal reflection exceeding unity, with the maximum at or slightly below the critical angle for total internal reflection (TIR). Using the analytical formula derived in Ref. [10], we have predicted the latter behavior for the parameters of our system.

However, of primary interest to the present study, is not an amplification of the incident light, but rather generation of a guided stimulated emission at the interface between low index R6G:PMMA and high index glass. Lasers and ASE sources harvesting optical gain with evanescent fields have been studied in the literature [6,11,12]. At this time, we report on realization of the miniature source of stimulated emission with evanescent gain, paving the road to micrometer-scale on-chip applications.

The experimental samples were optically pumped at λ=532 nm with the frequency doubled Q-switched Nd:YAG laser, t_{pulse} ~10 ns, at 57 degrees to the sample's normal. The pumped spot was nearly elliptical, with the area equal to ~27 mm^2.The emission was collected at 33 degrees to the sample's normal (Figure 1, Panel 2).

When the sample, R6G:PMMA film (λ=3.22 mm, c=5 g/l) deposited onto 1 mm glass slide, was pumped with low-energy pulses, <0.025 mJ, the emission spectra had maxima at λ=563 nm (Figure 1, Panel 3a), the emission intensities were small (Figure 1, Panel 3b), and the full widths at half maximum (FWHM) ranged between 34 nm and 40 nm (Figure 1, Panel 3c). The corresponding light spots, seen on the samples, are depicted in Figure 1, Panels 3d and 3e. With increase of the pumping energy (0.065 mJ), the bright spot became larger and got surrounded by a diffused light (Figure 1, Panel 3f).

At the further increase of the pumping energy (above the soft threshold at 0.14 mJ), a spectacular bright ring, followed by several other concentric rings (Figure 1, Panels 3g and 3h), appeared on the sample's surface. We numerated these bright rings with integer numbers m=1, 2, 3,…etc. Significantly less intense and often discontinuous emission rings could be seen in between the major "integer" rings; one of them is marked with red arrow in Figure 1, Panel 3h. We numerated the latter low intensity rings as m=1/2, 3/2, 5/2, etc.

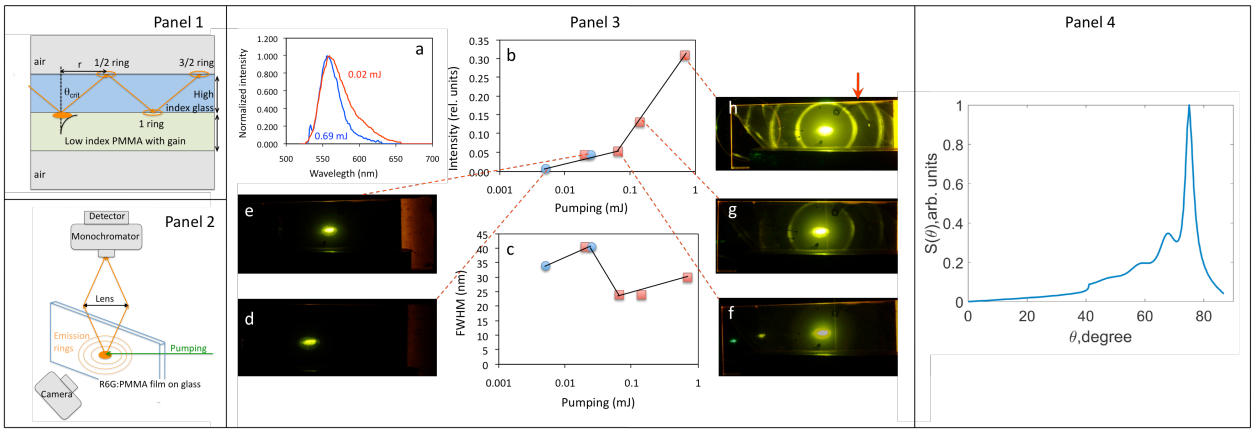

Figure 1. Panel 1: Schematics of the experimental sample; outcoupling and guiding of ASE. Panel 2: Schematics of the experimental setup. Panel 3: Emission spectra of R6G:PMMA (normalized to unity) measured at pumping energy of 0.02 mJ (red trace) and 0.69 mJ (blue trace). (b) Emission intensity plotted against the pumping energy. (c) Full width at half maximum (FWHM) plotted against the pumping energy. (d-h) Photographs of the emission patterns taken at pumping energies equal to 0.0051 mJ, 0.025 mJ, 0.065 mJ, 0.14 mJ, and 0.69 mJ, respectively. Panel 4: Angular profile of emission by a point dipolar source (located within PMMA layer) into the glass substrate.

No rings could be intercepted by a white card placed next to the sample's surface. However, an arched trace of light could be seen on a white card placed above the sample, suggesting that the emitted light was guided by the glass/polymer structure. Therefore, we attribute the rings to the scattering of the otherwise totally internally reflected (TIR) light by imperfect surfaces of glass slides and R6G:PMMA films.

The onset of the emission ring corresponded to a reduction of the emission bandwidth, down to FWHM=24 nm, and an increase of the emission intensity (see Figure 1, Panels 2b and 2c).

Rings radii r are proportional to the ring index m, as well as the thickness of the glass film and are independent of the thickness of PMMA film or pumping intensity (compare Panels 3g and 3h in Figure 1), in agreement with schematics shown in Fig.1, Panel 1. Based on the available data, the angle of emission q is very close to the critical angle at the glass/PMMA interface, $\theta_c=\arcsin(n_{PMMA}/n_{glass})=78.11^o$.

The experimental observations above are in agreement with theoretical simulations of emission within glass/doped PMMA/air stack that incorporates Green's function formalism (see Ref. [13] for details) and predicts that emission by point dipoles positioned within PMMA film is localized close to TIR angle in the glass substrate (Figure 1, Panel 4). Further analysis suggests that such angular profile is related to the existence of leaky guided mode that is responsible for both angular reshaping of emission and for providing feedback mechanism in for ASE.

The soft ASE threshold is observed in the studied metal-less surface wave geometry at the pumping energy density equal to E_{th}/S=0.24 mJ/cm^2, see Figs. 2b and 2g. According to the conservative estimate (based on the narrowing of the emission band), this value is forty five times smaller than the threshold of stimulated emission of SPP with gain, 10.9 mJ/cm^2 [3]. The reported demonstration of the low-threshold source of stimulated emission "fueled" by harvesting gain in an adjacent micrometer-thick dye-doped medium paves the way to on-chip realizations of low loss all-dielectric lasers with evanescent gain.

[1] G. E. Moore, Electronics, 38, pp. 114-117, (1965).

[2] N. Engheta, Science, 317, pp. 1698-1702 (2007).

[3] M. A. Noginov, et al., Phys. Rev. Lett. 101, 226806 (2008).

[4] R. V. Gibbons and T. J. Ahrens, Journal of Geophysical Research 76, pp. 5489-5498 (1971).

[5] M. N. Polyanskiy, https://refractiveindex.info.

[6] B. Ya Kogan, V. M. Volkov, and S. A. Lebedev, JETP Lett. 16, 100 (1972).

[7] G. N. Romanov and S. S. Shakhidzanov, JETP Lett. 16, 309 (1972).

[8] W. Lukosz and P. P. Herrmann, Opt. Commun. 17, 192 (1976).

[9] P. R. Callary and C. K. Carniglia, J. Opt. Soc. Am. 66, 775 (1976).

[10] H. Raether, *Surface Plasmons on Smooth and Rough Surfaces and on Gratings*, Springer, Berlin, Heidelberg (1988).

[11] C. J. Koester, IEEE Journal of Quantum Electronics, QE-2, 580-584 (1966).

[12] Y. Zhang et al., IEEE Photonics Journal, DOI: 10.1109/JPHOT.2019.2907469

[13] L. Nordin, et al., Appl. Phys. Lett. 116, 021102 (2020).

4.2 How Do the Purcell Factor, the Q-Factor, and the Beta Factor Affect the Laser Threshold? [5P]

[In collaboration with Jacob B. Khurgin at Johns University (primary author)]

As lasers get more and more miniaturized and their dimensions become comparable to the wavelength, two interconnected phenomena take place: the fraction of spontaneous radiation going into a specific laser mode (β-factor) increases and can ultimately reach unity, while the radiative lifetime gets shortened by the Purcell factor F_p. Often it is assumed that an increase of these two factors, along with the quality factor (Q-factor), almost invariably causes reduction of the lasing threshold. This assumption is tested on various photonic and plasmonic lasers, demonstrating that, while there is obvious correlation between the aforementioned factors and the laser threshold, the dependence is far from being straightforward and omnipresent. Depending on specific laser material and geometry, the threshold can decrease, increase, or stay unchanged when β-factor, Q-factor, and F_p increase. For the most part, the reduction of threshold is achieved simply by reducing the laser volume and this volume reduction can concurrently cause the increase in β-factor and/or Purcell factor, but it would be imprudent to say that the increase in either of these factors is the cause of the threshold reduction.

SECTION 5. CONCENTRATION DEPENDENCE OF TWO-PHOTON ABSORPTION IN PMMA POLYMERIC FILMS DOPED WITH RHODAMINE LASER DYES [6P]

Abstract: We studied polymeric (PMMA) films doped with R6G and RhB laser dyes as potential nonlinear material components for photonic applications at the nanoscale. The two-photon absorption cross sections and the optimal dye concentrations were determined.

Recent developments in plasmonics, metamaterials [1] and light-matter interaction at the nanoscale, in both weak and strong coupling regimes, have demonstrated multiple possibilities to control scores of physical and chemical phenomena of practical importance. Two-photon absorption (TPA) is a third order, $\chi^{(3)}$, nonlinear optical process [2], which has multiple applications in optical power limiting, 3-D optical memory, fluorescence microscopy, nanofabrication, photodynamic therapy, and *in vivo* imaging of biological tissues. However, many promising future applications require (i) the development of advanced materials with large two-photon-absorption (TPA) cross sections [3] or (ii) enhancement of TPA efficiency with rationally designed metal-dielectric environments, such as cavities [4], lamellar hyperbolic metamaterials [5], etc. The latter enhancement has been demonstrated for a linear absorption [5], suggesting that the enhancement of TPA is within reach.

Laser dyes of Rhodamine family have relatively large single-photon absorption and emission cross sections, large quantum yields, and superior chemical and photo-stability, which made them the material of choice in the 1970's, when dye lasers dominated the field of tunable lasers. Rhodamine dyes, in particular, Rhodamine 6G (R6G) and Rhodamine B (RhB), were reported to have relatively large TPA cross sections. However, the spread of the reported results is incredibly large, ~10 GM [6] to ~1.3×10^3 GM [7] (1 GM = 10^{-50} cm^4s $photon^{-1}$). Furthermore, if a particular dye is selected to be used in the

experiments aimed at enhancement of TPA with metal/dielectric environments, then what dye concentration should be chosen to maximize the TPA-excited emission?

The latter question motivated the present study, in which we fabricated a series of polymeric (PMMA) films doped with different concentrations of Rhodamine 6G (R6G) and Rhodamine B (RhB) laser dyes and investigated their TPA properties in emission and transmission experiments.

We have fabricated two series of polymeric films of poly(methyl methacrylate), PMMA, doped with Rhodamine 6G (R6G) perchlorate and Rhodamine B (RhB) perchlorate laser dyes. The amounts of dyes and PMMA were chosen to result in the dye concentrations ranging from 5 g/l to 400 g/l, in solid state. (For R6G, 1 g/l corresponds to 1.14×10^{18} cm^{-3}; and for RhB, 1 g/l corresponds to 1.11×10^{18} cm^{-3}). The dyes and the polymer were dissolved in dichloromethane (DCM). The resultant mixed solutions were spin coated onto glass substrates. After that, the solvent was allowed to evaporate slowly at room temperature. The films looked homogeneous and not scattering. Their thicknesses ranged from 370 nm to 4150 nm.

The results of the experimental studies can be summarized as follows:

- Expectedly, the intensity of the TPA-excited emission was proportional to the square of the pumping energy, Figs. 1a and 1b.

- By analyzing the concentration dependence of the emission intensity, we found that the concentration quenching rate is nearly proportional to the square of the dye concentration N.

- The TPA-excited emission is maximal at N≈20 g/l in the R6G doped film and N≈40 g/l in the RhB doped film, Fig. 1c.

- In the range of dye concentrations studied, 5 g/l to 400 g/l, the TPA-excited emission is several times stronger in the RhB doped samples than in the R6G doped samples, Fig. 1c.

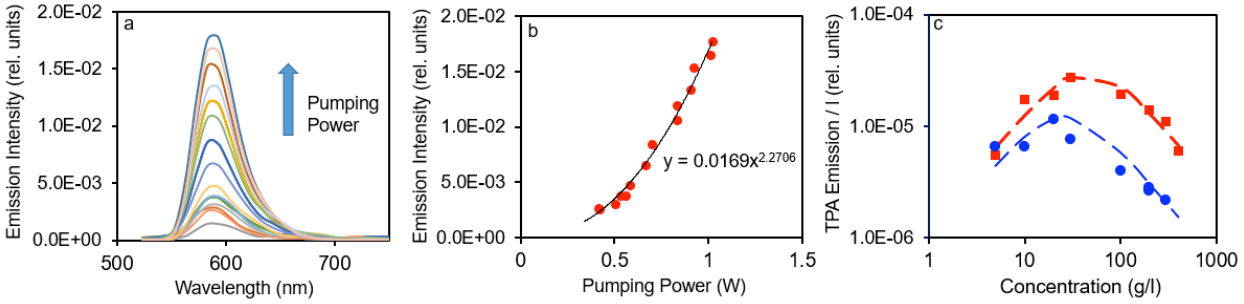

Figure 1 (a) Emission spectra of RhB:PMMA (N=30 g/l) pumped (at *l*=1064 nm) at multiple energy densities ranging from 1.17 J/cm^2 to 3.69 J/cm^2. (b) Nearly quadratic dependence of the TPA pumped RhB emission intensity. Similar results were obtained at different dye concentrations and in R6G doped PMMA films. (c) Experimental TPA emission intensities (measured at the spectral maxima), divided by the sample thickness *l*, in RhB-doped (red squares) and R6G-doped (blue circles) PMMA films at dye concentrations ranging from 5 g/l to 400 g/l; dashed lines - theoretical fitting.

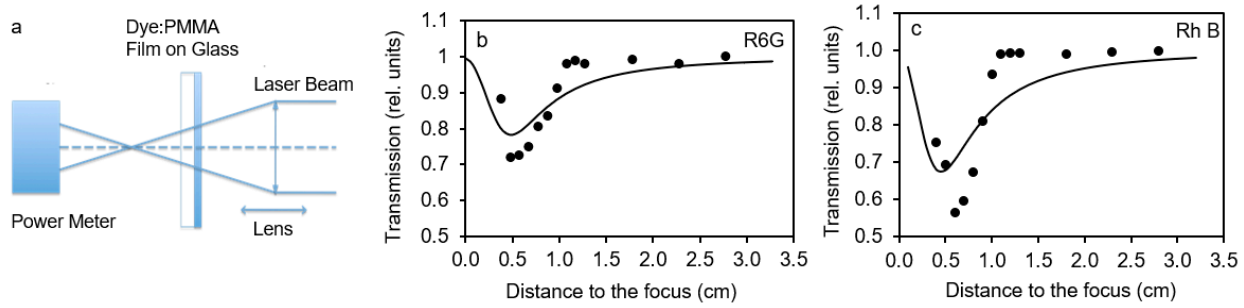

Figure 2. (a) Schematics of the TPA transmission experiment. (b) and (c) TPA transmission in the RhB and R6G doped PMMA films as the function of the distance from the sample to the focal point *d*. Black circles – experiment; black smooth lines – fit with the theoretical model: (b) R6G, (c) RhB.

- With an increase of the TPA pumping energy density, the sample's transmission experiences the reduction followed by an increase – in a good agreement with the theoretical prediction, Figs. 2a, 2b and 2c.

- The large values of TPA cross sections, determined in the TPA emission (~10^3 GM) and transmission (~10^4 GM) experiments, can be partly due to spatial non-uniformity of the pumped laser spot.

- The laser damage thresholds of Au and TiN thin films are significantly smaller than the characteristic pumping densities used in the TPA experiments reported above. Therefore, control of TPA with metallic (or alternative plasmonics) environments requires nonlinear $\chi^{(3)}$ materials with much larger TPA cross sections.

[1] M. A. Noginov and V. A. Podolskiy, Eds., Tutorials in Metamaterials (Series in Nano-optics and Nanophotonics) CRC Press, Taylor & Francis Group, Boca Raton (2011), 293 p.

[2] R. W. Boyd, Nonlinear Optics, 3rd ed., Academic Press, Burlington, MA (2008).

[3] M. Albota, D. Beljonne, J. L. Bredas et al. "Design of organic molecules with large two-photon absorption cross sections", Science, 281, 1653-1656 (1998).

[4] W.-H. Guo, J. O'Dowd, E. Flood, T. Quinlan, M. Lynch, A. L Bradley, J. F. Donegan, K. Bondarczuk, P. J. Maguire, Member, L. P. Barry, "Suppression of Residual Single-Photon Absorption Relative to Two-Photon Absorption in High Finesse Planar Microcavities", IEEE Photonics Technology Letters 20, 1426-1428 (2008).

[5] T. U. Tumkur, Lei Gu, J. K. Kitur, E. E. Narimanov, and M. A. Noginov, "Control of absorption with hyperbolic metamaterials", Appl. Phys. Lett. 100, 161103 (2012).

[6] A. Penzkofer and W. Leupacher, "S0-S1 two photon absorption dynamics of organic dye solutions," Opt Quant Electron 19, 327-349 (1987).

[7] Z. Dong, D. Yan, Y. Xia, D. Chen, and S. Su, "Two-photon absorption properties of rhodamine 6G in ethanol and PMMA," 2012 Int. Conf. Optoelectron. Microelectron. ICOM 2012, pp. 404-406 (2012).

Part 4

Aug. 1, 2021 – Sept. 28, 2022

ABSTRACT

The main goal of this project is to study how physical and chemical properties of organic matter can be controlled in strong and weak light-matter interaction regimes. In the first two years, the studied metal-dielectric environments were homogeneous plane films and lamellar stacks. In the third year, we studied effects of random nanostructured environments on the light-matter coupling, emission, energy transfer, and rates of electrochemical reactions. At this time, in the end of the fourth No Cost Extencion year, we concentrated on the following tasks: (i) Dispersion in reflection and emission of dye molecules strongly coupled to surface plasmon polaritons. (ii) Effect of metal-dielectric environments on photopolymerization of the [2,2′-bi-1H-indene]-1,1′-dione-3,3′-diyldiheptanoatecarboxylate monomer. (iii) Emission kinetics of HITC laser dye on top of arrays of Ag nanowires. (iv) Kelvin probe work-function studies of components of Fabry-Perot cavities and MIM waveguides. (v) Probing Charge Transport Kinetics in a Plasmonic Environment with Cyclic Voltammetry. (vi) Anomalous Dips in Reflection Spectra of Polymers Deposited on Plasmonic Metals. (vii) Effect of nanoscale dielectric environments on concentration quenching.

CONTENTS

The Technical Report is organized as follows:

PUBLICATIONS AND PRESENTATION

[1P] Md Golam Rabbani Chowdhury, Shamaar R. Howard, Kanij M. Khabir, Mikhail A. Noginov, "Dispersion of surface plasmon polaritons (SPPs) in weak and strong coupling regimes," Proc. SPIE PC12197, Plasmonics: Design, Materials, Fabrication, Characterization, and Applications XX, PC1219702 (3 October 2022); https://doi.org/10.1117/12.2633668.

[2P] Md Golam Rabbani Chowdhury, Shamaar R. Howard, Kanij Mehtanin Khabir, Mikhail A. Noginov, "Dispersion in reflection and emission of dye molecules strongly coupled to

surface plasmon polaritons," Proc. SPIE PC12195, Metamaterials, Metadevices, and Metasystems 2022, PC121951Y (3 October 2022); https://doi.org/10.1117/12.2635138.

[3P] Md G. R. Chowdhury, Shamar Howard, Kanij M. Khabir, Mikhail A. Noginov, “Anamalous Dispersion of Surface Plasmon Polaritons (SPPs) in Ultra Strong Coupling Regime”, Metamaterials 3.1, EPS Symposium on the Third Generation Metamaterials, 1-5 August, Cetraro, Calabria, Italy; paper # WED 4.3 (invited).

[4P] Md Golam Rabbani Chowdhury, Shamaar R. Howard, Kanij Mehtanin Khabir, Mikhail A. Noginov, “Dispersion in Reflection and Emission of Dye Molecules Strongly Coupled to Surface Plasmon Polaritons”, CLEO Conference, San JOSE, CA, USA and virtual, May 15 – May 19, 2022, paper FTh2B.2.

[5P] Leila Hesami, Chi Yang, Elias Anwar, Mikhail A. Noginov, “Effect of metal-dielectric environments on photopolymerization of the [2,2′-bi-1H-indene]-1,1′-dione-3,3′-diyldiheptanoatecarboxylate monomer”, 2022 MRS Spring Meeting and Exhibit, May 8 - 13.; Honolulu, Hawaii, USA.

[6P] L. Hesami, C. Yang, E. Anwar, N. Noginova, M. A. Noginov, “Effect of metal/dielectric substrates on photopolymerization of BITh thin films”, Sci. Rep. 12, 19109 (2022). https://doi.org/10.1038/s41598-022-23243-4.

[7P] Sangeeta Rout, Vanessa N Peters, Sangram K Pradhan, Carl E Bonner, Mikhail A Noginov, “Emission kinetics of HITC laser dye on top of arrays of Ag nanowires”, Nanophotonics, 2021, pp. 000010151520210374. https://doi.org/10.1515/nanoph-2021-0374.

[8P] Kanij Mehtanin Khabir, Mohammad Shahabuddin, Jalyn-Rose L. Clark, Natalia Noginova, Mikhail A. Noginov, "Kelvin probe work-function studies of components of Fabry-Perot cavities and MIM waveguides," Proc. SPIE PC12195, Metamaterials, Metadevices, and Metasystems 2022, PC121951Z (3 October 2022); https://doi.org/10.1117/12.2635137.

[9P] K. M. Khabir, M. Shahabuddin, N. Noginova, M. A. Noginov, “Workfunction studies of constituents of Fabri-Perot cavities and MIM waveguides”, 2022 MRS Spring Meeting and Exhibit, May 8 -13.; Honolulu, Hawaii, USA.

[10P] Ashleigh K. Wilson, Paula Fortuno, Mohammad Shahabuddin, Natalia Noginova, "Effect of electrochromic polymer switching on surface plasmon polaritons," Proc. SPIE 12195, Metamaterials, Metadevices, and Metasystems 2022, 121950I (3 October 2022); https://doi.org/10.1117/12.2633586.

[11P] Md Golam Rabbani Chowdhury, Ayanna N. Shorter, Sangeeta Rout, and Mikhail A. Noginov "Anomalous Dips in Reflection Spectra of Optical Polymers Deposited on Plasmonic Metals", Proc. SPIE 12195, Metamaterials, Metadevices, and Metasystems 2022, 1219533 (3 October 2022); https://doi.org/10.1117/12.2635133.

[12P] Md Golam Rabbani Chowdhury, Ayanna Shorter, Sangeeta Rout, Mikhail A. Noginov, “Anomalous Dips in Reflection Spectra of Polymers Deposited on Plasmonic Metals”, CLEO Conference, San JOSE, CA, USA and virtual, May 15 – May 19, 2022, paper JTu3B.14.

[13P] Sangeeta Rout , Samantha R. Koutsares, Devon Courtwright, Ezekiel Mills, Ayanna Shorter, Srujana Prayakarao, Carl E. Bonner and Mikhail A. Noginov, “Effect of nanoscale

dielectric environments on concentration quenching", Nanophotonics, 000010151520210132. (2021) https://doi.org/10.1515/nanoph-2021-0132.

TECHNICAL REPORT

(i). Dispersion in reflection and emission of dye molecules strongly coupled to surface plasmon polaritons

Abstract: We have studied coupling of dye molecules with surface plasmon polaritons in the Kretschmann geometry and found that the coupling strength and the multi-segment dispersion curves in reflection are strongly different from those in emission [1P - 4P].

Strong coupling of light and matter is of great interest for both fundamental science and applications [1-4], including control of emission, energy transfer, chemical reactions, resistivity, surface potentials, polaritonic lasers, and many others. Although reflection and emission are among the most studied strong coupling phenomena, we have observed their highly unusual dispersion behavior, which was strongly different for reflection and emission and, according to our knowledge, newer reported in the literature.

The dispersion curve of surface plasmon polaritons (SPPs) excited in the Kretschmann geometry (high index prism / plasmonic metal / low index dielectric) is very well known [5] (Fig. 1a). If the dielectric has an absorption band of (quantum) emitters, which are strongly coupled with SPPs, this results in an avoided crossing and Rabi splitting of the dispersion curve [3]. Two absorption bands (or a band in a shoulder) result in two open gaps [4], *etc*. The coupling strength (proportional to the square root of the concentration of the dye molecules) is expected to affect the magnitude of the Rabi splitting but not the spectral positions and the very existence of the dispersion branches and gaps [3].

Experimentally, we fabricated a series of the Kretschmann geometry samples, with concentrations of dye (Rh590) in the polymer (PMMA) ranging between 0 g/l (pure PMMA) and 1260 g/l (pure Rh590) and studied their reflection spectra collected at multiple incidence angles. The angular and spectral positions of the dips in the experimental reflection spectra resulted in the dispersion curves discussed below.

In the absence of dye, the dispersion curve, expectedly, had no gaps or splitting (Fig. 1a). At the dye concentrations equal to n=4 g/l and n=16 g/l, two gaps were observed in the experimental dispersion curve (Fig. 1b). The spectral position of the lower gap approximately corresponded to the peak of the Rh590 absorption band. At the same time, the agreement between the spectral position of the upper gap in the dispersion curve and the shoulder of the Rh590 absorption band was not perfect.

The most intriguing behavior has been observed when the dye concentration was equal to or exceeded n=64 g/l. At n=64 g/l, the number of branches in the dispersion curve increased to four, although they were noisy and not highly pronounced (Fig. 1c). At n=256 g/l, a clearer "staircase" structure of the branches of the dispersion curve started forming; and at n=512 g/l and n=1260 g/l, a well defined "staircase" structure, with the number of the branches equal to six, has been formed (Fig. 1d). To the best of our knowledge, this is the largest number of the segments of the Kretschmann geometry dispersion curves reported in the literature. The latter numbers of segments and their spectral positions did not match precisely the main peak and the shoulder of the R590 spectral band. The theoretical model describing dispersion of the strong coupling observed in the *reflection spectra* will be presented at the conference.

Our next particular experiment aimed at the dispersion of *spontaneous emission* of dye molecules coupled with SPPs in the prism geometry. The dispersion of emission is expected to be different from that in reflection due to a variety of reasons, including a large Stokes shift in Rh590 molecules [6]. Experimentally, SPPs were excited, at λ=532 nm, via the prism in the Kretschmann geometry, and the spectra of outcoupled SPP emission, at $\lambda \geq 570$ nm, were collected (via the same prism) at multiple angles. The angular and spectral positions of the emission maxima were used to plot the dispersion curves of the dye's spontaneous emission coupled with SPPs. At *n*=16 g/l and *n*=64 g/l, no obvious Rabi splitting was observed in the dispersion curves for emission (Figs. 1b and 1c). At the same time, at *n*=32 g/l, the splitting, if existed, was not highly pronounced and its shape was significantly different from that in reflection. More experimental data and analysis will be presented at the conference.

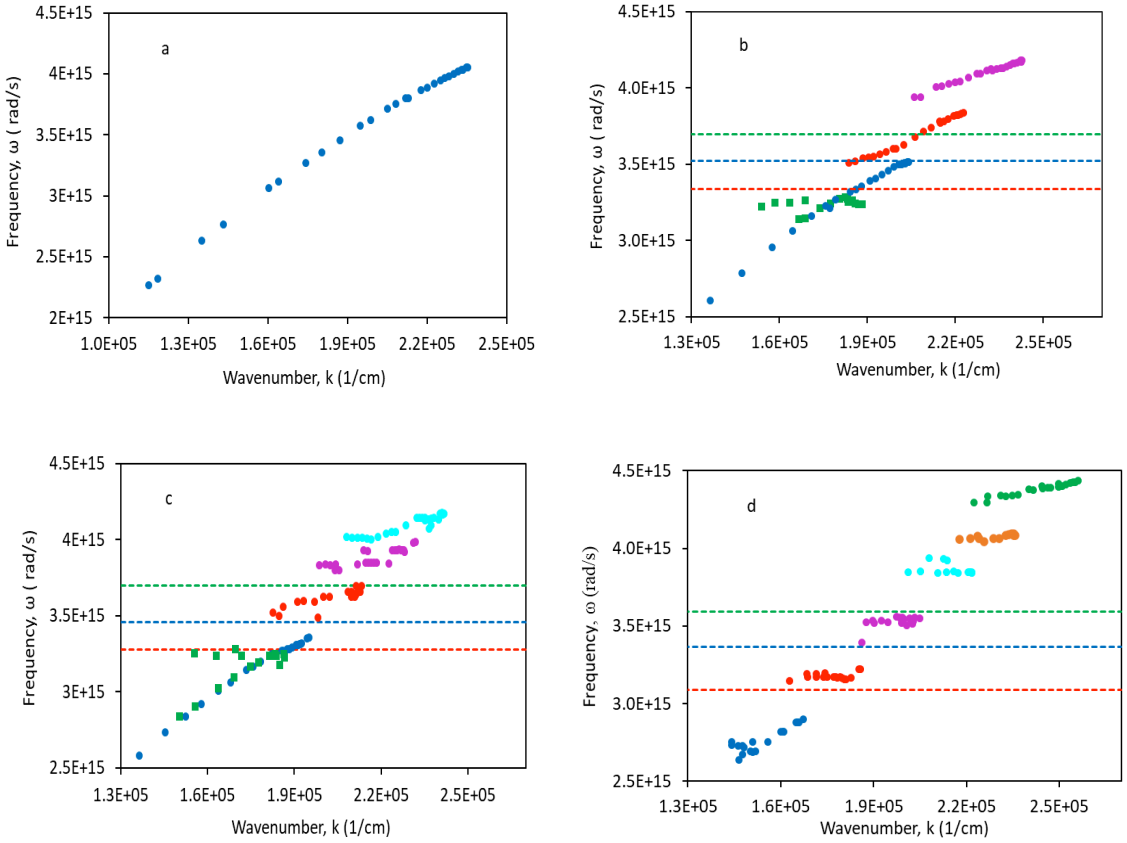

Figure 1. Dispersion curves for SPPs coupled with dye doped polymer (Rh590:PMMA) in the Kretschmann geomtry, at the dye concentrations equal to 0 g/l (pure PMMA) (a), 16 g/l (b), 64 g/l (c) and 1260 g/l (pure Rh590) (d). Circles: dispersion curves for reflection; squares: dispersion curves for emission. Red lines: Spectral maxima of Rh590 emission; blue lines: spectral maxima of Rh590 absorption; green lines: Rh590 absorption shoulder.

[1] Hutchison, J. A., Schwartz, T., Genet, C., Devaux, E., & Ebbesen, T. W. (2012). Modifying chemical landscapes by coupling to vacuum fields. *Angewandte Chemie International Edition*, *51*(7), 1592-1596.

[2] Wang, S., Mika, A., Hutchison, J. A., Genet, C., Jouaiti, A., Hosseini, M. W., & Ebbesen, T. W. (2014). Phase transition of a perovskite strongly coupled to the vacuum field. *Nanoscale*, *6*(13), 7243-7248.

[3] Törmä, P., & Barnes, W. L. (2014). Strong coupling between surface plasmon polaritons and emitters: a review. *Reports on Progress in Physics*, *78*(1), 013901.

[4] Hakala, T. K., Toppari, J. J., Kuzyk, A., Pettersson, M., Tikkanen, H., Kunttu, H., & Törmä, P. (2009). Vacuum Rabi splitting and strong-coupling dynamics for surface-plasmon polaritons and rhodamine 6G molecules. *Physical review letters*, *103*(5), 053602.

[5] Reather, H. (1988). Surface plasmons on smooth and rough surfaces and on gratings. *Springer tracts in modern physics*, *111*, 1-3.

[6] On, C., Tanyi, E. K., Harrison, E., & Noginov, M. A. (2017). Effect of molecular concentration on spectroscopic properties of poly (methyl methacrylate) thin films doped with rhodamine 6G dye. *Optical Materials Express*, *7*(12), 4286-4295.

(ii). Effect of metal-dielectric environments on photopolymerization of the [2,2′-bi-1H-indene]-1,1′-dione-3,3′-diyldiheptanoatecarboxylate monomer

We have studied effects of metal-dielectric substrates on photo-polymerization of [2,2'-Bi-1H-indene]-1,1'-dione-3,3'-diyl diheptanoate (BITh) monomer. We synthetized BITh and spin-coated it onto a variety of dielectric, metallic, and metal-dielectric substrates [5P]. The films were exposed to radiation of a UV-visible Xe lamp, causing photo-polymerization of monomer molecules. The magnitude and the rate of the photo-polymerization were monitored by measuring the strength of the ~480 nm absorption band, which existed in the monomer but not in the polymer. Expectedly, the rate of photo-polymerization changed nearly linearly with the change of the pumping intensity. In contrast with our recent study of photo-degradation of semiconducting polymer P3HT, the rate of photo-polymerization of BITh is getting modestly higher if the monomer film is deposited on top of silver separated from the monomer by a thin insulating MgF_2 layer preventing a charge transfer. This effect is partly due to a constructive interference of the incident and reflected light waves, as well as known in the literature effects of metal/dielectric substrates on a variety of spectroscopic and energy transfer parameters. At the same time, the rate of photopolymerization is getting threefold larger if monomer is deposited on Ag film directly and charge transfer is allowed. Finally, Au substrates cause modest (~50%) enhancement of both monomer film absorption and the rate of photo-polymerization.

(iii). Emission kinetics of HITC laser dye on top of arrays of Ag nanowires

Control of spontaneous emission and energy transfer are among key functionalities of photonic materials and devices. It has been shown that metamaterials with hyperbolic dispersion (lamellar metal-dielectric structures and arrays of metallic nanowires grown in pores of alumina membranes, whose dielectric permittivities in orthogonal directions have opposite signs have high photonic densities of states (PDOS) and, in accord with the Fermi's Golden Rule, can manipulate both rates and directionality of spontaneous emission. In turn, Förster energy transfer was shown to be affected by lamellar hyperbolic metamaterials, cavities, metallic films and nanoporous random structures with sponge morphology. In particular, it was shown that the same nonlocal metal-dielectric environments, which boost spontaneous emission, inhibit the energy transfer. [7P]

(iv). Kelvin probe work-function studies of components of Fabry-Perot cavities and MIM waveguides

Work function is an important material's property playing important roles in electronics, photovoltaics, and, more recently, in nanophotonics. We have studied effects of organic and inorganic dielectric materials on work functions of Au films [8P, 9P]. We found that measured

work function of a metallic surfaces can be affected by dielectric materials situated 10 nm-100 nm away from the surface. Our samples were single- and multi-layered Au and dye-doped polymeric films (Rh590:PMMA) deposited on glass. We have found that (i) glass reduces work functions of Au surfaces separated from glass by ≈50 nm gold slabs. (ii) Rh590:PMMA increases the work function of a gold film deposited on top of the polymer and (iii) reduces it if Rh590:PMMA is deposited on top of Au. (iv) With increase of the Rh590 concentration in PMMA, n, the work function first decreases (at n<30 g/l) and then increases (at n>30 g/l). (v) The work function of a Fabry-Perot cavity or an MIM waveguide is almost the same as that of single Au films of comparable thickness. The experimental results can be qualitatively explained in terms of a simple model taking into account adhesion of charged molecules to a metallic surface and formation of a double layer of charges accelerating or decelerating electrons exiting the metal and decreasing or increasing the work function.

(v). Effect of electrochromic polymer switching on surface plasmon polaritons

Electrochromic polymers incorporated into plasmonic systems provide a possibility to control plasmonic properties with the applied voltage. Using gold-polyaniline (PANI) bilayers, we study the effect of coloration switching on surface plasmon polaritons propagating at the PANI-gold interface. The width of the resonance, magnitude of the plasmon wave-vector and dielectric permittivity of PANI are estimated as the function of the applied voltage. [10P]

(vi). Anomalous Dips in Reflection Spectra of Polymers Deposited on Plasmonic Metals

Abstract: Anomalous dips in reflection spectra of optical polymers deposited on plasmonic metals have been observed and discussed in terms of singularity of surface plasmon polaritons (SPP's) in the ultraviolet (UV) part of the spectrum [11P, 12P].

Controlling spectroscopic properties of quantum emitters with metal-dielectric environments, including metamaterials [1], metasurfaces [2], Fabry-Perot cavities [3], and Metal-Insulator-Metal (MIM) waveguides [4,5], is of great importance to fundamental studies and applications of nanophotonics [6], metamaterials [1] and plasmonics [7]. In our recent studies (unpublished) we have observed that reflection spectra of thin PMMA polymeric films doped with rhodamine 590 (Rh590) or HITC laser dyes deposited on Ag and Au feature strong bands (reflection dips) at λ~380 nm (Figs.1a-1c), in addition to the expected $S_0 \rightarrow S_1$ absorption maxima at λ~530 nm (Rh590) and λ~760 nm (HITC), respectively. These λ~380 nm absorption bands are in the spectral range of high-energy transitions (presumably, $S_0 \rightarrow S_2$) of the Rh590 and HITC dyes. No significant λ~380 nm bands were observed in transmission spectra of the Rh590 and HITC films on top of glass, Figs. 1a-1c.

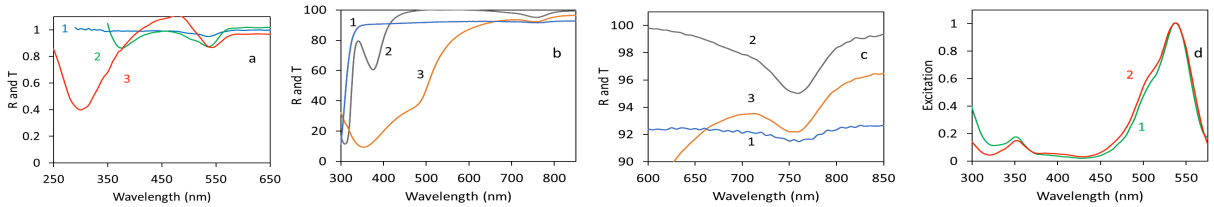

Figure 1. (a) Transmission (1) and reflection (2,3) spectra of Rh590:PMMA deposited on glass (1), Ag (2) and Au (3). (b) Same for HITC:PMMA films. (c) Zoomed fraction of Figure 1b. (d) Excitation spectra of Rh590 emission on top of glass (1) and Ag (2).

Intriguing spectroscopic properties and potential applications of the λ~380 nm reflection dips motivated the present study. Surprisingly, we found that the λ~380 nm absorption bands are irrelevant to the Rh590 and HITC laser dyes. Instead, they are likely related to singularities of Surface Plasmon Polaritons (SPPs) in the UV part of the spectrum, excited by unintentional scatterers. In the first series of experiments reported below, we observed large dips (at λ~380 nm) in the reflection spectra of Rh590:PMMA films deposited on top of the 150 nm Ag film. This was in addition to observation of the $S_0 \rightarrow S_1$ absorption band at λ~530 nm, Fig. 1a. At the same time, no significant l~380 nm bands were seen in the transmission spectra of Rh590:PMMA films deposited on glass, Fig. 1a. Furthermore, when Rh590:PMMA was deposited on top of the 162 nm Au film, the UV spectral band became even more pronounced and shifted to 300 nm, Fig. 1a. Similar results were obtained when the laser dye was HITC (with the maximum of the $S_0 \rightarrow S_1$ transition at λ~760 nm) rather than Rh590, Figs. 1b,1c. Although this observation is consistent with enhancement of the high-energy transition (presumably, $S_0 \rightarrow S_2$) by Ag and Au, it is not conclusive. In the next particular experiment, we collected *excitation* spectra of the of the R6G:PMMA emission (at λ~600 nm, $S_1 \rightarrow S_0$) on top of glass and Ag substrates (Fig. 1d), and did not see any significant bands at λ~380 nm, while we have routinely seen them in the *reflection* spectra measured on top of Ag. This is the strong evidence that the λ~380 nm band in the reflection spectrum has nothing to do with absorption of Rh590 molecules but has a completely different origin.

The most decisive evidence proving that the λ~380 nm reflection band was not due to Rh590 or HITC molecules was obtained when *undoped* PMMA, PVP and PS polymers were deposited on Ag substrates: all these spectra had λ~380 nm spectral bands, whose exact spectral positions depended on the refractive index: the smaller the index, the shorter the dip's wavelength, see Figs. 2a and 2b.

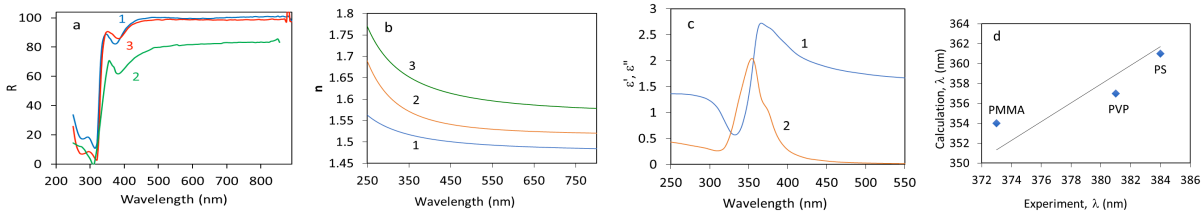

Figure 2. (a) Reflection spectra of polymers PMMA (1), PVP (2), PS (3) on top of Ag, featuring dips at λ~380 nm. (b) Spectra of refractive indexes of PMMA (1), PVP (2), and PS (3). (c) Calculated spectra of real (1) and imaginary (2) parts of refractive indexes of SPPs propagating at the interface between Ag and PMMA. (d) Calculated vs experimental wavelengths of the dips in the reflection spectra.

The existence of the ~380 nm dips in the reflection spectra of polymers (with or without dye) deposited on Ag, can be tentatively explained in terms of SPPs excited at the interface between metal and dielectric. The effective refractive index of SPPs is given by the formula,

$$n_{SPP} = \sqrt{\frac{\varepsilon_m \cdot \varepsilon_d}{\varepsilon_m + \varepsilon_d}} \qquad n_{SPP} = \sqrt{\frac{\varepsilon_m \varepsilon_d}{\varepsilon_m - \varepsilon_d}} \tag{1}$$

where ε_m and ε_d are the dielectric permittivities of metal and dielectric, respectively [8]. We calculated the corresponding SPP dispersion curves and found that real and imaginary parts of n_{SPP} have "wave-like" and "bell-shaped" singularities in vicinity of λ~360 nm, Fig. 2c, close to the positions of the spectral bands observed in the experimental reflection spectra of polymers on Ag, Fig 2a, 2d. The order of the above spectral features, $\lambda_{PMMA}<\lambda_{PVP}<\lambda_{PS}$, was the same as the order of the experimental dips in the reflection spectra, Fig.2a, and the order of refractive indexes of the same three polymers in the UV range of the spectrum, $n_{PMMA}<n_{PVP}<n_{PS}$ (Fig. 2b). We, thus, tentatively conclude that the dips in the reflection spectra of the polymers on top of Ag are due to singularities in n_{SPP} occurring when the real part of the denominator in the formula above is equal to zero. The modest disagreement between the spectral positions of the experimental (λ~380 nm) and calculated (λ~360 nm) spectral bands can be due to the fact that the dielectric permittivities in our experiment were not exactly the same as those used in the calculations [9]. The key question pertaining to the explanation above is how the SPP was excited without any prism or grating. We infer that the excitation of SPPs was mediated by unintentional subwavelength scatterers. The effect of the scattering strength on the excitation of SPPs and the experimentally observed dips in the reflection spectra is the subject of future studies to be published elsewhere. Alternatively, the observed anomalous dips in the reflection spectra can be attributed to a Berreman-like leaky mode in the light cone [10] or strong field enhancement in the Epsilon Near Zero (ENZ) regime.

[1] Noginov, Mikhail A., and Viktor A. Podolskiy, eds. *Tutorials in metamaterials*. CRC press, 2011.

[2] Chen et al. "A review of metasurfaces: physics and applications." *Reports on progress in physics* 79.7 (2016): 076401.

[3] Faruk et al. "Emission of R6G dye in Fabry–Perot cavities in weak and strong coupling regimes." *JOSA B* 37.11 (2020): 3200-3212.

[4] Peters et al. "Control of physical and chemical processes with nonlocal metal–dielectric environments." *Acs Photonics* 6.12 (2019): 3039-3056

[5] Miyazaki et al. "Controlled plasmon resonance in closed metal/insulator/metal nanocavities." *Applied physics letters* 89.21 (2006): 211126.

[6] Kirchain, Randolph, and Lionel Kimerling. "A roadmap for nanophotonics." *Nature Photonics* 1.6 (2007): 303-305.

[7] Maier, Stefan A. *Plasmonics: fundamentals and applications*. Vol. 1. New York: springer, 2007.

[8] Reather, Heinz. "Surface plasmons on smooth and rough surfaces and on gratings." *Springer tracts in modern physics* 111 (1988): 1-3.

[9] Ni et al. "PhotonicsDB: Optican Constants." Nanohub.org, 30 March 2018, https://nanohub.org/tools/photonicsdb

[10] Vassant, Simon, et al. "Berreman mode and epsilon near zero mode." *Optics express* 20.21 (2012): 23971-23977.

(vii). Effect of nanoscale dielectric environments on concentration quenching

We have studied the dependence of concentration quenching of luminescence (donor-acceptor energy transfer) on the thickness d of dye-doped polymeric films (HITC:PMMA) and found its strong inhibition at small values of d [13P]. This phenomenon is tentatively explained by the limited number of acceptors, which can be reached by donors' excitation in thin samples, if the film's thickness is comparable to the diffusion length of the energy transfer (determined by the Förster radius and the dye concentration). The same phenomenon is consistent with inhibition of the concentration quenching of dye embedded in anodic alumina membranes. The elongation of the emission kinetics in thick HITC:PMMA films is cautiously attributed to the samples' crystallinity.

The photonic density of states (PDOS) and, correspondingly, the radiative decay rates of emitters implanted into a dielectric matrix are getting reduced in vicinity of a dielectric-air interface. The same mechanism should cause a reduction of spontaneous emission rates in thin HITC:PMMA films in our study. However, the comparison of the model and our experiment suggests that the PDOS reasoning is insufficient to explain the strong reduction of the decay rates observed at high dye concentration v=40 g/l (~2.5-fold). This and seeming absence of the PDOS effect in low doped HITC:PMMA thin films, v=2 g/l and v=3.6 g/l, is the subject of the further study to be published elsewhere.